NASA CR-112268

ELASTO-PLASTIC BENDING OF CRACKED PLATES, INCLUDING THE EFFECTS OF CRACK CLOSURE

David Paul Jones

Report SM-83A

October 1972

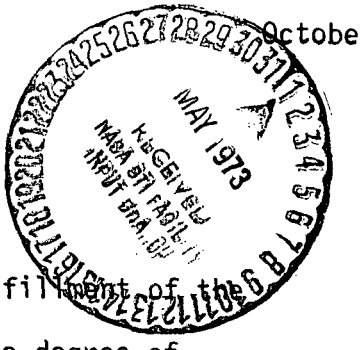

Submitted in partial fulfillment of the

requirements for the degree of

Doctor of Philosophy at Carnegie-Mellon University

N73-18915

(NASA-CR-112268) ELASTO-PLASTIC BENDING OF CRACKED PLATES, INCLUDING THE EFFECTS OF CRACK CLOSURE Ph.D. Thesis (Carnegie Inst. of Tech.) 135 p HC $8.75 CSCL 20K

~~N73-21948~~

Unclas

G3/32 68981

Department of Mechanical Engineering

Carnegie Institute of Technology

Carnegie-Mellon University

Pittsburgh, Pennsylvania

ACKNOWLEDGMENTS

The author wishes to thank his thesis advisor, Dr. J. L. Swedlow of Carnegie-Mellon University who was a constant source of encouragement throughout the course of this work. Thanks are also due to members of the thesis committee, Drs. D. S. Griffin, T. A. Cruse, and C. L. Dym. The author is grateful for the patience and understanding of his wife Janet, who was happy to see this work begin and delighted to see it end. The author acknowledges the Doctoral Program of the U. S. Atomic Energy Commission at Westinghouse Bettis Atomic Power Laboratory for providing financial assistance during his Ph.D. studies. Also, much of the computer support was provided under NASA grant #NGR 39-002-023 for which the author is grateful. And finally, special thanks to Gerry Straker who typed the manuscript.

TABLE OF CONTENTS

page

LIST OF FIGURES

LIST OF TABLES

LIST OF SYMBOLS

A	One-half plate length in x direction
a	One-half crack length
B	One-half plate width in y direction
C_{ij}	$\int_{-h/2}^{h/2} ZE_{ij}dZ$
D_{ij}	$\int_{-h/2}^{h/2} Z^2E_{ij}dZ$
D	Plate rigidity, $Eh^3/12(1-\nu^2)$
E_{ij}	Two dimensional compliance relation
E	Young's Modulus
$F(\theta,\lambda)$	Angular function in Williams [19] solution
H_{ij}	Hermite interpolation formulas
h	Plate thickness
J_1,J_2,J_3	Stress deviator invariants
K_I	Opening mode stress intensity factor
K_B	Bending mode stress intensity factor
m	Number of constraint equations
M_o	Applied boundary moment
M_x,M_y,M_{xy}	Moment resultants
N_x,N_y,N_{xy}	In-plane force resultants
N	Number of system degrees of freedom
NEL	Total number of elements

S_{ij}	Deviator of stress tensor σ_{ij}
X	Surface measure
T_i	Surface traction
u,v,w	Displacement components
V	Volume measure
$W^{(p)}$	Plastic strain energy density
x,y,z	Plate cartesian coordinates
r,θ,z	Plate cylindrical coordinates
α_i	Magnitude of search in ith direction
β_i	Orthogonalization constant
γ	Scalor defined by Equation (3-5)
∇^4	Biharmonic operator
$\varepsilon_x,\varepsilon_y,\gamma_{xy}$	Strain components
ε_{ij}	Strain tensor
κ	Scalor in loading function
Λ	Constant of proportionality
Φ	Loading function
μ,ν	Elastic constants (shear modulus, Poisson's ratio)
ψ	Airy stress function
η	Unit outward normal vector to a surface
π,π^*	Objective functionals
σ_o	Applied boundary stress
$\sigma_x,\sigma_y,\tau_{xy}$	Stress components
σ_{ij}	Stress tensor
$\tau_{eq},\varepsilon_{eq}$	Equivalent stress, strain components
τ_{OCT},γ_{OCT}	Octahedral stress, strain components

$[A]$, $[A]$	Master stiffness matrix
$\{B\}$	Element nodal force vector
$[C]$	Connection matrix
$\{D\}$	Constraint vector
$E_{ijk\ell}$, $C_{ijk\ell}$	Plasticity compliance tensors
$\{F\}$	Work equivalent force vector
$\{H\}$	Solution vector to $\delta\pi = 0$
$[k^{ij}]$	$i,j = u,v,w$; Element stiffness matrix entries
$\{p_i\}$	Direction of search vector
$\{P(x,y)\}$	Polynomial vector made up of H_{ij} H_{ij} products
$\{R\}$	Residual vector
$\{X\}$	State variable vector made up of system degrees of freedom
$\{Y\}$	Element degrees of freedom
$[\alpha^n]$	Element communication data. Maps element degrees of freedom onto system degrees of freedom.
$\{\lambda\}$	Lagrange multiplier vector

Superscripts (e), (p) refer to elastic and plastic portions. The dot over a symbol refers to time derivatives. The usual summation convention on i,j,k,ℓ is assumed except in Section III, where the subscripts refer to particular vectors and not their components.

ABSTRACT

A capability for solving elasto-plastic plate bending problems is developed using assumptions consistent with Kirchhoff plate theory. Both bending and extensional modes of deformation are admitted with the two modes becoming coupled as yielding proceeds. The material work-hardens and, consistent with the fundamental theory of elasto-plasticity, loading is incremental and local unloading is permitted to occur. Equilibrium solutions are obtained numerically by determination of the stationary point of a functional which is analogous to the potential strain energy. The stationary value of the functional for each load increment is efficiently obtained through use of the conjugate gradient method (CGM) at modest computer storage requirements. The CGM was modified to take advantage of initial search direction vectors to provide possible reductions in computing time from one load increment to the next.

This technique is applied to the problem of a large centrally through cracked plate subject to remote circular bending. Comparison is drawn between two cases of the bending problem. The first neglects the possibility of crack face interference with bending, and the second includes a kinematic prohibition against the crack face from passing through the symmetry plane. Results are reported which isolate the effects of elasto-plastic flow and crack closure.

CHAPTER I

INTRODUCTION

1.1 General Comments

The stress and strain fields in a plate containing a perfectly sharp crack subject to a variety of loading conditions has been the principal focus of a great deal of past and present research. The solution to the elastic extensional problem was given by Inglis [1]* in 1913. It was not until 1951 that Williams [2], using Kirchhoff fourth order plate theory, first published a solution to the problem of elastic bending of a centrally cracked plate. In 1961, Knowles and Wang [3] solved this same centrally cracked plate bending problem using sixth order Reissner plate theory. The principal deficiency with either the Williams or the Knowles and Wang solutions to the bending problem is their inability to account for the crack closure phenomena, i.e., both solutions model the crack face as a free surface either in the Kirchhoff or Reissner sense. This allows the material to overlap onto itself on the compressive side as bending and crack face rotation proceeds.

The bending/extension interaction problem has been mainly attempted through superposition of elastic bending and extensional solutions. The work of Folias [4] and Wynn [5] are noted in this area. Specifically, the crack closure problem does not exist if the extensional load is large enough to open the crack sufficiently to preclude contact of the crack

---

*Numbers in parentheses indicate references listed in the Bibliography.

face on the compressive side due to the bending load. Unfortunately, this crack face interaction does exist in many practical instances and its effect needs to be quantified.

The extension/bending problem becomes even more insideous when material yielding is present. Under these conditions, not only is the bending/extension behavior coupled through interaction of the closed crack face, it is also coupled through material property considerations.

Elasto-plastic solutions are available for the extensional case in the form of numerical solutions [(6), (7), and (8)] and closed form solutions in the case of special plasticity assumptions [(9), (10), and (11)]. Unfortunately, the bending problem has not been attacked with such success. The principal reasons for this is the additional complications of crack closure, free surface approximations for Kirchhoff boundary conditions, and the elastic core that persists in plate bending problems for the case of work hardening materials. Gonzalez and Brinson [12] have applied the Dugdale Strip model to the bending problem with some success but their solutions are limited both due to lack of crack closure considerations and not accounting for an elastic core.

1.2 Scope of Research

Ideally, the analysis of a plate with a centrally placed through crack subject to circular bending of such a magnitude to cause large amounts of yielding would include both the effects of crack closure and coupling between bending and extension as yielding proceeds. A first step in that direction is provided in this work.

The bending theory used in this study is based on classic Kirchhoff plate assumptions. Higher order theories for the bending analysis were deemed prohibitive when considered in conjunction with elasto-plastic material properties. The general elasto-plastic extension/bending theory is developed through use of a functional whose minimum corresponds to the equilibrium state for the elasto-plastic plate. Determination of this minimum through a numerical procedure constitutes the finite element approach used. Using this capability, the circular bending of an elasto-plastic plate with a centrally located crack is treated. The problem is essentially broken down into two parts: The first problem using the classic boundary conditions for a stress free surface (in the Kirchhoff sense) of the crack face (i.e., no closure) and the second which modifies these boundary conditions to reflect the physically realistic phenomenon of crack closure. This is accomplished by adding to the functional, constraint equations that require the normal displacement of the crack face on the compressive surface to be zero. This couples in-plane and bending behavior through the constraint of the crack face and not by extending exterior plate boundaries to relieve the crack face interference.

It should be pointed out that no corrections of the results are to be made concerning crack face warpage due to either three dimensional effects at the crack tip or to the wedging effect as the crack closes. Experimental evidence [13] indicates that these effects are important for crack length to plate thickness ratios of less than four, for which these

results do not apply. Also, no geometric non-linearities are introduced either through the bending or stretching theories. However, since a circular bending field is applied to the plate, a developable surface is expected and the geometric non-linearities due to bending, should be small.

1.3 Summary of Principal Findings

Principal findings of this study clearly show that the mechanics of a centrally cracked plate subject to circular bending is strongly influenced both by the effects of crack closure and elasto-plastic flow. Results are given for in-plane and transverse deflections, transverse slopes, neutral axis shifts, stress and strain distributions, growth of yielded zones, and stress intensity factors for plates with and without closure effects accounted for. Comparison of these results between the two problems allow reduction of systemic errors and even though Kirchhoff plate theory was used, a good indication of the effects of elasto-plasticity and crack closure was obtained.

CHAPTER II

REVIEW OF LITERATURE

Many theoretical and experimental studies have been performed concerning the problem of a stationary through crack in a plate subject to bending and/or extensional loading. Although the bulk of these studies deals with elastic behavior only, elastic-plastic results are available for the extensional problem mostly in the form of numerical determination of the stress state or asymptotic studies of crack tip singularities in plastic materials. There has been relatively little work reported on the elasto-plastic bending problem.

2.1 Elastic Bending and Extension

The early work by Williams [2,14] dealt with the bending problem by considering a wedge-shaped section and applying boundary conditions along radial edges of the section. Williams solved the biharmonic equation $\nabla^4 w = 0$ of Kirchhoff plate theory by assuming a solution of the form $w(r,\theta) = r^{\lambda+1}F(\theta,\lambda)$. He then determined the functional form $F(\theta,\lambda)$ which solved the differential equations and obtained eigen solutions appropriate for various boundary conditions. Williams [15] then made the analogy between the plane extension $\nabla^4\Psi = 0$ and bending $\nabla^4 w = 0$ where Ψ is the Airy stress function and using the developed techniques, solved for various boundary condition combinations. In this paper, he suggested that the wedge-shaped section for the extensional problem be extended to 360^o for the free-free boundary condition case. These conditions represent a

semi-infinite V-shaped notch in an infinite plate. In [16], Williams published the results of the V-shaped notch or crack for the extensional case using the technique developed in [15].

In 1957, Irwin [17] presented the results of using the Westergard stress function [18] as applied to the through cracked plate. The singular stresses at the crack tip for the extensional case are

$$\sigma_{xx} = \frac{K_I}{\sqrt{(2\pi r)}} \cos\frac{\theta}{2}\left(1 - \sin\frac{\theta}{2}\sin\frac{3\theta}{2}\right)$$

$$\sigma_{yy} = \frac{K_I}{\sqrt{(2\pi r)}} \cos\frac{\theta}{2}\left(1 + \sin\frac{\theta}{2}\sin\frac{3\theta}{2}\right)$$

$$\tau_{xy} = \frac{K_I}{\sqrt{(2\pi r)}} \sin\frac{\theta}{2}\cos\frac{\theta}{2}\cos\frac{3\theta}{2} \qquad (2\text{-}1)$$

$$\sigma_{zz} = \nu(\sigma_{xx} + \sigma_{yy})$$

$$\tau_{xz} = \tau_{yz} = 0$$

$$K_I = \sigma_o(\pi a)^{\frac{1}{2}}$$

The significant points of this work are the $1/\sqrt{r}$ singularity, the ratio of the normal stresses at the crack tip (unity), and the angular variation of the stresses.

Williams [19] continued his eigen solution technique and in 1961 published his results employing fourth-order classical bending theory with Kirchhoff boundary conditions. His singular stresses were modified by Sih, Paris, and Erdogan [20] to identify a bending stress and shear stress intensity factor. Using this later notation K_B, these singular stresses are (see Figure 2-1 for plate geometry)

$$\sigma_{rr} = \frac{7 + \nu}{2(3 + \nu)} \frac{K_B}{\sqrt{2r}} \frac{z}{h} \left[\frac{3 + 5\nu}{7 + \nu} \cos \frac{\theta}{2} - \cos \frac{3\theta}{2} \right]$$

$$\sigma_{\theta\theta} = \frac{7 + \nu}{2(3 + \nu)} \frac{K_B}{\sqrt{2r}} \frac{z}{h} \left[\frac{5 + 3\nu}{7 + \nu} \cos \frac{\theta}{2} + \cos \frac{3\theta}{2} \right] \qquad (2\text{-}2)$$

$$\tau_{r\theta} = \frac{7 + \nu}{2(3 + \nu)} \frac{K_B}{\sqrt{2r}} \frac{z}{h} \left[- \frac{(1 - \nu)}{(7 + \nu)} \sin \frac{\theta}{2} + \sin \frac{3\theta}{2} \right]$$

$$K_B = \frac{6M_o}{h^2} (\pi a)^{\frac{1}{2}}$$

Sih, Paris, and Erdogan [20] went on to calculate K_B for various crack configurations using the method of complex variables as applied to planar problems by Muskhelishvili [21].

Williams [19] results showed that the ratio of the normal stresses at the crack tip in the plane of the crack are not unity as in Irwin's extensional problem and, although the $(1/r)^{\frac{1}{2}}$ singularity was the same, the angular variation was different between the extensional and bending case.

FIGURE 2-1
CENTRALLY THROUGH CRACKED PLATE

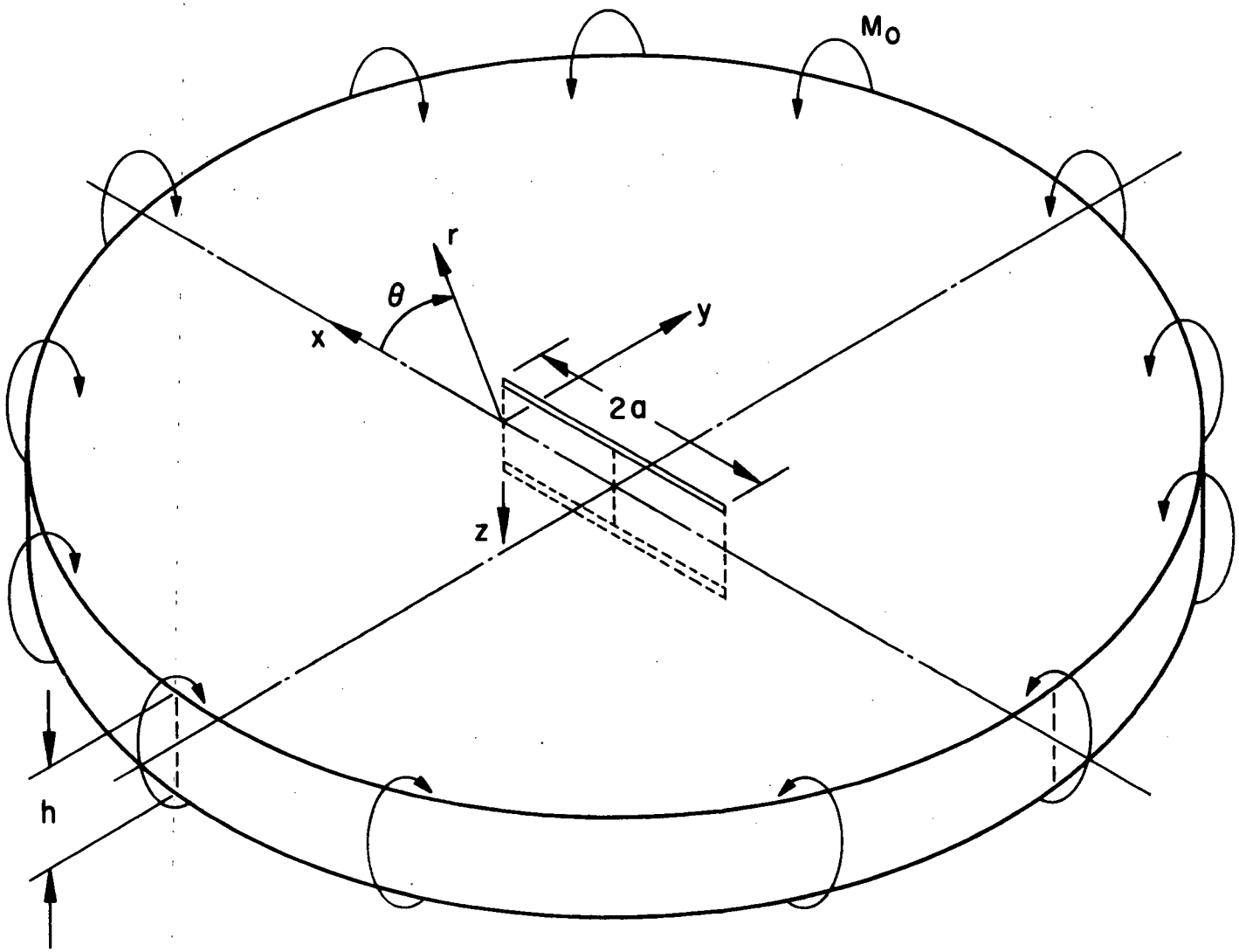

Knowles and Wang [3] used sixth order Reissner plate theory and showed that the functional form of the stress distribution is the same as in the extensional case. Moreover, the stress ratio is unity as in the extensional problem. The difference between Williams [19] and Knowles and Wang's results is due to the use of approximate Kirchhoff boundary conditions for the free surface, while the Reissner theory allows for the satisfaction of three separate boundary conditions, i.e., vanishing normal moment, twisting moment, and shear stress on the crack face.

In 1969, Hartranft and Sih [22] applied Reissner plate theory to an infinite plate of finite thickness and showed that the bending stress intensity was a function of plate thickness. For vanishingly thin plates, these results reduced to those of Knowles and Wang [3].

2.2 Experimental Investigations

In all of the theoretical studies mentioned above, the crack face was taken to be stress free in either the Kirchhoff or the Reissner sense. In reality, however, this is not the case; on the compression side of the plate, the crack physically closes on itself. There is ample experimental evidence that such is the case. For instance, Erdogan et al. [23] found that even in cases of some extension normal to the crack surface, the crack closes upon itself on the compression side of the plate. Smith and Smith [13,24], using a photoelastic technique, also found a strong influence of crack closure on the stress results and in fact found that crack closure could produce a non-conservative effect of as much as 40%. Smith and Smith [24] indicated a shift in the neutral axis that was

associated with the crack closure phenomenon. They compared their experimental results with the theoretical work of Hartranft and Sih [22] and found that as three-dimensional effects became prominent (i.e., crack length becomes small compared to plate thickness) crack closure effects dropped off.

2.3 Elasto-Plastic Bending and Extensional Solutions

A considerable amount of effort has been directed toward the extension of an elasto-plastic plate containing a stationary crack. There is much current work being done attempting to identify and make use of parameters which characterize near tip singularities of elasto-plastic solutions from both analytical and numerical approaches.

Due to the complexity that non-linear material behavior adds to this problem, most of the analytic efforts reported in the literature have made use of various idealizations such as perfect plasticity or power law hardening materials. For example, for rigid-perfectly plastic materials, Rice [25] has shown that the shear strain exhibits a 1/r crack tip singularity. Also, both Hutchinson [9], and Rice and Rosengren [10] have found near tip solutions to power law hardening materials which have stress and strain type singularity of $n/(1+n)$ and $1/(1+n)$ where n is the hardening exponent. Much has been learned from elasto-plastic finite element solutions presented by Lee and Kobayashi [8], Swedlow et al. [6], Miyamoto et al. [7], and others concerning the growth and shape of plastic yield zones, transition between elastic and plastic behavior, and the stress and strain behavior in the vicinity of the crack tip.

Experimental evidence [27] has shown that the detailed shape of the stress-strain curve is of great importance when considering crack geometries. This has led many investigators to develop numerical capabilities to handle materials with general work hardening properties (i.e., [6], [7], and [8]). Swedlow, Yang, and Williams [6] using finite element techniques, indicate that for elasto-plasticity, the singularity of stresses at the crack tip decreases with load, while that for strain increases. Efforts (Rice and Tracey [26] and Levy, et al. [28]) have been made to develop elasto-plastic singularity elements with limited success. This is mostly due to the changing nature of the singularity as the plasticity develops, the dependence of the singularity on the details of stress-strain curve, and the difference between stress and strain singularities at the crack.

Very little theoretical or experimental work has been done concerning the elasto-plastic bending of plates containing stationary cracks. Gonzalez and Brinson [12] have extended the Dugdale extensional model to the bending case. They performed an experimental study and found that the plastic zone varied with thickness in both tension and compression at the crack tip with the compressive zone continuing along the crack front on the compressive side of the plate. They also found experimentally a shift in the neutral axis due to the effects of crack closure which were not included in their theoretical considerations.

2.4 Combined Bending and Extension

Theoretical solutions to the elastic combined extension/bending problem for the most part have been obtained by superposition of local stress fields due to the extensional load onto local stress fields due to the bending moment [5], [44]. These solutions do not account for the crack closure phenomena unless the extensional load is large enough to preclude contact of the crack face on the compressive surface due to bending. Adjusting the extensional load and bending moment such that the crack face is always open was suggested by Wynn [5] as a method of eliminating the crack closure problem. However, as Wynn's work pointed out, there are many practical instances of combined extension/bending where crack closure is of major importance. No elasto-plastic results are reported in the literature for the case of combined bending and extensional loading.

CHAPTER III

DISCRETE ELEMENT FORMULATION

As pointed out in Chapter II, theoretical solutions are not yet available for the problem of a through stationary crack in a plate subjected to bending and extension where the effects of crack closure are important. Experimental evidence indicates that analytical techniques are needed that can adequately reflect the shift in neutral axis due to crack closure and couple the resulting in-plane loadings to the transverse plate behavior. In the elasto-plastic problem, this is further complicated by the coupling between stretching and bending that occurs as yielding proceeds.

3.1 Solution Technique

Traditionally, for elastic behavior, minimum potential and complementary energy theorems have been used either to derive equilibrium equations with complete boundary conditions or to determine approximate solutions to complicated boundary value problems. These theorems are also used in the development of general numerical capabilities for the solution of elastic structural problems, namely, the finite element method. Also, by discretizing the structure in question and treating the potential energy expression as a functional to be minimized, it is possible to cast the equilibrium problem as a mathematical programming problem. The minimization process may then be carried out by any

number of numerical algorithms developed from the mathematical programming point of view. For non-linear material behavior, minimum potential and complementary energy theorems are not valid. However, for incremental plasticity, rate formulations analogous to the minimum potential and complementary energy theorems can be obtained. Conceptually these new functionals may be treated similarly to the potential and/or complementary energy with the interpretation being applied on an incremental rather than a total state basis.

The problem addressed here is that of a flat plate that is loaded in such a way as to cause both extentional and bending modes of deformation at least locally. These displacements are considered to be small enough so that kinematic assumptions consistent with Kirchhoff plate theory can be made. Although the deflections are considered to be small, the resulting stress field is allowed to be of such a magnitude to cause considerable yielding of the material. The theory for this elasto-plastic material behavior relating increments in stress and strain to increments of applied load has been obtained by coupling the Prandtl-Reuss relations with Drucker's work-hardening hypothesis, [6] and [29].

Due to the complexity of the field equations and boundary condition describing the stretching-bending elasto-plastic plate behavior, only the simplest cases can be solved in closed form. However, because the problem is basically quasi-linear (see Swedlow [29]), it is possible to cast the boundary value problem as a set of linear sub-problems to be solved

in succession. Each sub-problem is associated with a load increment and accumulated values of stress and strain. The solution to the complete elasto-plastic boundary value problem then consists of solving a succession of linear, anisotropic, inhomogeneous elasticity problems.

The approach taken in this study is to discretize the structure and solve the resulting equilibrium problem of an assemblage of elements approximating the total plate structure. A functional is developed whose minimum corresponds to the equilibrium point of an elasto-plastic plate subjected to in-plane and transverse loadings. The assemblage of the discretized approximations to this functional is then numerically minimized for a succession of loads incrementally applied allowing the plasticity effects to build up with each increment.

The plate element used in this work was constructed using two dimensional cubic Hermite interpolation functions. Bogner, Fox, and Schmit [30] used these displacement functions to develop an elastic plate bending element. The attractive feature of using cubic Hermite interpolation polynomials as displacement functions is that they have the property of continuity of displacement and slope at intraelement boundaries. Tong and Pian [31] have shown that such an element satisfies kinematic admissibility for the entire plate while Birkhoff, Schultz, and Varga [32] have shown that the error bounds are proportional to the mesh size squared. The extension of this elastic element to the inelastic case was done using deformation theory for the case of pure bending and no stretching by Fox and Stanton [33].

The discretized element representation used here incorporates the kinematic admissibility properties of the bicubic Hermite interpolation polynomials in addition to the incremental plasticity constitutive relations. The spatial variation of the material properties caused by the yielding is approximated by bilinear Hermite interpolation between additional nodes interior to the element that partition the element into four sections. The thickness integration is accomplished by a Lobotav quadrature of nine points.

Using the discretized representation for the plate, a quadratic functional is developed whose minimum corresponds to the equilibrium point for the particular displacement-equilibrium problem. A modified version of Beckman's [34] conjugate gradient quadratic programming algorithm is used to minimize the functional and obtain the equilibrium solution. The modifications used take direct advantage of initial guess of both solution and direction of search. These modifications become extremely important as far as elasto-plastic solutions are concerned. Here, the solution from the previous load increment can be used for the initial guess and direction vector for the next increment.

The primary advantage of the energy search technique to solve the equilibrium problem is that of computer storage. By calculating the total potential energy as the summation of the energy contributions from each element, very large problems can be solved without requiring the assembly of the master stiffness matrix. Also, bandwidth becomes unimportant as zeros are taken advantage of regardless of their position

in the matrix. In plasticity solutions where direct advantage of initial guess solutions may be made, significant reduction in computation time may be realized.

In this Chapter, the plate element stiffness matrix is derived and the conjugate gradient method developed.

3.2 Constitutive Relations

Since the mathematical theory of plasticity has received extensive treatment in the literature (e.g., [29]), there is little need to present a detailed derivation here. Rather, an outline of the steps and assumptions necessary to obtain the elasto-plastic flow rule used in subsequent calculations is presented.

A flow rule for elasto-plastic deformation can be derived based on the following assumptions [29]:

1. elastic and plastic strains are separable;
2. quasi-thermodynamic postulate known as Drucker's hypothesis is imposed; and,
3. the existence of a surface is presumed in stress space, known as a loading function, which is of the form

$$\phi(J_2, J_3) - \kappa \leq 0 \qquad (3\text{-}1)$$

where ψ is an arbitrary function having the dimensions of stress whose arguments are

$$J_2 = \frac{1}{2} \underline{S}_{ij} \underline{S}_{ji}$$
$$J_3 = \frac{1}{3} \underline{S}_{ij} \underline{S}_{jk} \underline{S}_{k\ell}. \tag{3-2}$$

Here, $\underline{S}_{ij} = \sigma_{ij} - \frac{1}{3} \sigma_{kk} \delta_{ij}$ is the deviator of the stress tensor σ_{ij}. The scalar κ is a function of the plastic strain energy density $W^{(p)}$ given by

$$W^{(p)} = \int \sigma_{ij} d\varepsilon_{ij}^{(p)} \tag{3-3}$$

From Drucker's hypothesis, the plastic strain increment vector can be written as

$$d\varepsilon_{ij}^{(p)} = \Lambda \frac{\partial \phi}{\partial \sigma_{ij}} \tag{3-4}$$

here Λ is a constant of proportionality yet to be determined. Under these circumstances, the plastic strain increment is

$$d\varepsilon_{ij}^{(p)} = \frac{\gamma^2}{2\mu} \phi_{ij} \phi_{k\ell} d\sigma_{k\ell} \tag{3-5}$$

The scalar γ^2 is given by

$$\gamma^2 = \frac{\mu}{\mu_{eq}^{(p)}} \frac{\phi}{\phi_{ij}\phi_{ij}}$$

and

$$\phi_{ij} = \frac{\partial \phi}{\partial \sigma_{ij}}$$

$$2\mu_{eq}^{(p)} = \frac{d\tau_{eq}}{d\varepsilon_{eq}^{(p)}}$$

$$\phi = \tau_{eq}$$

The total strain increment can be divided into recoverable and irrecoverable portions. This suggests the superposition of elastic and plastic strain increments.

$$d\varepsilon_{ij} = d\varepsilon_{ij}^{(e)} + d\varepsilon_{ij}^{(p)} \tag{3-6}$$

The elastic portion is described by Hooke's law. Combining (3-5) and (3-6), the flow rule takes the form

$$2\mu d\varepsilon_{ij} = d\sigma_{ij} - \frac{\nu}{1+\nu} d\sigma_{kk}\delta_{ij} + \gamma^2 \phi_{ij}\phi_{k\ell}\, d\sigma_{k\ell} \tag{3-7}$$

The inverse of (3-7) is

$$d\sigma_{ij}/2\mu = d\varepsilon_{ij} + \frac{\nu}{1-2\nu} d\varepsilon_{kk}\delta_{ij} - \frac{\phi_{ij}\,\phi_{k\ell}\, d\varepsilon_{k\ell}}{\phi_{mn}\phi_{mn} + 1/\gamma^2} \tag{3-8}$$

Equation (3-8) can be divided by dt and by noting that the material derivative $d\sigma_{ij}/dt$ can be written as $\partial\sigma_{ij}/\partial t = \dot{\sigma}_{ij}$ for a quasi-static process, it is possible to write the flow rule independent of the time scale [6]. Hence the constitutive relations Equation (3-8) take the form

$$\dot{\sigma}_{ij} = E_{ijk\ell}\dot{\varepsilon}_{k\ell} \qquad \text{or} \qquad \dot{\varepsilon}_{ij} = E^{-1}_{ijk\ell}\dot{\sigma}_{k\ell} \tag{3-9}$$

(Note: $E_{ijk\ell}$ is given in Appendix A for plane stress.)

Equation (3-9) has been derived for a monotonically increasing equivalent stress, equivalent strain curve.

3.3 Variational Formulation

Force equilibrium for a static process is expressed by

$$\sigma_{ij,j} + F_i = 0 \tag{3-10}$$

For a quasi-static process in which the displacements are small and F_i is both small enough not to cause yielding and independent of time, differentiation with respect to time yields

$$\dot{\sigma}_{ij,j} = 0 \tag{3-11}$$

Defining $\delta\dot{u}_i$ as the first variation in the displacement field corresponding to a change in applied forces and integrating $\dot{\sigma}_{ij,j}\ \delta\dot{u}_i$ over the volume requires that

$$\int \dot{\sigma}_{ij,j}\ \delta\dot{u}_i\ dV = 0 \tag{3-12}$$

Equation (3-12) can be integrated by parts and the divergence theorem used to change the volume integration to one along the surface S.

$$\int_{S_u} \dot{\sigma}_{ij}\ \delta\dot{u}_i\ \eta_j\ dS - \int_V \dot{\sigma}_{ij}\ \delta\dot{u}_{i,j}\ dV = 0 \tag{3-13}$$

Cauchy's stress equilibrium expression $\dot{T}_i^{\eta} = \dot{\sigma}_{ij}\eta_j$ is used along the surface to produce the equation

$$\int \dot{\sigma}_{ij}\ \delta\dot{u}_{i,j}\ dV - \int_{S_u} \dot{T}_i^{\eta}\ \delta\dot{u}_i\ dS = 0 \tag{3-14}$$

The strain rate, displacement rate equations $\dot{\varepsilon}_{ij} = \frac{1}{2}(\dot{u}_{i,j} + \dot{u}_{j,i})$ can now be used resulting in a rate form analogous to the Principle of Virtual Work.

$$\int_V \dot{\sigma}_{ij}\ \delta\dot{\varepsilon}_{ij}\ dV = \int_{S_u} \dot{T}_i^{\eta}\ \delta\dot{u}_i\ dS \tag{3-15}$$

Using the constitutive Equations (3-9), the stationary principle required to determine equilibrium can be established. That is,

$$\int_V E_{ijk\ell}\dot{\epsilon}_{k\ell}\delta\dot{\epsilon}_{ij}dV = \int_{S_u} \dot{T}_i^{\eta}\,\delta\dot{u}_i\,dS \tag{3-16}$$

Defining the functional

$$\pi = \int_V \frac{E_{ijk\ell}}{2}\,\dot{\epsilon}_{k\ell}\,\dot{\epsilon}_{ij}dV - \int_{S_u} \dot{T}_i^{\eta}\,\dot{u}_i\,dS \tag{3-17}$$

and since $E_{ijk\ell}$ and $\dot{T}_i$ remain constant at an instant in time, Equation (3-16) gives rise to the stationary principle

$$\delta\pi = 0 \tag{3-18}$$

The statement for Equation (3-18) is as follows:

Theorem I.

Of all displacement rates $\dot{u}_i$ satisfying the given boundary conditions, those which satisfy the equations of equilibrium are distinguished by a stationary (extreme) value of the functional π.

For the case of elasticity, it is clear from Equation (3-17) that the functional π reduces to the potential energy and that Theorem I is the minimum potential energy theorem. In the same sense that Equation (3-18)

is the analogue to the minimum potential energy theorem, a functional π^* can be developed to be analogous to the complementary energy theorem. This functional is

$$\pi^* = \int_V \frac{C_{ijk\ell}}{2} \dot{\sigma}_{ij} \dot{\sigma}_{k\ell} \, dV - \int_{S_u} \dot{T}_i^n \dot{u}_i \, dS \qquad (3\text{-}19)$$

Since the volume is fixed and $C_{ijk\ell}$ and $\dot{u}_i$ remain constant at an instant in time, the adjunct to Theorem I is

$$\delta\pi^* = 0$$

Therefore, the second theorem is:

Theorem II.

Of all the stress rate tensor fields $\dot{\sigma}_{ij}$ that satisfy the equations of equilibrium and boundary conditions where traction rates are prescribed, the "actual" one is distinguished by a stationary (extreme) value of the functional π^*.

3.4 Discrete Element Representation

The basis for the displacement solution is the determination of the stationary point associated with the functional in Equation (3-18). Viewing this functional as the summation of contributions from an assemblage of discrete elements, it is clear that the displacement state that minimizes Equation (3-18) corresponds to the equilibrium solution.

By assuming a displacement rate state over each discrete element, the volume integration can be completed with only the coefficients of the assumed displacement state as unknowns. Therefore, the most important phase in the development of the discrete element is the selection of the individual element displacement rate functions. As pointed out by Bogner [30] and Shieh [36], the displacement rate functions must meet several criteria to guarantee that the stationary point of the functional of the assemblage of elements corresponds to the global stationary point for the complete structure. The formulation for the functional indicates the requirements that must be met by a displacement rate function. These requirements are:

1. Satisfy global kinematic admissibility by satisfying boundary conditions and enforcing intraelement continuity of displacement and slope rates.
2. It must have at least as many undetermined parameters as degrees of freedom.
3. The assumed displacement rate shape should be complete in the sense that increasing the number of elements monotonically increases accuracy of results.
4. It must allow for rigid body displacements otherwise element equilibrium could be violated.

As indicated by Bogner [30], Stanton and Schmit [37], and others, the use of displacement rate states written as the sum of two-point Hermite

interpolation polynomials make the satisfaction of kinematic admissibility very convenient. By allowing for two in-plane and one out-of-plane displacement rates, there are 12 constants and 12 degrees of freedom per corner of a rectangular element. Using the two-point bicubic Hermite interpolation polynomials, these degrees of freedom are matched exactly with those of the polynomials. Also, rigid body displacements are accounted for exactly. As Key [38] has shown for the special case of pure bending of a flat plate, the element displacement rates are complete and assure monotonic convergence.

For these reasons, the displacements rate shapes considered here are written as two-point Hermite interpolation polynomials.

When values of $f(x)$ and $df(x)/dx = f'(x)$ are known at two points, then, using Hermite interpolation,

$$f(x) = \sum_{i=1}^{2} [H_{0i}(x)f(x_i) + H_{1i}(x)f'(x_i)] \tag{3-21}$$

The one dimensional cubic Hermite interpolation polynomials $H_{0i}(x)$, $H_{1i}(x)$ may be found in Hildebrand [39]. For an interval $0 \leq x \leq a$, they are

$$\begin{aligned} H_{01}(x) &= 1/a^3\,[2x^3 - 3ax^2 + a^3] \\ H_{11}(x) &= 1/a^2\,[x^3 - 2ax^2 + a^2x] \\ H_{02}(x) &= -\,1/a^3\,[2x^3 - 3ax^2] \\ H_{12}(x) &= 1/a^2\,[x^3 - ax^2] \end{aligned} \tag{3-22}$$

For two-dimensional interpolates, products of two, one-dimensional interpolation formulas are formed to describe the function over the rectangular domain of interest. The undetermined parameters are the values of the function, first derivatives with respect to the arguments, and a cross derivative.

3.5 Rectangular Bending-Membrane Plate Element

For the plate analysis to follow, several assumptions are made in addition to those already mentioned. These are:

1. Geometrically, deflections are small compared to plate dimensions.
2. The plate is thin and a state of plane stress exists, i.e., $\sigma_{zz} = \tau_{xz} = \tau_{yz} = 0$ (see Figure 3-1).
3. Lines orthogonal to the middle surface of the plate before bending, remain so after bending.

Expanding Equation (3-17) for the case of plane stress consistent with assumption 2 yields

$$\pi = \int_0^a \int_0^b \int_{-h/2}^{h/2} \tfrac{1}{2} \{E_{11}\, \dot{\varepsilon}_x^2 + 2E_{12}\, \dot{\varepsilon}_x \dot{\varepsilon}_y + E_{22}\, \dot{\varepsilon}_y^2 + 2E_{13}\, \dot{\varepsilon}_x\, \dot{\gamma}_{xy} + 2E_{23}\, \dot{\gamma}_{xy}\, \dot{\varepsilon}_y + E_{33}\, \dot{\gamma}_{xy}^2\} \, dx\,dy\,dz - \int_S \dot{T}_i^{\eta}\, \delta\dot{u}_i \, dS \tag{3-23}$$

FIGURE 3 - 1
DISCRETE PLATE ELEMENT

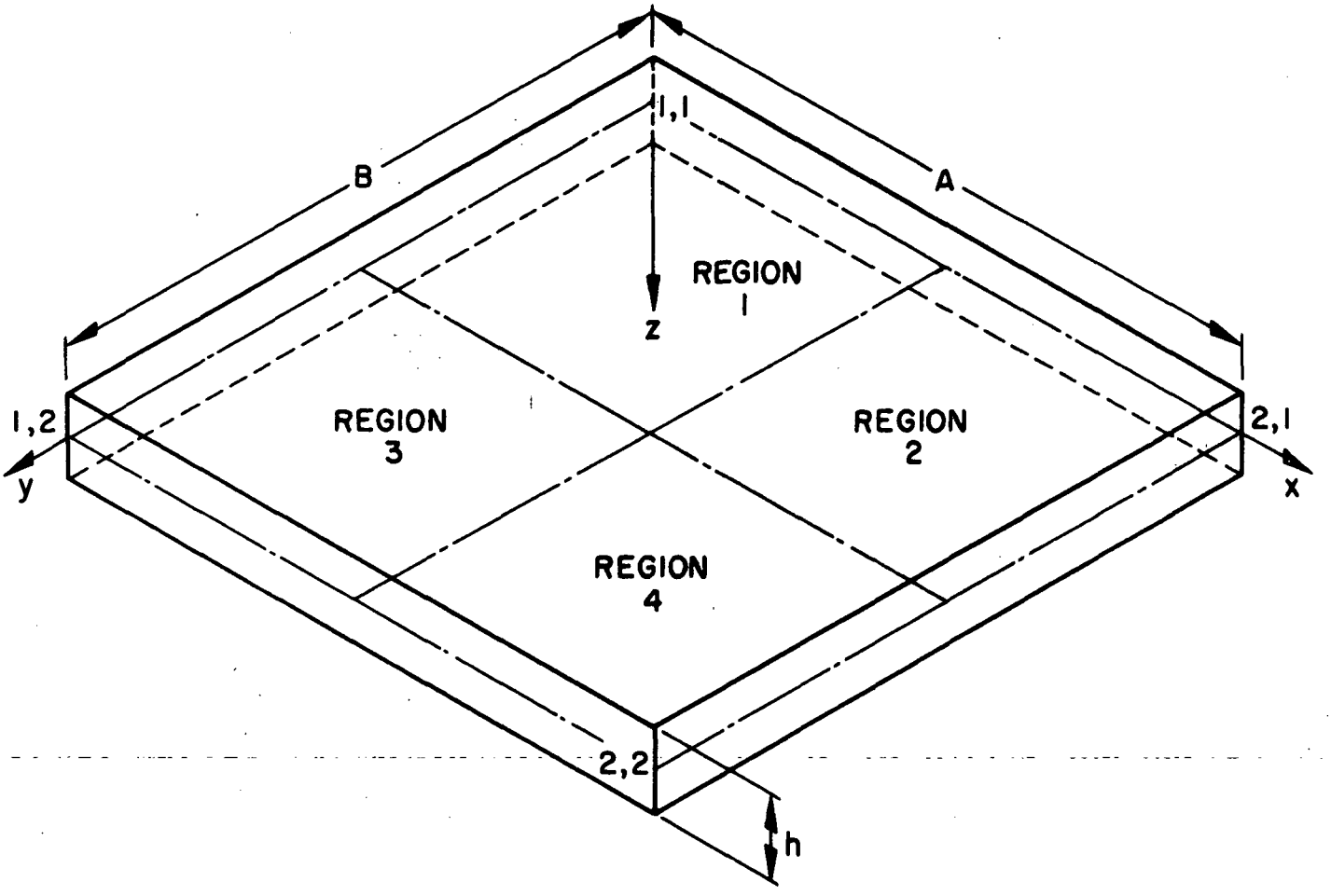

Taking advantage of assumption 3, the strain-rate displacement-rate equations are

$$\dot{\varepsilon}_x = \frac{\partial \dot{u}}{\partial x} - Z \frac{\partial^2 \dot{w}}{\partial x^2}$$

$$\dot{\varepsilon}_y = \frac{\partial \dot{v}}{\partial y} - Z \frac{\partial^2 \dot{w}}{\partial y^2} \qquad (3\text{-}24)$$

$$\dot{\gamma}_{xy} = \frac{\partial \dot{u}}{\partial y} + \frac{\partial \dot{v}}{\partial x} - 2Z\left[\frac{\partial^2 \dot{w}}{\partial x \partial y}\right]$$

Using bicubic Hermite interpolation formulas for the displacement shapes, the displacement rate state for the rectangular element over region $0 \le x \le a$, $0 \le y \le b$ where the unknowns are corner parameters of a typical element is (see Figure 3-1 for numbering scheme of i,j).

$$\dot{u}(x,y) = \dot{u}_{ij} H_{0i}(x) H_{0j}(y) + \frac{\partial \dot{u}_{ij}}{\partial x} H_{1i}(x) H_{0j}(y)$$

$$+ \frac{\partial \dot{u}_{ij}}{\partial y} H_{0i}(x) H_{1j}(y) + \frac{\partial^2 \dot{u}_{ij}}{\partial x \partial y} H_{1i}(x) H_{1j}(y) \qquad (3\text{-}25)$$

This equation can be rewritten in matrix form as

$$\dot{u}(x,y) = \{\dot{u}\}^T \{P(x,y)\} \qquad (3\text{-}26)$$

Complete vectors $\{\dot{u}\}$ and $\{P(x,y)\}$ are given in Appendix B.

Combining (3-23), (3-24), and (3-26) results in

$$\pi^n = \tfrac{1}{2} \begin{Bmatrix} \dot{u} \\ \dot{v} \\ \dot{w} \end{Bmatrix}^T \left[\begin{array}{c|c|c} k^{uu} & k^{uv} & k^{uw} \\ \hline k^{uv} & k^{vv} & k^{vw} \\ \hline k^{uw} & k^{vw} & k^{ww} \end{array}\right] \begin{Bmatrix} \dot{u} \\ \dot{v} \\ \dot{w} \end{Bmatrix} - \begin{Bmatrix} \dot{u} \\ \dot{v} \\ \dot{w} \end{Bmatrix}^T \{\dot{B}^n\} \qquad (3\text{-}27)$$

where $\{\dot{B}^n\}$ is the vector of external forces applied on the nodes of the element, and each of the k^{ij} are 16 x 16 symmetric entries defined by the volume integrals as follows:

$$[k^{uu}] = \int_V \left[E_{11} P_x P_x^T + 2E_{13} P_x P_y^T + E_{33} P_y P_y^T \right] dv$$

$$[k^{uv}] = \int_V \left[2E_{12} P_x P_y^T + 2E_{13} P_x P_x^T + 2E_{23} [P_y P_y^T] + 2E_{33} P_y P_x^T \right] dv$$

$$[k^{uw}] = -\int_V \left[2ZE_{11} P_x P_{xx}^T + 2ZE_{12} P_x P_{yy}^T + 4ZE_{13} P_x P_{xy}^T + 2ZE_{13} P_y P_{xx}^T + 2ZE_{23} P_y P_{yy}^T + 2ZE_{33} P_y P_{xy}^T \right] dv$$

$$[k^{vv}] = \int_V \left[E_{22} P_y P_y^T + 2E_{23} P_x P_y^T + E_{33} P_x P_x^T \right] dv$$

$$[k^{vw}] = -\int_V \left[2ZE_{12} P_y P_{xx}^T + 2ZE_{13} P_x P_{xx}^T + 2ZE_{22} P_y P_{yy}^T + 2ZE_{23} P_x P_{yy}^T + 4ZE_{23} P_y P_{xy}^T + 2ZE_{33} P_x P_{xy}^T \right] dv$$

$$[k^{ww}] = \int_V \Big[E_{11} Z^2 P_{xx} P_{xx}^T + 2E_{12} Z^2 P_{xx} P_{yy}^T + 4E_{13} Z^2 P_{xx} P_{xy}^T + E_{22} Z^2 P_{yy} P_{yy}^T + 4E_{23} Z^2 P_{yy} P_{xy}^T + 4Z^2 E_{33} P_{xy} P_{xy}^T \Big] dV$$

In these expressions the P's are the Hermite polynomial vectors listed in Appendix B. The subscripts on P indicate differentiation with respect to particular variables.

Since the material properties E_{ij} are in general functions of both the stress state and spatial coordinates, special consideration of them is due before the volume integration can be performed. To accomplish the x-y integration, the element is broken up into four subregions. Values of

$$\bar{E}_{ij}^k(x,y) = \int_{-h/2}^{h/2} E_{ij}(x,y)dZ$$

$$C_{ij}^k(x,y) = \int_{-h/2}^{h/2} ZE_{ij}(x,y)dZ \qquad (3\text{-}29)$$

$$D_{ij}^k(z,y) = \int_{-h/2}^{h/2} Z^2 E_{ij}(x,y)dZ$$

$k \equiv$ region number as per Figure 3-1

are subject to bilinear Hermite interpolation within each subregion where the values of the four adjacent corners are the unknown parameters. This permits closed form integration in the x-y plane with numerical evaluation of $\overline{E}_{ij}$, C_{ij}, D_{ij} required only at the nine connecting nodes of the four subregions. This numerical integration in the thickness direction is accomplished using the Lobotav quadrature with nine thickness points. For the elastic case, $k^{uw} = k^{vw} = [0]$.

Equation (3-27) represents the contribution to π for the n^{th} element. The total value of the functional π is the sum of π^n over all the elements or

$$\pi = \sum_{i=1}^{NEL} \pi^n \quad \text{where NEL = number of elements} \tag{3-30}$$

The equilibrium position for the plate is the stationary value of the functional π.

3.6 Minimization Algorithm

The total value of the functional π is obtained by summing over all elements their respective contributions to π as indicated in Equation (3-27). By calling the element degress of freedom $\{Y\}$ and element stiffness matrices $[K^n]$, Equations (3-27) and (3-30) can be rewritten as

$$\pi^n = \tfrac{1}{2} \{Y^n\}^T [K] \{Y^n\} - \{Y^n\}^T \{B^n\} \tag{3-31}$$

Defining a transformation of the element degrees of freedom $\{Y^n\}$ to the system degrees of freedom $\{X\}$ such that

$$\{Y^n\} = [\alpha^n]\{X\} \tag{3-32}$$

it is possible to write Equation (3-30) in the form

$$\pi = \sum_{n=1}^{NEL} \pi^n = \tfrac{1}{2}\{X\}^T[A]\{X\} - \{X\}^T\{F\} \tag{3-33}$$

where

$$[A] = \sum_{n=1}^{NEL} [\alpha^n]^T[K^n][\alpha^n]$$

and

$$\{F\} = \sum_{n=1}^{NEL} [\alpha^n]^T\{B^n\}$$

Since [A] is a positive definite symmetric matrix, the stationary point of the quadratic functional in (3-33) is a minimum. It is now possible to cast the equilibrium problem in terms of a mathematical programming problem, i.e.,

$$\begin{aligned} &\text{Minimize:} \quad \pi(x) = \tfrac{1}{2}\{X\}^T[A]\{X\} - \{X\}^T\{F\} \\ &\text{Subject:} \quad \text{No constraints.} \end{aligned} \tag{3-34}$$

In this representation, {X} is the state variable vector of dimension N (number of system degrees of freedom), [A] is a positive definite N x N matrix, and {F} is the N-dimensional work equivalent force vector.

There are many techniques for minimizing Equation (3-34). Essentially, they fall into two categories: direct search methods and gradient methods. Most success in structural mechanics problems has been through the use of gradient techniques [30], [35], [37], [40]. Although Gisvold and Moe [40] applied Powell's (see [42]) method of direct search in solving buckling problems with satisfactory results, it has been pointed out by both Box [42] and Beveridge and Schechter [41] that gradient methods rather than direct search methods are best suited for unconstrained minimum problems. This is especially true when an analytic form of the gradient of the objective function can be determined. It is for these reasons that a modified version of the conjugate gradient method as outlined in Beckman's paper [34] is used in this work.

All gradient techniques locate the solution {H} to the minimization problem as the limit of a sequence $\{X_0\}$, $\{X_1\}$, $\{X_2\}$,..., where $\{X_0\}$ is an initial approximation to {H}. (Note that subscripts refer to particular vectors and not their components.) The movement from one approximation $\{X_i\}$ to the next approximation $\{X_{i+1}\}$ proceeds along some specified direction $\{p_i\}$ a distance α_i. That is

$$\{X_{i+1}\} = \{X_i\} + \alpha_i\{p_i\} \tag{3-35}$$

The techniques of determining α_i and $\{p_i\}$ comprise the primary differences between the various methods. By constructing the $\{p_i\}$ to be linearly independent, one forms a basis for the solution space $\{H\}$ and hence, in linear problems, convergence to the solution in N steps is guaranteed. Beckman [34] constructs the $\{p_i\}$'s by a Gram-Schmidt orthogonalization process using the gradient of π evaluated at the $\{X_i\}$'s. Hence the name, conjugate gradient. The distance of travel α_i is determined by minimizing $\pi(X_{i+1})$ with respect to α_i. This gives the maximum distance of travel along any direction vector.

It should be noted that in this method as in the conjugate gradient methods used by Stanton and Schmit [37], Bogner [35], Bogner, et al. [30], and Fox and Stanton [33], the initial direction vector is in the direction of steepest descents. A common characteristic of this starting direction is that the number of iterations to convergence for a particular problem is independent of the initial guess $\{X_o\}$ and hence $\{p_o\}$. This behavior was found by Beckman [34] and Stanton and Schmit [37]. Although this characteristic may be an advantage in many instances, for incremental elasto-plastic problems, a distinct advantage could be gained by making use of the solution at the previous load step as a starting point for the present load step.

The following method is based on Beckman's method but instead of starting in steepest descent direction, an arbitrary initial direction is used. Constructing the solution vector sequentially as

$$\{H\} = \{X_o\} + \alpha_o\{p_o\} + \alpha_1\{p_1\} + \alpha_2\{p_2\} + \ldots + \alpha_{N-1}\{p_{N-1}\}$$

it is possible to size α_i such that the distance α_i in the direction $\{p_i\}$ minimizes the objective function π. This is if

$$\{X_{i+1}\} = \{X_i\} + \alpha_i\{p_i\}$$

Then α_i is such that

$$\frac{d\pi(X_{i+1})}{d\alpha_i} = 0$$

Carrying out this operation gives

$$\alpha_i = \frac{\{p_i\}^T\{R_i\}}{\{p_i\}^T[A]\{p_i\}}$$

where the residual vector $\{R_i\}$ is defined as

$$\{R_i\} = \{F\} - [A]\{X_i\}$$

It is now necessary to pick a new direction vector. This vector is determined by an [A] - orthogonalization of $\{p_0\}$, $\{R_1\}$, $\{R_2\}$, ..., $\{R_{N-1}\}$ using a Gram-Schmidt process. This results in a set of linearly independent vectors spanning the N-space describing the solution vector of Equation (3-34).

The algorithm described above may be summarized as follows:

1. $\{X_0\}$ = An arbitrary initial guess to $\{H\}$.

   $\{R_0\} = \{B\} - [A]\{X_0\}$

   $\{p_0\}$ = an arbitrary initial guess to the direction from $\{X_0\}$ to $\{X_1\}$, or $\{R_0\}$.

2. $$\alpha_i = \frac{\{p_i\}^T\{R_i\}}{\{p_i\}^T[A]\{p_i\}}$$

   $$\{X_{i+1}\} = \{X_i\} + \alpha_i\{p_i\}$$

3. $$\{R_{i+1}\} = \{F\} - [A]\{X_{i+1}\}$$

   or

   $$\{R_{i+1}\} = \{R_i\} - \alpha_i[A]\{p_i\}$$

4. $$\beta_i = -\frac{\{R_{i+1}\}^T[A]\{p_i\}}{\{p_i\}^T[A]\{p_i\}}$$

5. $$\{p_{i+1}\} = \{R_{i+1}\} + \beta_i\{p_i\}$$

Steps 2 thru 5 are now repeated until the solution to the desired accuracy is obtained. This takes at most N-steps for linear problems.

The choosing of the initial guess $\{X_0\}$ and direction $\{p_0\}$ is very critical in this routine. However, for linear problems, choosing $\{X_0\}$ to be $\{0\}$ and $\{p_0\}$ to be proportional to the solution, results in the exact solution in only one iteration. This is easily seen as α_0 then simply scales $\{p_0\}$ to the correct magnitude. For elasto-plastic analysis, this is very helpful for it has been found that from one load step to the next, the displacement states are roughly proportional. Hence, using the old solution for both $\{X_0\}$ and $\{p_0\}$ should provide very rapid convergence behavior. For elastic problems, approximate solutions are often available that may be used as $\{X_0\}$ and $\{p_0\}$. If not, $\{p_0\}$ may either remain arbitrary or determined by steepest descents with convergence still guaranteed in at most N-iterations.

In the course of their work using the conjugate gradient method for geometric non-linear structural problems, Fox and Stanton [33] uncovered a strong scaling effect significant in the convergence of their problems. Essentially, the difficulty stemmed from large variation in diagonal terms of the [A] matrix. They found that by making all diagonal terms equal (say 1.) and the sum of off-diagonal terms as small as possible, convergence of the conjugate gradient algorithm was greatly increased. This behavior was suggested by Gerschgorin's disk theorem. Geometrically, this scaling transforms the N-dimensional hyperellipsoid described by $\pi(X)$ = constant into a more hyperspheroidal shape. The scaling transformation is accomplished by premultiplying the state vector $\{X\}$ by a diagonal matrix whose diagonal entries are $d_{ii} = 1./\sqrt{A_{ii}}$.

Convergence may be determined by one or both of two methods. Either the magnitude of the residual vector may be forced to be very small or convergence to a certain digit accuracy of the objective function may be required. In practice, both methods can work well. The minimum residual vector criteria seems to be more restrictive, however, its value does not necessarily decrease monotonically from iteration to iteration. On the other hand, the objective function does converge monotonically to the minimum value and is thus attractive as a convergence criteria.

It should be pointed out that linear constraint equations of the form

$$[C]\{X\} + \{D\} = 0 \tag{3-41}$$

can be introduced into Equation (3-34) through the use of Lagrange multiplier concepts. For the linear constraint equations of Equation (3-41), Equation (3-34) can be written as

$$\pi = \tfrac{1}{2}\{X\}^T[A]\{X\} - \{X\}^T\{B\} - \{\lambda\}^T[C]\{X\} - \{\lambda\}^T\{D\}. \tag{3-42}$$

or

$$\pi = \tfrac{1}{2}\{\underset{\sim}{X}\}^T[\underset{\sim}{A}]\{\underset{\sim}{X}\} - \{\underset{\sim}{X}\}^T\{\underset{\sim}{B}\} \tag{3-43}$$

where

$$\{\underset{\sim}{X}\} = \begin{Bmatrix} X \\ \hline \lambda \end{Bmatrix} \quad [\underset{\sim}{A}] = \begin{bmatrix} A & -C^T \\ \hline -C & 0 \end{bmatrix} \quad \{\underset{\sim}{B}\} = \begin{Bmatrix} B \\ \hline D \end{Bmatrix}$$

For m linear constraint equations, [C] is a nxm connection matrix, $\{\lambda\}$ is an m dimensional Lagrange multiplier vector, and {D} is an m dimensional constraint vector where n is the dimension of the original {x} vector. With zeroes along the main diagonal, $[\underset{\sim}{A}]$ is no longer positive definite. However, $[\underset{\sim}{A}]^T[\underset{\sim}{A}]$ is positive definite and a new conjugate gradient method for this case can be derived (see Beckman [34]) following the same reasoning as above.

3.7 Numerical Implementation

The procedures outlined in the previous sections were assembled into a computer program called PLATER [47]. An outline of the program organization is shown in Figure 3-2. As input to the program, material properties, element geometry, and intraelement communication data are required. Boundary conditions and constraint equations are necessary on an incremental basis. The material properties include elastic constants and discrete point values of octahedral stress vs. octahedral plastic strain. Figure 3-3 shows the PLATER element along with nodal load and displacement sign conventions.

From an operational standpoint, the program evaluates the constitutive relations of Equation (3-7) for each element at the beginning of each load step. The properties are then considered constant over the subsequent

FIGURE 3-2

PLATER Program Flow Diagram

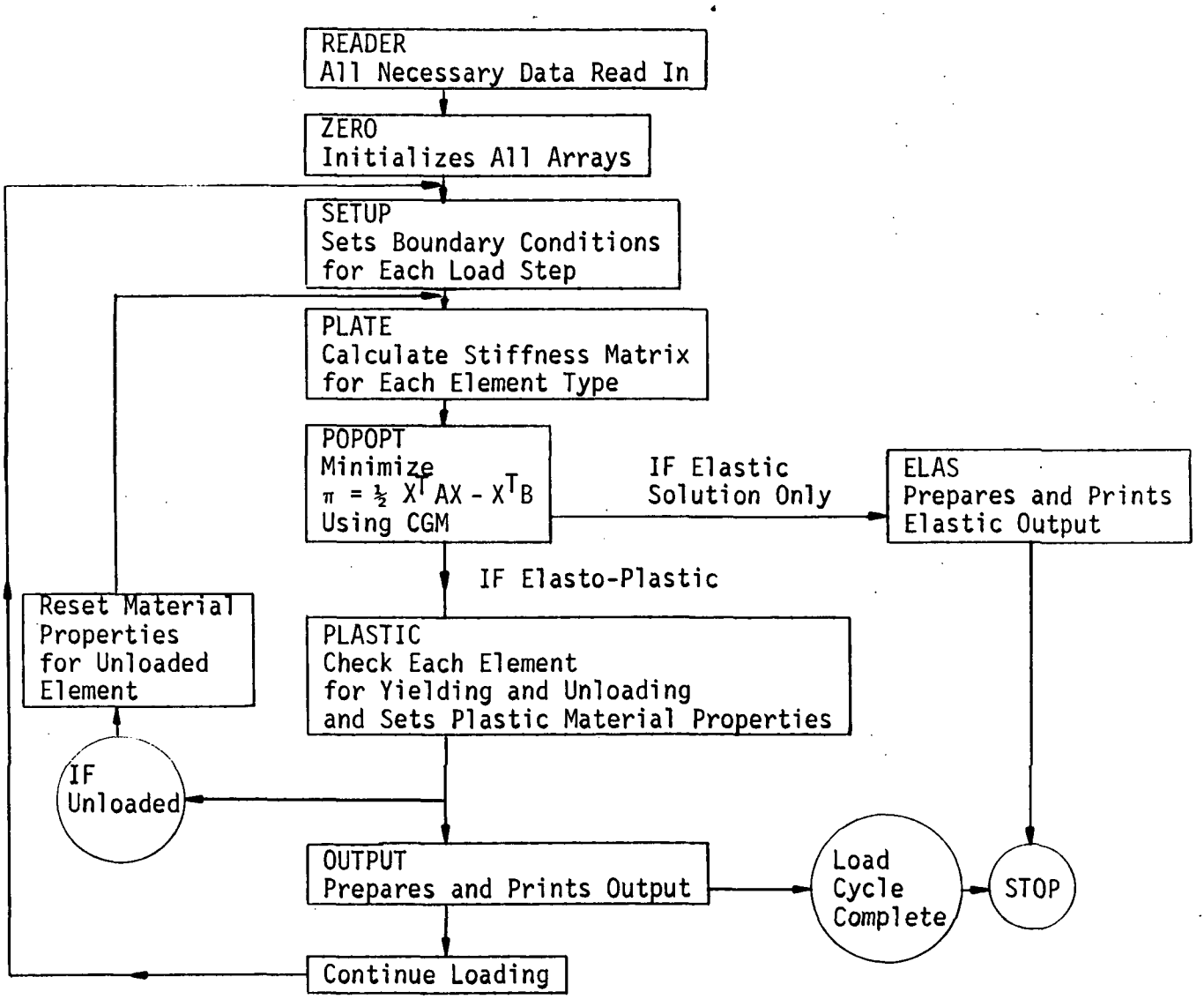

FIGURE 3-3
PLATER NODAL LOADS AND DISPLACEMENT
SIGN CONVENTION

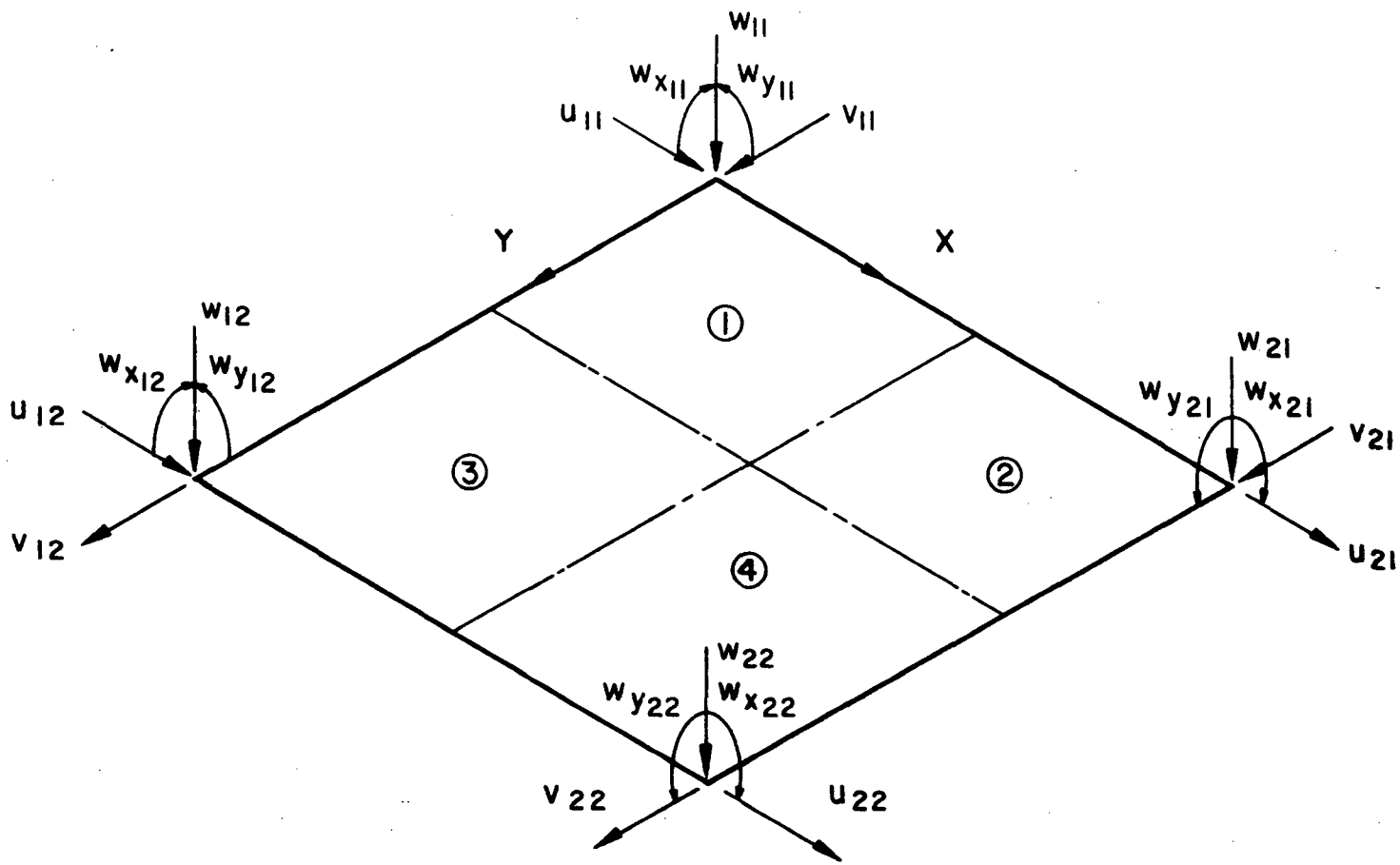

NOTE:
POSITIVE NODAL LOADS ARE
IN THE SAME DIRECTION AS THE
CORRESPONDING DISPLACEMENT

loading increment. Elastic unloading is systematically accounted for in the procedure. Isotropic hardening is assumed for subsequent yielding.

The program was verified by comparing available closed form solutions with numerical results from PLATER. A variety of boundary conditions were used for bending, extensional, and combined bending/extension problems. Table 3-1 lists the verification problems and gives some results for stresses and displacements. An indication of the discretization error is given in Table 3-1 by comparing the results as the number of elements is increased. Obviously, certain types of problems require higher degrees of discretization than others. For example, resolution of stress results under point loads is poor until the number of elements in the vicinity of the load gets large. However, as Table 3-1 indicates, as the number of elements in a given area was increased, the results (displacements and stresses) converged monotonically toward the correct answer.

The convergence properties of the conjugate gradient method (CGM) were also investigated extensively. Particular attention was paid both to ill-conditioned master stiffness matrices and to the effects of initial guess values of both $\{x_o\}$ and $\{p_o\}$. In this context, ill-conditioned matrices imply those which have large weighting of off diagonal terms. Ill-conditioned matrices were examined since it was expected that zeroes would appear on the main diagonal and that there would be large weighting of off diagonal terms due to extension/bending stiffness representations.

TABLE 3-1

Verification Solutions for PLATER

ELASTIC PROBLEMS

Bending Results							
Number of Elements	Circular Bending Square Plate		Simply Supported Square Plate				Clamped Square Plate
			Center Load		Uniform Load		Center Load
	$w\rfloor_{max}$	$M_x\rfloor_{max}$	$w\rfloor_{max}$	$M_x\rfloor_{max}$	$w\rfloor_{max}$	$M_x\rfloor_{max}$	$w\rfloor_{max}$
	$\frac{M_o a^2}{D(1+\nu)}$	M_o	$\frac{Pa^2}{D}10^3$	$\frac{10^2}{Pa^2}$	$\frac{qa^2}{D}10^3$	$\frac{10^2}{qa^2}$	$\frac{Pa^2}{D}10^3$
1	1.0	1.0	11.11	---	---	---	5.32
2	1.0	1.0	11.25	---	3.45	4.98	5.37
4	1.0	1.0	11.45	1.65	4.00	4.80	5.47
8	1.0	1.0	11.59	1.88	4.03	4.79	5.54
EXACT* Solution	1.0	1.0	11.60	1.88	4.06	4.78	5.60

Number of Elements	Extension/Bending Results				
	Circular Bending Plus Uniform Compression				
	$v\rfloor_{max}$	$u\rfloor_{max}$	$w\rfloor_{max}$	$\sigma_y\rfloor_{MEMBRANE}$	$\sigma_y\rfloor_{BENDING}$
1	$+.12 \times 10^{-2}$	$-.36 \times 10^{-3}$	.0605	1000.	3000.
EXACT	$+.12 \times 10^{-2}$	$-.36 \times 10^{-3}$	.0605	1000.	3000.

* NAVIER Solution, see Ref. [43].

TABLE 3-1 (con't)

Verification Solutions for PLATER

ELASTO-PLASTIC PROBLEMS

Bilinear Stress-Strain Curve; $E^{(E)} = 10 \times 10^6$, $E^{(P)} = 40 \times 10^4$					
Circular Bending			Applied Twisting Edge Moment		
	PLATER	EXACT		PLATER	EXACT
M_o^{yield}	5490	5490	M_o^{yield}	3130	3130
w_{max}^{yield}	1.82	1.82	w_{max}^{yield}	1.95	1.95
The Following Data is for $M_o = 8125 \frac{\text{IN-LBS}}{\text{IN}}$			The Following Data is for Edge Twisting Moment of $M_{xy}^o = 4630 \frac{\text{IN-LBS}}{\text{IN}}$		
$w\rfloor_{max}$	4.85	4.85	$w\rfloor_{max}$	5.55	5.55
z/h	Normal Stress Distribution		z/h	Shear Stress Distribution	
0.5	37500	38500	0.5	20100	20300
0.4	36000	37000	0.4	19600	19800
0.3	34500	35500	0.3	19000	19200
0.2	32700	33700	0.2	18300	18500
0.1	17500	18500	0.1	10500	10750
0.0	0	0	0.0	0	0

Results of these studies indicate the following:

1. Convergence of the CGM is strongly influenced by ill-conditioning of the [A] matrix. This can be somewhat alleviated by the scaling transformation suggested by Fox and Stanton [3 3].
2. The initial solution guess vector $\{X_0\}$ has very little effect on the convergence properties.
3. The selection of the initial search direction vector $\{p_0\}$ has a strong influence on convergence. However, the selection of $\{p_0\}$ for a multidimensional problem is very difficult and the steepest descents direction (used in standard CGM formulations) is better than a bad guess for $\{p_0\}$. Much advantage can be obtained where good approximate $\{p_0\}$ vectors can be found from previous solutions. In particular, incremental plasticity solutions can take direct advantage of this property by constructing $\{p_0\}$ from one load increment to the next.
4. CGM convergence properties can be greatly influenced by judicious choice in orientation and numbering of both system degrees of freedom and element descriptions. The more uniform the element map, the better the convergence. No attempt to optimize a particular element map was made. Non-uniformity of the element map has a much greater effect on the convergence properties than having elements with large aspect ratios involved.

CHAPTER IV

STATIONARY THROUGH CRACK IN A PLATE SUBJECT TO CIRCULAR BENDING

The elasto-plastic plate bending capability, PLATER, is now applied to the study of the through cracked plate. The plate is to be of sufficient dimension as to model an infinite plate where the crack length is large compared to the plate thickness. The plate width and length to crack length ratios are to be large enough so that the plate exterior boundaries do not interfere with the crack behavior. Essentially, two problems are to be analyzed. The first one neglects the effects of crack closure and the second includes these effects. Comparison of the two solutions permits elimination of any systemic errors resulting from the numerical procedures and isolates the closure phenomena. Geometrically, both problems are dimensioned as show in Figure 4-1. The boundary conditions for the two problems are identified in this chapter.

The exterior dimensions are set so that the finite plate models as closely as possible an infinite plate. No corrections for finite plate effects are made. Also, no corrections are made for crack face warping. Although crack face warping may be expected physically, the Kirchhoff assumption of planes remaining plane preclude the realization of the warping effect. However, as indicated by Smith and Smith [13], at crack length to plate thickness ratios greater than four, three dimensional effects become less important compared to crack closure effects. As shown in Figure 4-1, the plate under consideration does have $2a/h = 4.0$.

FIGURE 4-1
CRACKED PLATE GEOMETRY

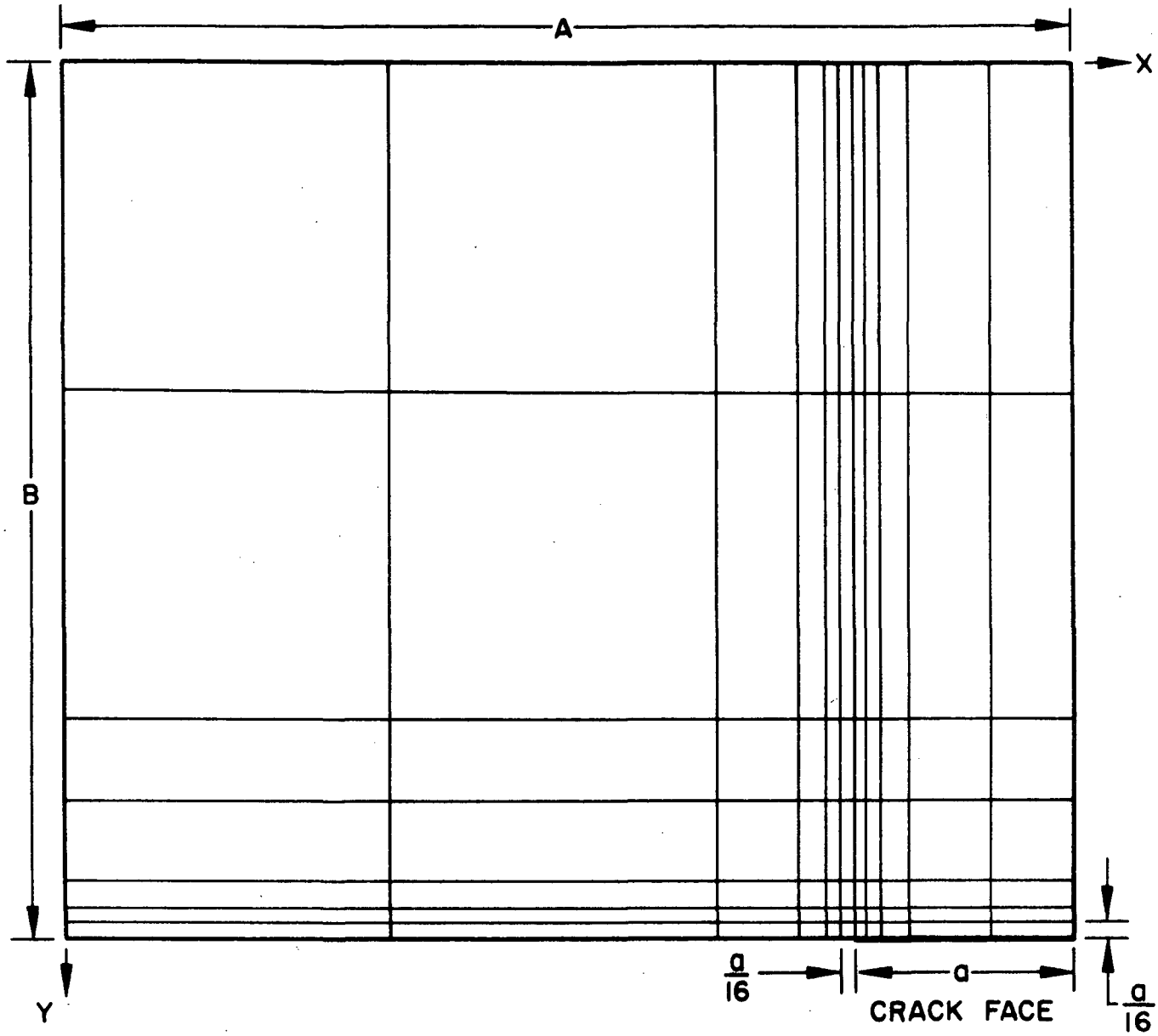

$\frac{A}{a}$ = 4.125

$\frac{B}{a}$ = 4.000

$\frac{2a}{h}$ = 4.000

77 ELEMENTS

96 NODES

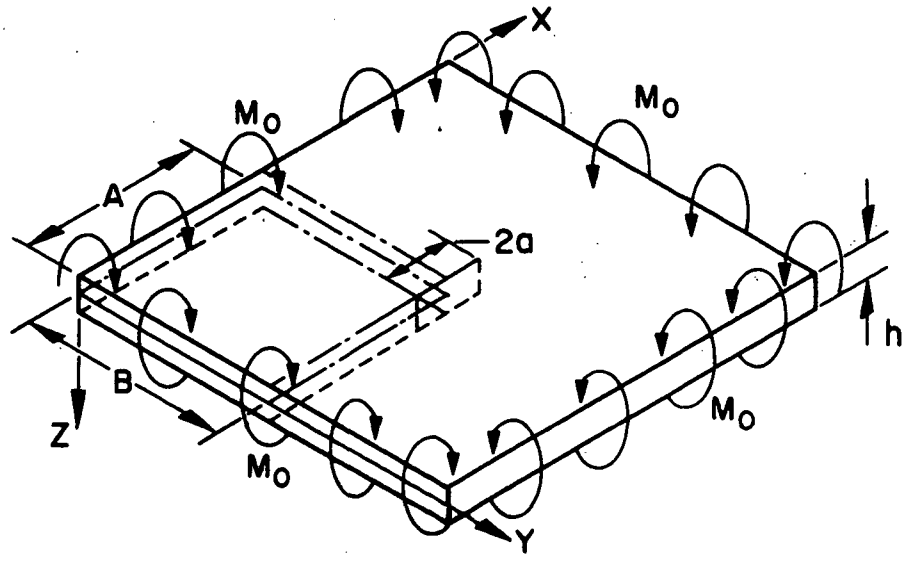

The material properties are listed in Figure 4-2. The work hardening material chosen is felt to be rather typical of many common materials. The Ramsberg-Osgood power law is cited only for convenient comparison to other published results [6] as the PLATER program uses discrete points on the τ_{oct} vs. $\gamma_{oct}^{(p)}$ curve. This curve is shown in Figure 4-2.

4.1 Boundary Conditions Without Closure

The boundary conditions for the first problem neglecting the crack closure behavior are identical with the ones used by Williams [16], i.e., the crack face is modeled as a free surface while the exterior plate boundaries are subjected to constant applied normal moment.

The free surface boundary conditions in Kirchhoff plate theory are obtained by coalescing three conditions (i.e., normal moment, twisting moment, and average shear force equal to zero) into two conditions admissible by fourth order differential theory [43]. These conditions along a line parallel to the y axis are

$$(M_x)_{x=a} = 0$$

$$V_x = \left(Q_x - \frac{\partial M_{xy}}{\partial y}\right)_{x=a} = 0 \qquad (4\text{-}1)$$

Also, reaction forces at the crack tip and plate corners warrent particular attention in Kirchhoff theory. As shown in Appendix D, no additional contributions to the boundary conditions are required for this analysis.

FIGURE 4-2
MATERIAL PROPERTIES

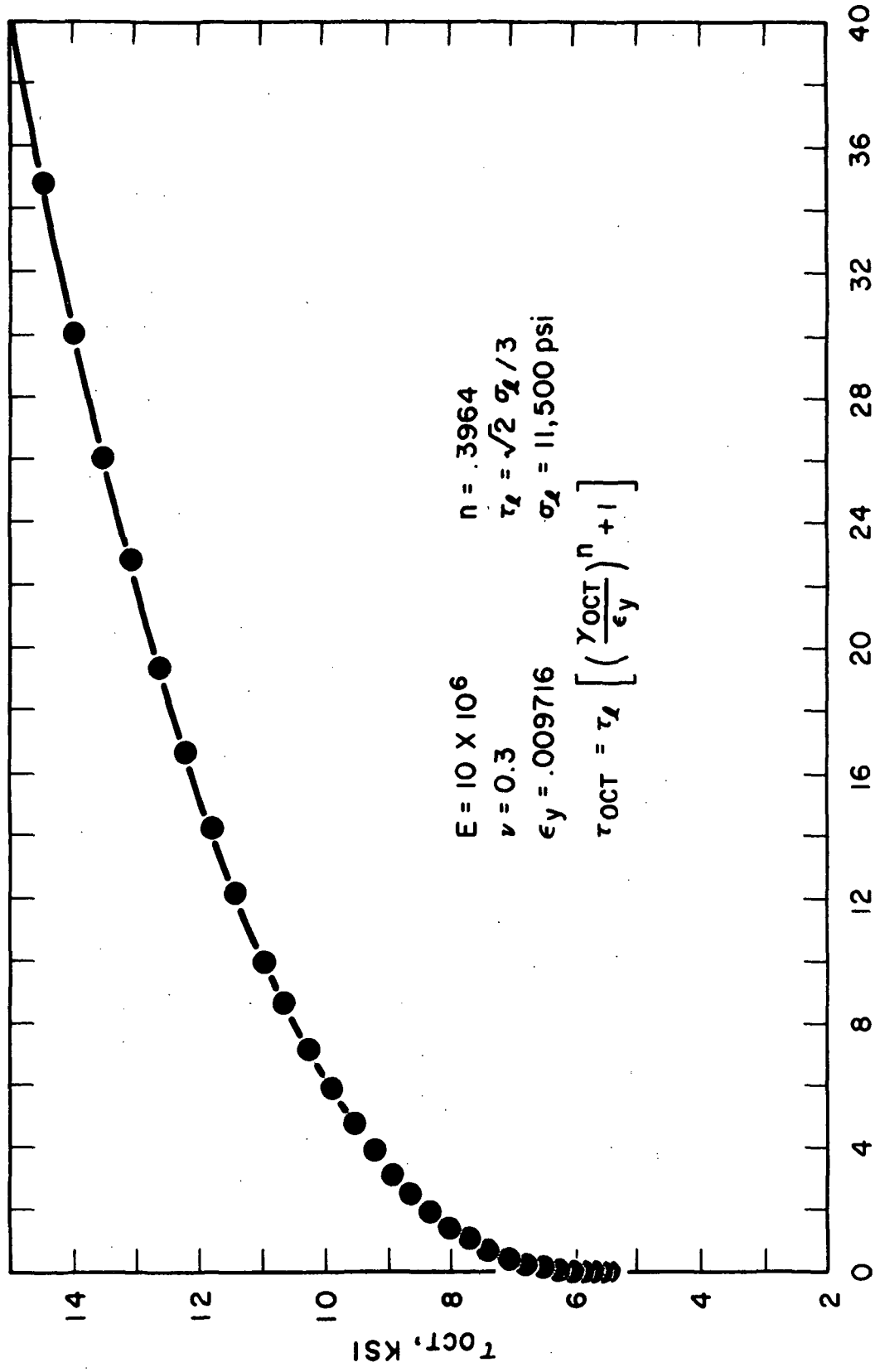

The complete boundary conditions for the plate with no closure considerations are as follows:

Along Y axis,

$X = 0, Y = Y$	$N_x = 0$	$M_x = M_o$
	$N_{xy} = 0$	$V_x = 0$

Along X axis,

$X = X, Y = 0$	$N_y = 0$	$M_y = M_o$
	$N_{xy} = 0$	$V_y = 0$

Along line $X = A$,

$X = A, Y = Y$	$u = 0$	$u - z \frac{\partial w}{\partial x} = 0$
	$\tau_{xy} = 0$	$\frac{\partial u}{\partial y} + \frac{\partial v}{\partial x} - 2z \frac{\partial w}{\partial x \partial y} = 0$

Along line $Y = B$

$0 \leq X \leq A-a, Y = B$	$v = 0$	$v - z \frac{\partial w}{\partial y} = 0$
	$\tau_{xy} = 0$	$\frac{\partial u}{\partial y} + \frac{\partial v}{\partial x} - 2z \frac{\partial w}{\partial x \partial y} = 0$

Along crack face,

$A-a < X \leq A, Y = B$	$N_y = 0$	$M_y = 0$
	$N_{xy} = 0$	$V_y = 0$

At $X = A, Y = B$ $\quad w = 0$

The applied moment, M_o, is applied incrementally by scaling the first elastic load so that the most sensitive element is brought to the proportional limit. The next three load steps are at 5% of this initial yield load. The remaining load steps are applied at 10% the initial yield load. Table 4-1 lists the load increment and accumulated load level for the no closure problem.

4.2 Boundary Conditions With Closure Effects

The problem described in the above section is to be reanalyzed including the effects of the crack face interference as the crack face rotates due to applied moments. Clearly, the only boundary conditions to change are those along the crack face. For this problem, the crack is no longer traction free but subject to a normal compressive load due to the crack face interaction which prevents material overlap as the plate is bent. Since the PLATER program is quasi-three dimensional (the through thickness behavior being assumed in the Kirchhoff sense) the wedging effects of the compressive surface must be modeled in terms of mid-surface quantities. The constraint of the crack face on the compressive surface can be obtained from the Kirchhoff displacement relations of Equation (3-24). Referring to Figure 4-3, the displacement in the Y-direction (v) of the compressive contact edge (Z = - h/2) is required to be zero. The Kirchhoff displacement relation is

$$v(x,y) = v_S(x,y) - Z \frac{\partial w(x,y)}{\partial y} \qquad (4\text{-}3)$$

TABLE 4-1

Incremental Load Steps and Accumulated Values for the No Closure Problem

Load Step	Applied Edge Moment $\left[\frac{\text{IN-LBS}}{\text{IN}}\right]$	Accumulated Value $\left[\frac{\text{IN-LBS}}{\text{IN}}\right]$
1	266.7	266.7
2	13.3	280.0
3	13.3	293.3
4	26.67	320.0
5	26.67	346.7
6	26.67	373.4
7	26.67	400.0
8	26.67	426.7
9	26.67	463.3
10	26.67	490.0
11	26.67	526.7
12	26.67	553.3
13	26.67	580.0
14	26.67	606.7
15	26.67	633.3
16	26.67	660.0
17	26.67	686.7
18	26.67	713.3
19	26.67	740.0
20	26.67	766.7
21	26.67	793.3
22	26.67	820.0
23	26.67	846.6
24	26.67	873.3
25	26.67	900.0

FIGURE 4-3
BOUNDARY CONDITIONS FOR THE CLOSURE PROBLEM

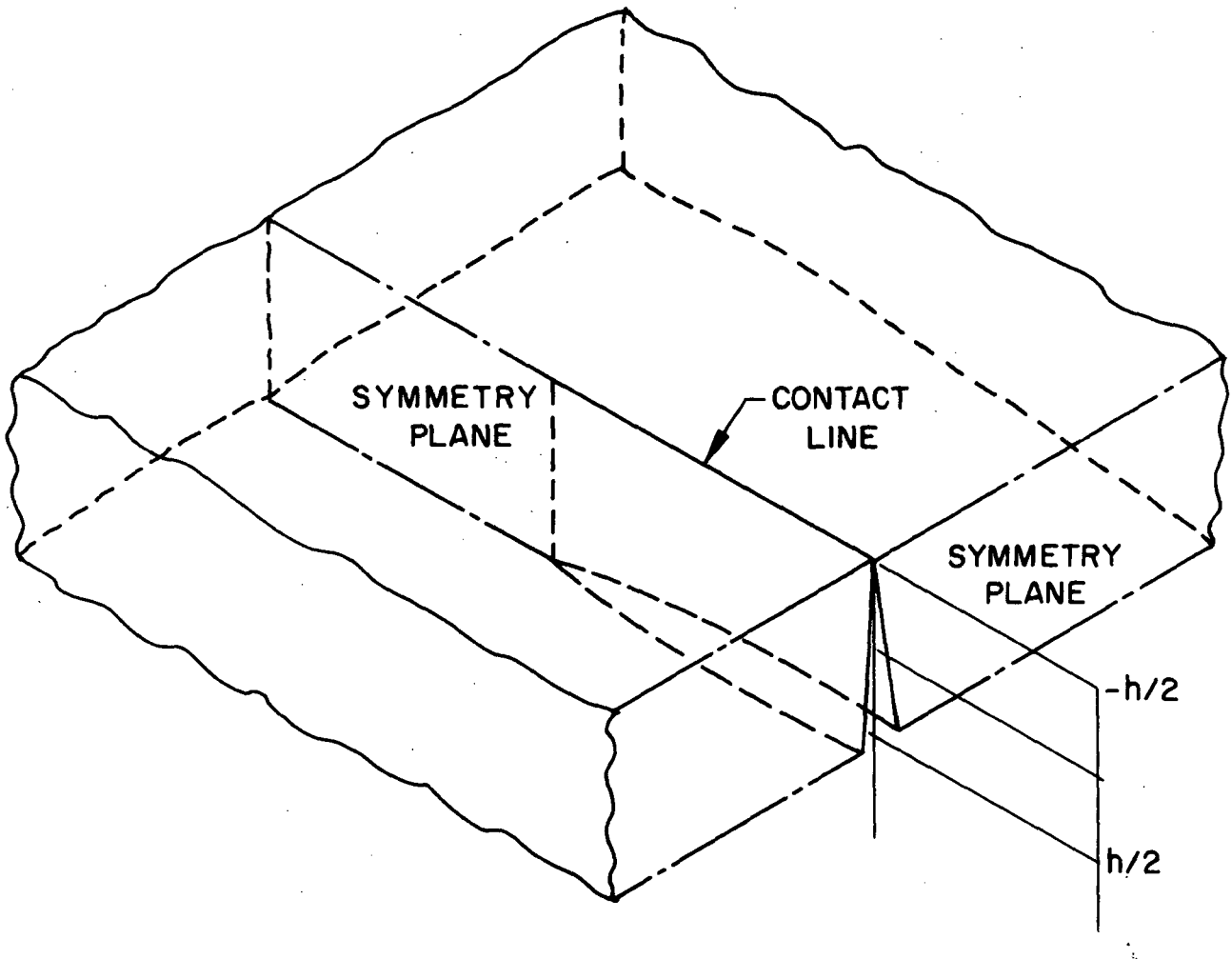

Along the crack face,

$$v(x,B) = 0 = v_S(x,B) + \frac{h}{2}\frac{\partial w}{\partial y}(x,B) \qquad (4\text{-}4)$$

Therefore the constraint equations are

$$\{V_S\} + \frac{h}{2}\left\{\frac{\partial w}{\partial y}\right\} = 0 \qquad (4\text{-}5)$$

When these constraint equations are used in PLATER, the in-plane extension and transverse bending behavior are coupled. The constraint equations are introduced into PLATER through the use of Lagrange multiplier concepts. The resulting Lagrange multipliers are given the interpretation of in-plane loads and transverse moments. Although the mid-surface line along the crack face is actually free, these Lagrange multiplier couples give rise to pseudo-stresses in the results. Physically, this result is very realistic with the neutral surface shifting reflecting the wedging effect of the crack face.

Loading was incremental for this problem as it was for the no closure problem. Table 4-2 lists the load increments and accumulated values for the closure problem.

TABLE 4-2

Incremental Load Steps and Accumulated Load Values for the Closure Problem

Load Step	Applied Edge Moment $\left[\frac{\text{IN-LBS}}{\text{IN}}\right]$	Accumulated Value $\left[\frac{\text{IN-LBS}}{\text{IN}}\right]$
1	370.	370.
2	18.5	389.
3	18.5	407.
4	37	444.
5	37	481.
6	37	518.
7	37	555.
8	37	592.
9	37	629.
10	37	666.
11	37	703.
12	37	740.
13	37	777.
14	37	814.
15	37	851.
16	37	888.
17	37	925.
18	37	962.
19	37	999.
20	37	1036.
21	37	1073.
22	37	1110.
23	37	1147.
24	37	1184.
25	37	1221.

4.3 Discretization of the Crack Problems

Geometrically, both problems have 77 elements and 96 nodes with the elements in the vicinity of the crack tip being (a/16) square. For the no closure problem where bending variables only are considered, there are 353 system degrees of freedom. For the closure problem, both bending and extensional modes of deformation are excited which results in 1046 degrees of freedom plus 9 constraint equations.

CHAPTER V

NUMERICAL RESULTS

The numerical data extracted from the PLATER analysis of the centrally cracked plate bending problems are put into graphical form for ease in distinguishing the effects of crack closure and material yielding. The detailed elastic results reported are from the first load increment of the elasto-plastic incremental solutions normalized to a common load level. The elastic results for the no closure case allow not only for direct comparison with the closure case but for detailed verification of the finite element solution with the analytic solutions of Williams [19], Equation (2-2).

5.1 Elastic Displacement Data

The deformed shapes of the elastic plate with and without closure effects are shown in Figure (5-1). These figures clearly indicate that the kinematic boundary conditions on the plate were met. Of particular interest is that the in-plane displacement normal to the crack face along the compressive surface of the plate was essentially zero (on the order of 10^{-13} in.). Also of importance is that the crack face remains flat, consistent with Kirchhoff plate theory.

Figures (5-2) are contour plots of the transverse displacement, w. These plots have been normalized to the quantity $M_o/2D(1+\nu)$ which is the coefficient of the (x^2+y^2) solution to the circular bending problem of a plate without a crack. These contours are circles whose radius is the

FIGURE 5-1
ELASTICALLY DEFORMED PLATE

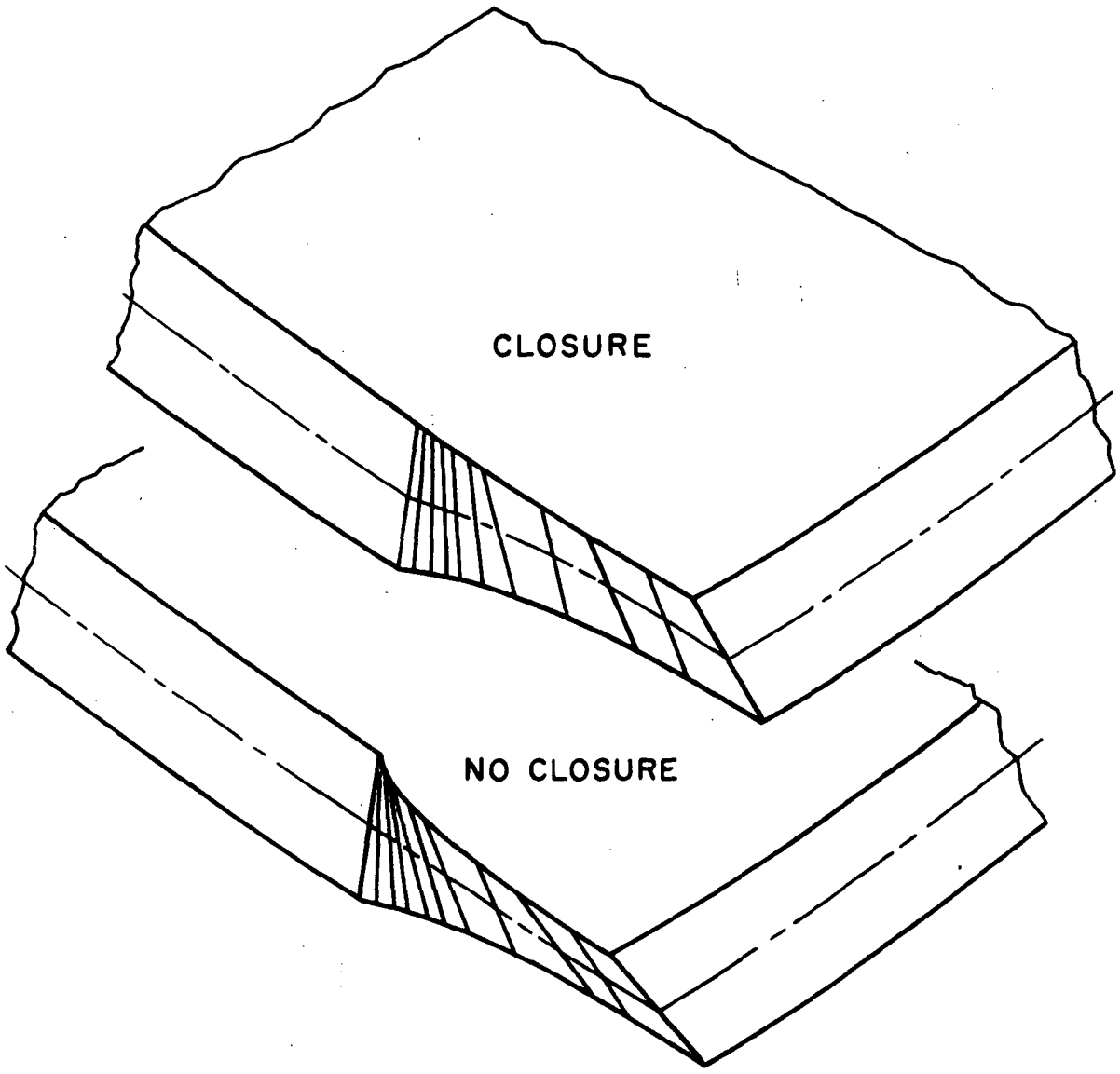

FIGURE 5-2
CONTOURS OF TRANSVERSE DEFLECTION $W[2D(1+\upsilon)/M_o]$,
FOR ELASTIC PROBLEMS

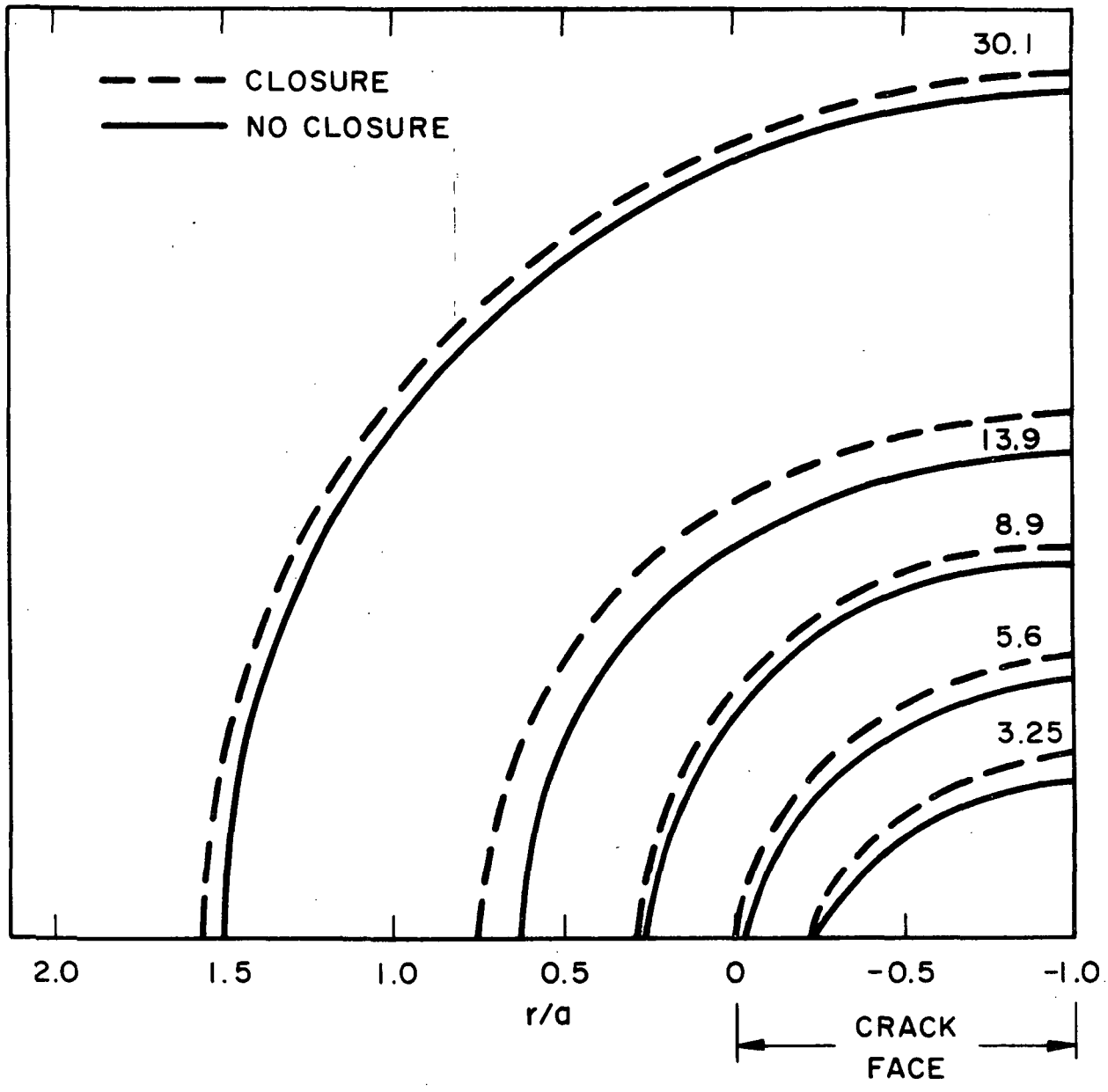

square root of the quantity plotted. As can be seen, the presence of the crack changes the circle into an ellipse around the crack. The ellipse for the crack closure model has a larger minor axis than that for no closure. Note that the transverse displacement is not a particularly sensitive parameter in studying the closure phenomena and that the elliptical contours of the transverse displacement caused by the crack, quickly (within three plate thicknesses) degenerate into circular contours. This circular contour is the developable surface of a sphere which is generated by the circular bending of a plate without a crack. Hence, it is expected that the errors due to neglecting large transverse displacements are small, especially since the transverse displacements are small (compared to the plate thickness) in the vicinity of the crack tip. In all cases, the slopes are small (approximately 0.03).

Figures (5-3) and (5-4) are contour plots of the transverse slopes $\frac{\partial w}{\partial x}$ and $\frac{\partial w}{\partial y}$. These quantities are normalized to $M_o/D(1+\nu)$ so that comparison with the solution of the plate with no crack can be made. Note that without a crack, $\frac{\partial w}{\partial x}$ is straight line parallel to the Y axis and $\frac{\partial w}{\partial y}$ is a straight line parallel to the X axis. Deviations from this straight line behavior are indicative of the crack presence in the analysis. Comparisons of Figures (5-4a) and (5-4b) shows that $\frac{\partial w}{\partial x}$ is affected by the crack presence but not markedly different with and without the closure effects present. Since this is the slope parallel to the crack face, this result is expected. On the other hand, Figures (5-4a) and (5-4b) show that the

FIGURE 5-3
CONTOURS OF TRANSVERSE SLOPE,
$\partial w/\partial x[D(1+\upsilon)/M_0]$, FOR ELASTIC PROBLEMS

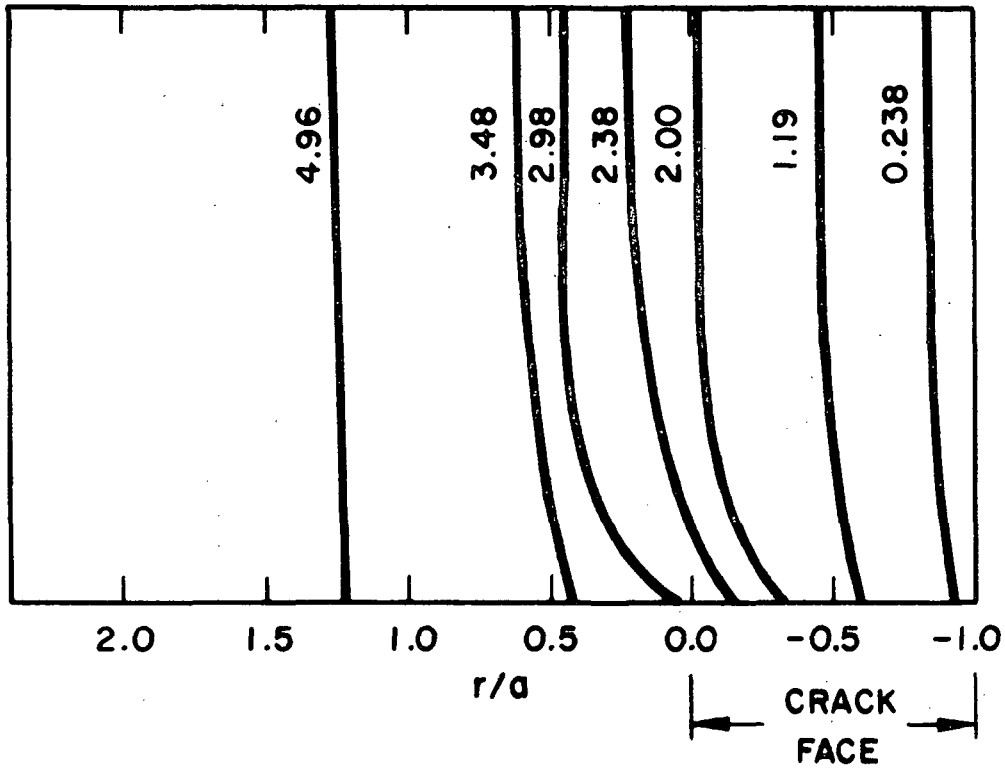

a) NO CLOSURE

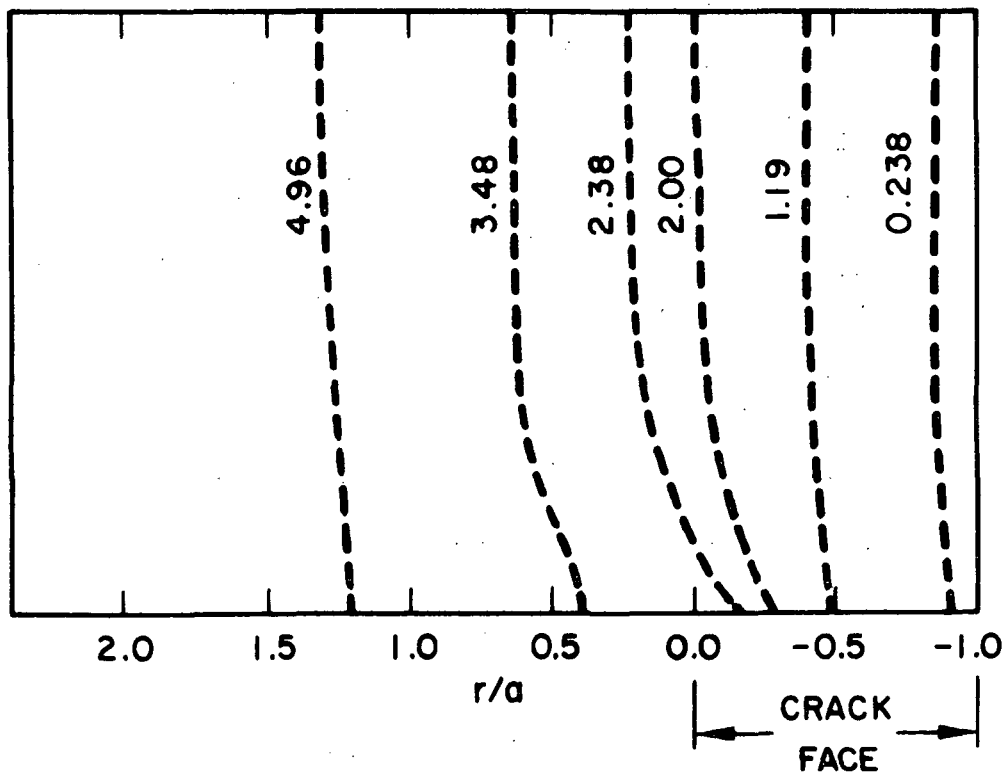

b) CLOSURE

FIGURE 5-4
CONTOURS OF TRANSVERSE SLOPE $\partial w/\partial y[D(1+\upsilon)/M_o]$,
FOR ELASTIC PROBLEMS

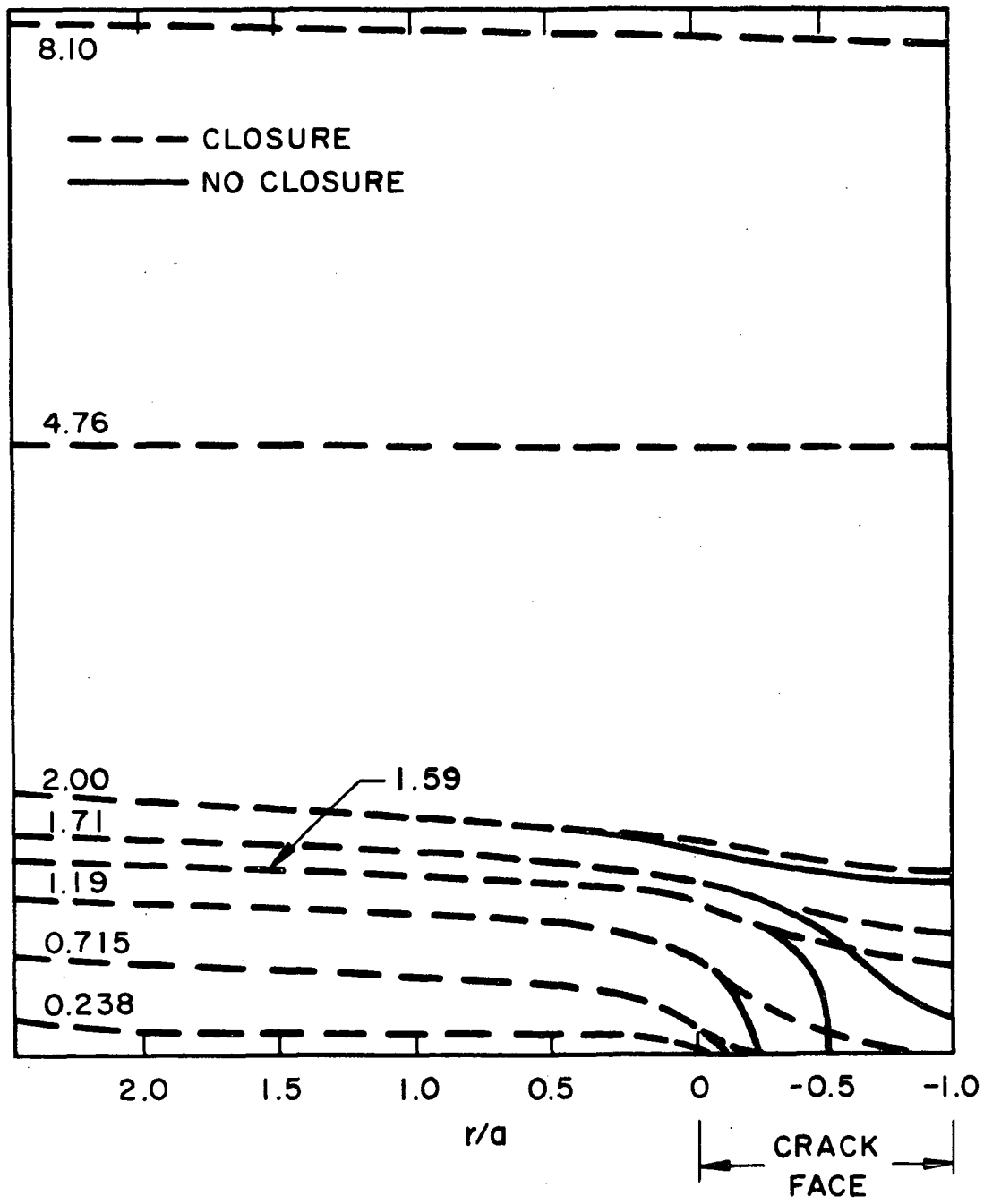

transverse slope normal to the crack face is strongly influenced by the presence of the crack and exhibits a very pronounced change due to crack closure effects. Hence, $\frac{\partial w}{\partial y}$ is a very sensitive measure of the crack closure phenomenon. Again, $\frac{\partial w}{\partial x}$ and $\frac{\partial w}{\partial y}$ indicate that the region of influence of the crack is about 3h.

The in-plane displacement normal to the crack face is plotted in Figure (5-5). A plan view of the tensile side of the plate is shown so that the overlap of material is indicated by negative displacements. This is the case for the no closure model with the compressive edge being overlapped onto itself (shown in Figure (5-5)) and the centroidal surface being at zero displacement. The closure model shows the compressive edge being at zero displacement and the centroidal surface being displaced exactly one-half of the value on the tension surface. The crack opening displacement is seen to be higher for the closure model. This implies a higher stress intensity factor if a linear elastic fracture mechanics approach is taken. (For further discussion of this, see Section 5.3.)

5.2 Elastic Stress Results

In Figures (5-6a), (5-7a), and (5-8a), the moment components, (M_x, M_y, M_{xy}) are plotted vs. r/a along the $\theta = 0$ axis for the elastic response. These moment distributions for the no closure problem compare favorably to the Williams [19] solution near the crack tip. For example, M_x and M_y exhibit the $(r)^{-\frac{1}{2}}$ singularity with M_x/M_y going negative near the crack tip as a consequence of Kirchhoff boundary conditions. Also present is

FIGURE 5-5
ELASTIC CRACK OPENING

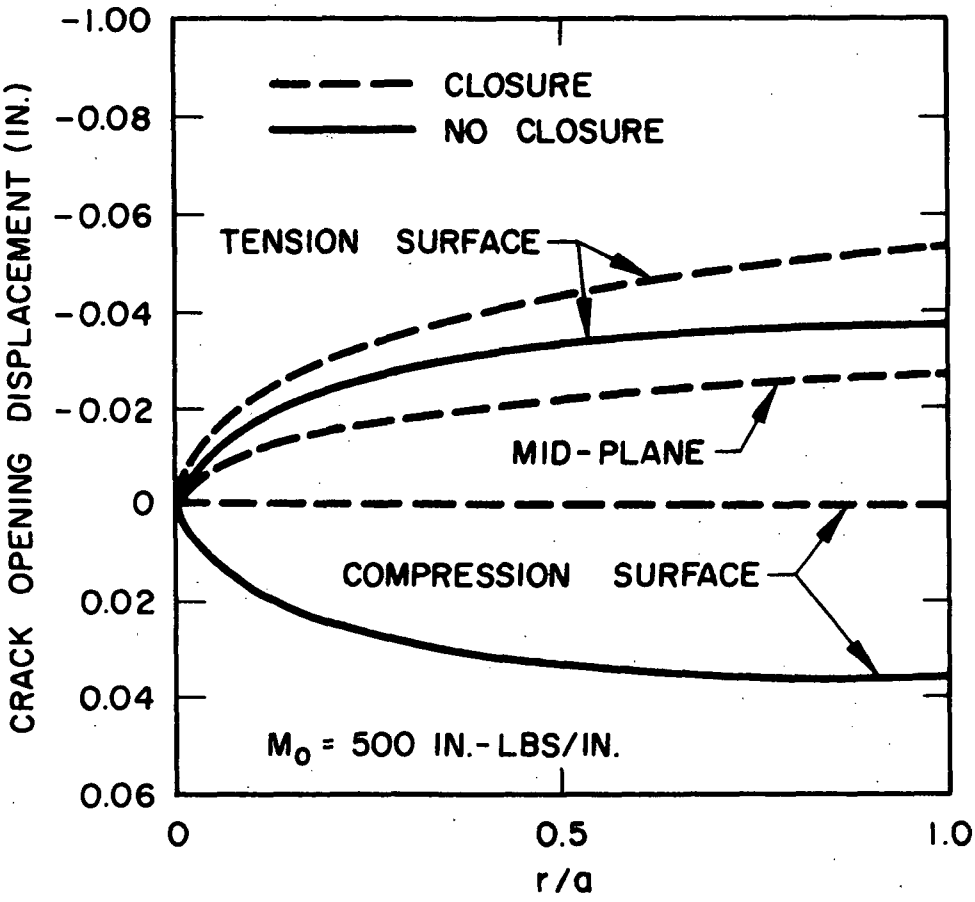

FIGURE 5-6
ELASTIC MOMENT (M_x/M_o) AND STRESS DISTRIBUTIONS (σ_x/σ_o)

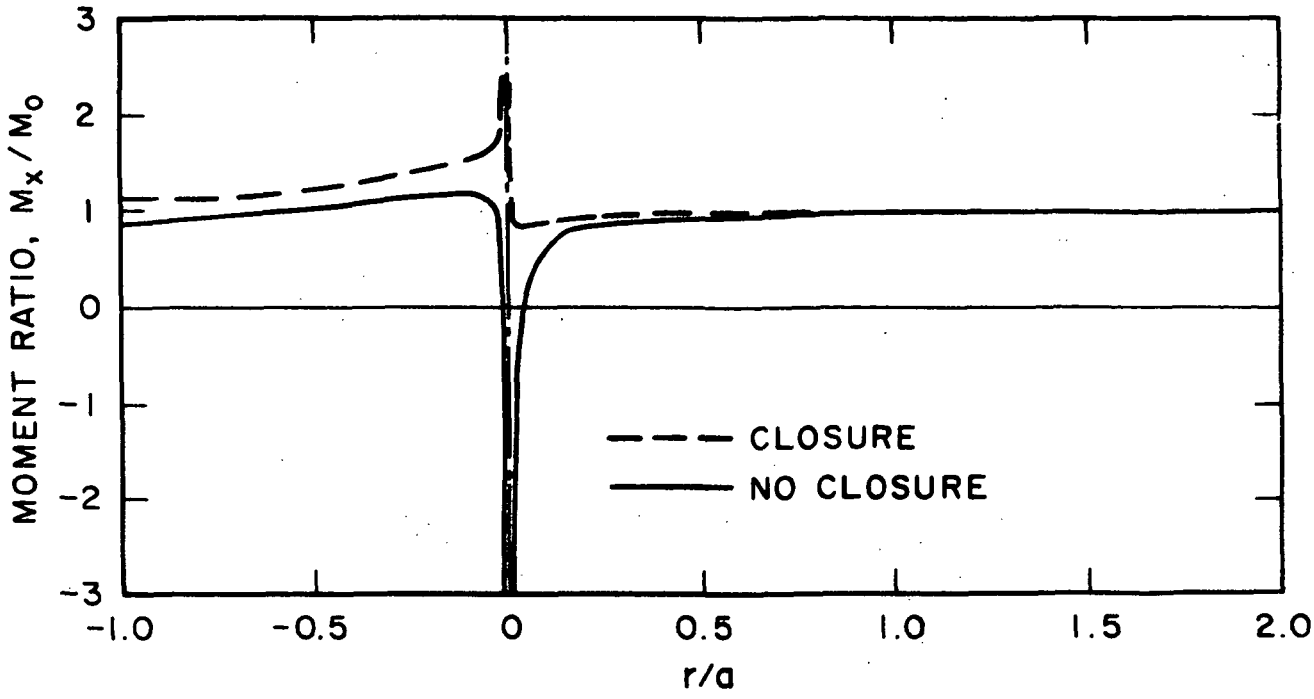

a) MOMENT DISTRIBUTION ALONG $\theta = 0°$ AXIS

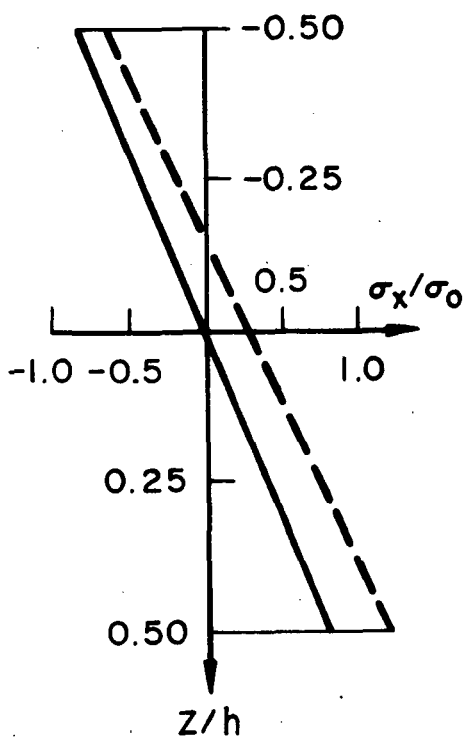

b) σ_x/σ_o VS Z/h FOR $\theta = 0°$, r/a = 3/16

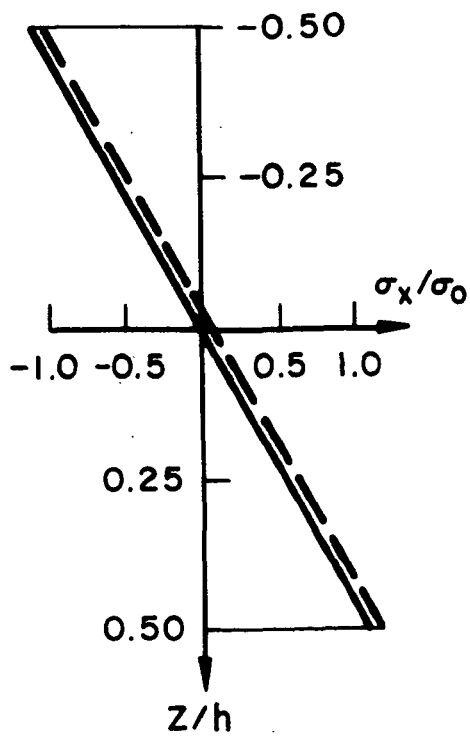

c) σ_x/σ_o VS Z/h FOR $\theta = 90°$, r/a = 3/16

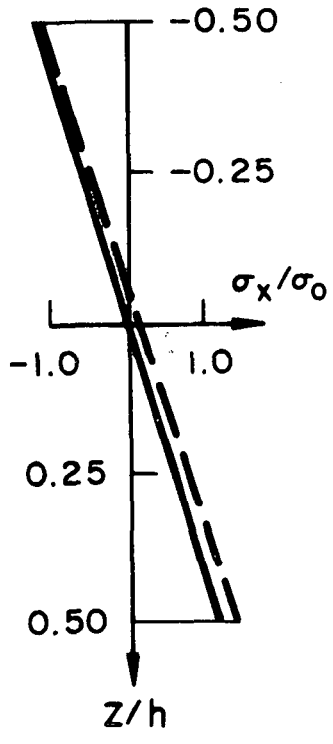

d) σ_x/σ_o VS Z/h FOR $\theta = 180°$, r/a = 3/16

FIGURE 5-7
ELASTIC MOMENT (M_y/M_o) AND STRESS (σ_y/σ_o) DISTRIBUTIONS

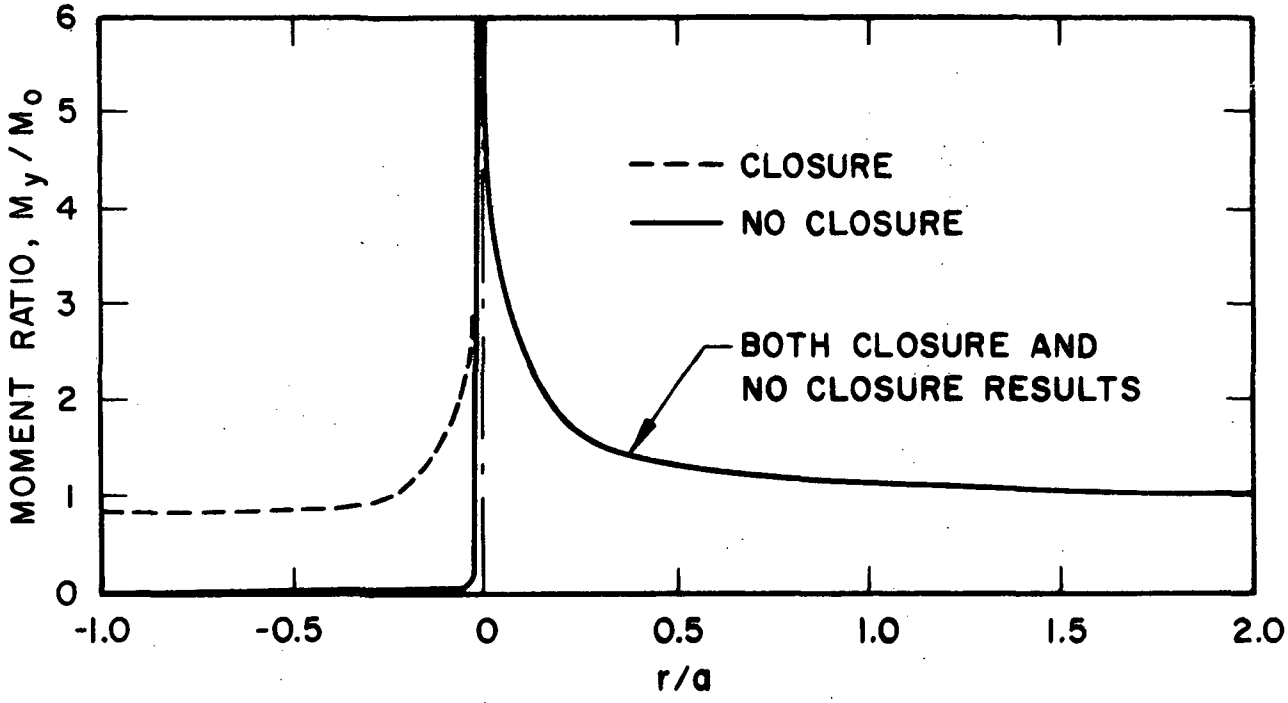

a) MOMENT DISTRIBUTION ALONG $\theta = 0°$ AXIS

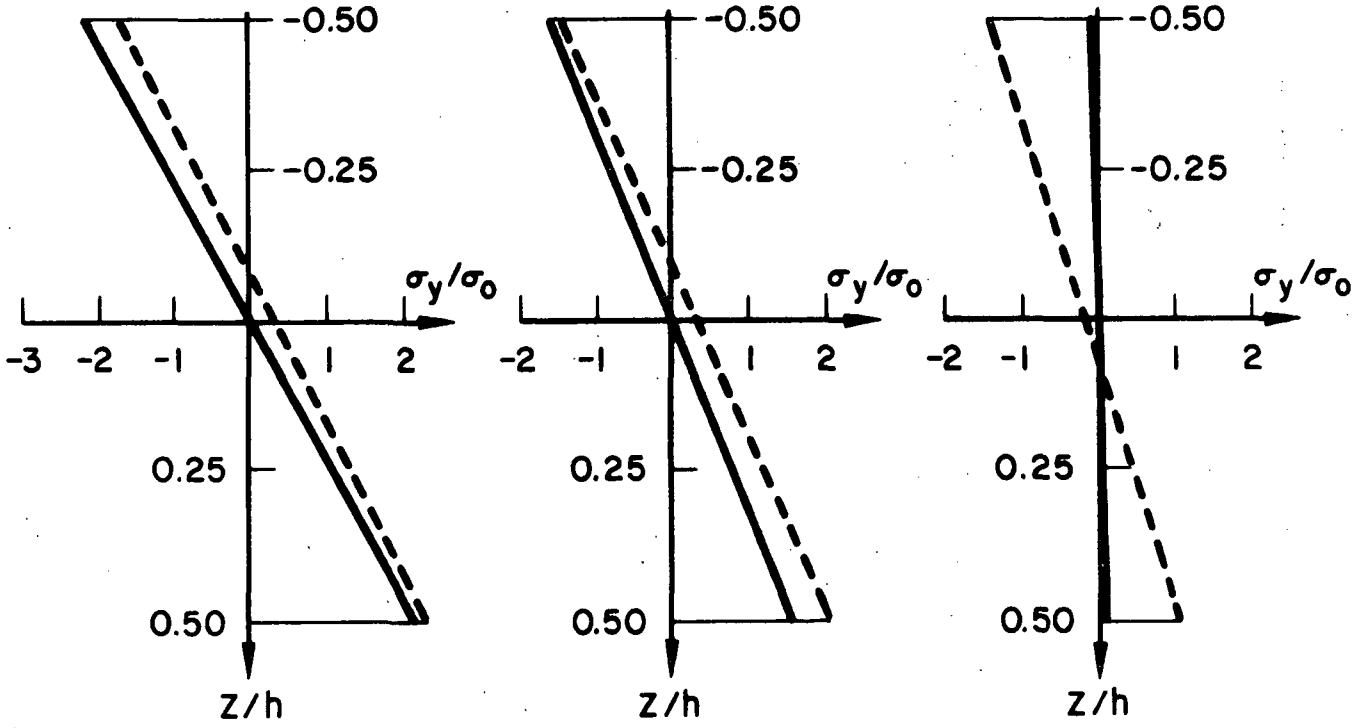

b) σ_y/σ_o VS Z/h FOR $\theta = 0°$, r/a = 3/16

c) σ_y/σ_o VS Z/h FOR $\theta = 90°$, r/a = 3/16

d) σ_y/σ_o VS Z/h FOR $\theta = 180°$, r/a = 3/16

FIGURE 5-8

TWISTING MOMENT (M_{xy}/M_0) AND SHEAR STRESS (τ_{xy}/σ_0) DISTRIBUTIONS FOR ELASTIC RESPONSE

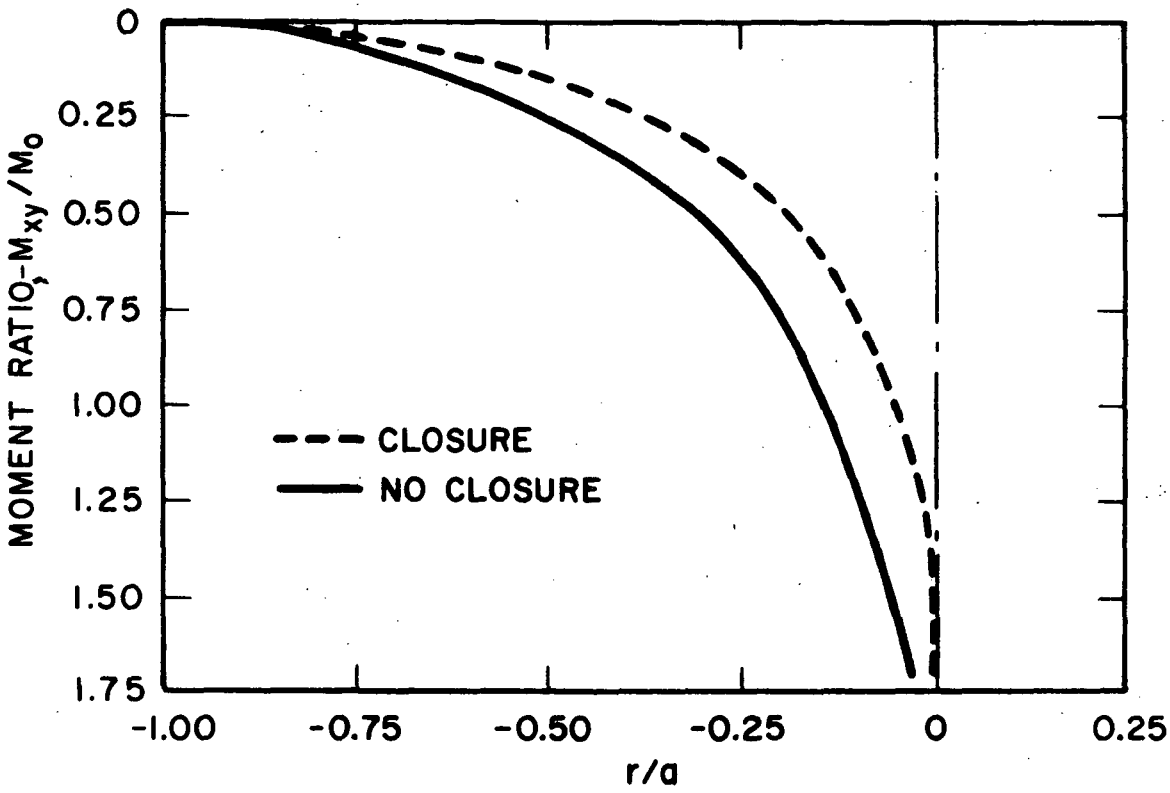

a) TWISTING MOMENT DISTRIBUTION ALONG $\theta = 0°$ AXIS

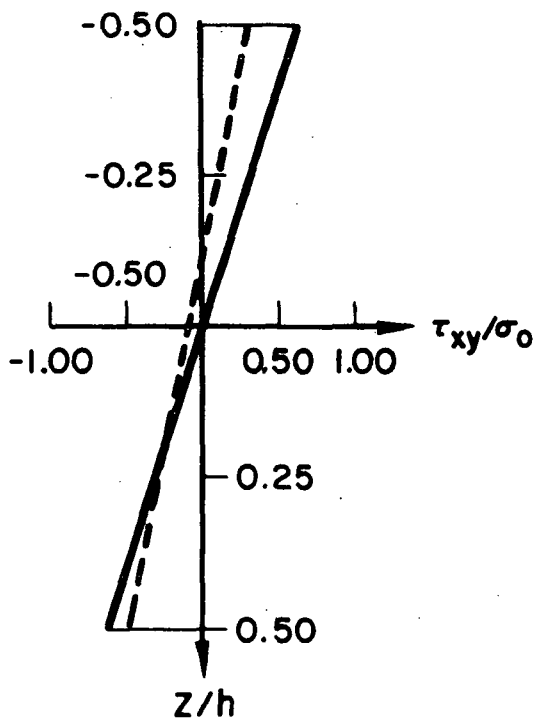

b) τ_{xy}/σ_0 VS Z/h FOR $\theta = 90°$, r/a = 3/32

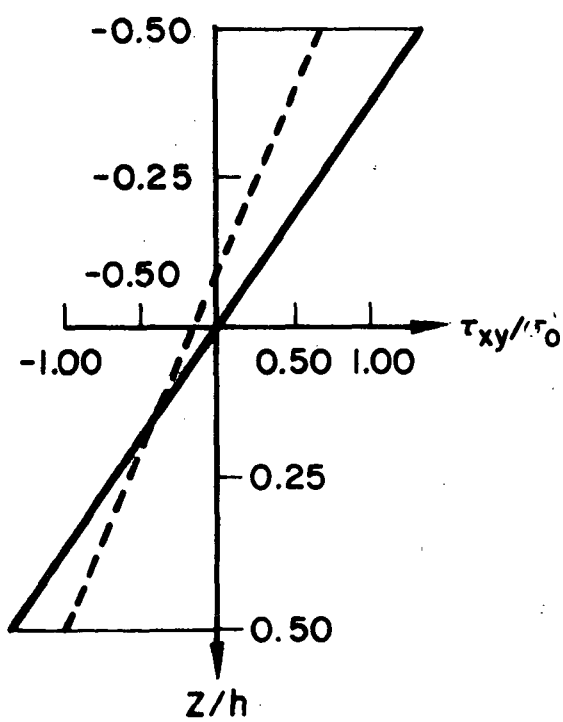

c) τ_{xy}/σ_0 VS Z/h FOR $\theta = 180°$, r/a = 3/32

the singular behavior of M_{xy} at the crack tip as approached along the crack face. This is a consequence of the approximate nature of the free surface assumption in Kirchhoff theory. It should be noted that the force boundary conditions remote from the crack are satisfied and that the zero normal moment along the crack face is also satisfied for the no closure problem.

Figure (5-7a) shows the non-zero normal moment along the crack face for the closure problem. This moment is the result of the wedging of the crack face during crack closure. As shown in Figure (5-9), there is actually an in-plane load normal to the crack face generated as a result of the crack face interference along the compressive edge during bending. Transferring this load to the centroidal surface of the plate (Figure (5-9)) requires the addition of a couple to satisfy equilibrium. As shown in Figure (5-9), although the mid-surface is actually a free surface, there are these pseudo forces and moments calculated at the mid-plane of the plate. The shift in the neutral axis resulting from the in-plane load is further discussed in Section 5.4.

In Figures (5-6b,c,d), (5-7b,c,d) and (5-8b,c,d), the stress distributions through the thickness are shown for (r/a) = 3/32 and $\theta = 0^{o}$, 90^{o}, 180^{o}. For the no closure case, these plots show the symmetrical stress distribution (about the mid-plane) required by pure bending. Also, the linearity of stress and the resolution of the zero σ_y at the crack face for no closure ($\theta = 180^{o}$) is noted. The shift in neutral surface and the moment at the crack face is evident in the closure case.

FIGURE 5-9
VARIATION OF IN-PLANE MEMBRANE LOADS
FOR THE ELASTIC CLOSURE PROBLEM

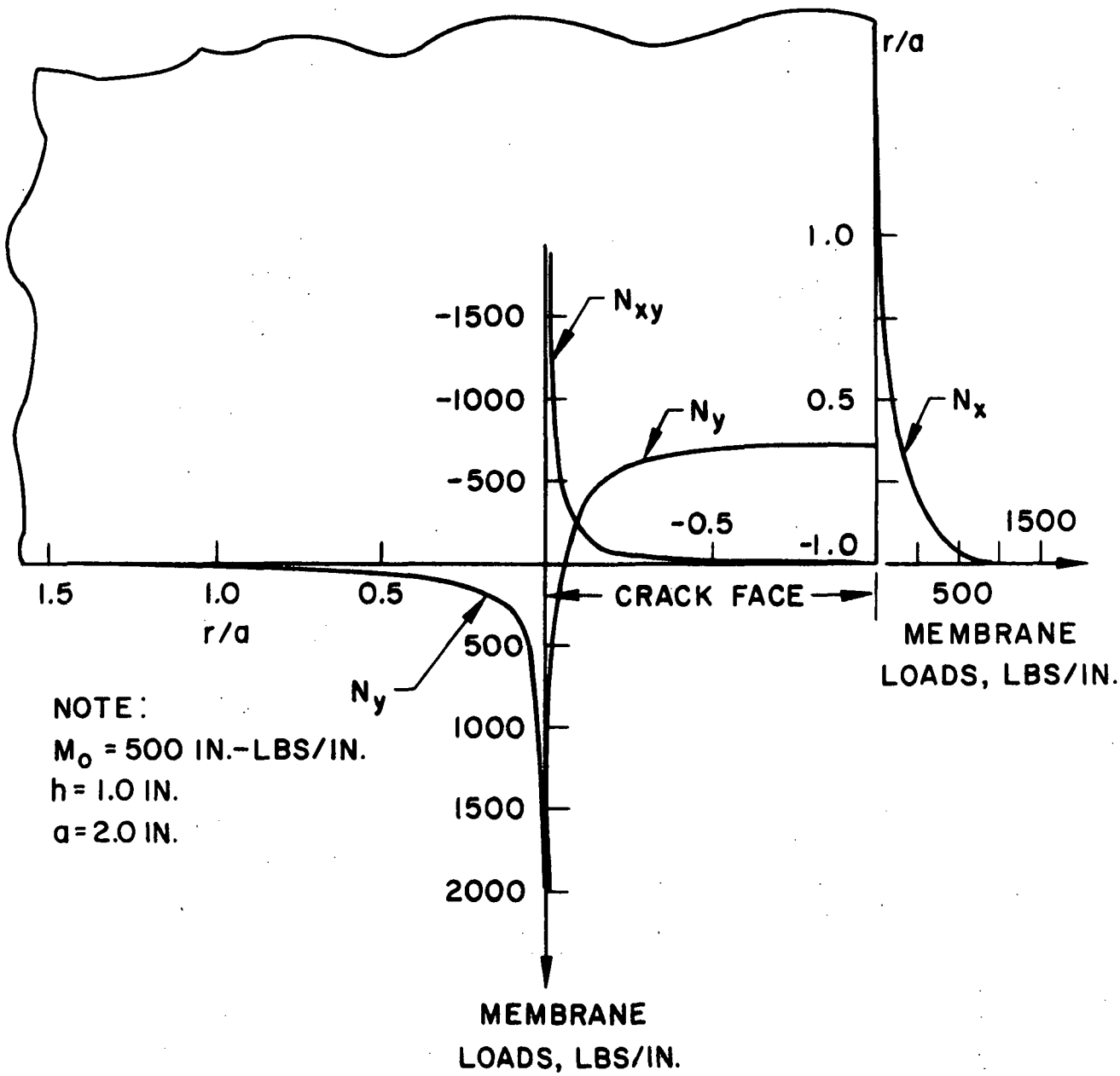

The variation of the stress components with the angle around the crack tip are compared with the Williams solution in Figures (5-10), (5-11), and (5-12). Fairly good agreement is achieved with the usual difficulty in resolving finite element stress results across inter-element boundaries being present.

5.3 Fracture Mechanics Interpretation

As discussed in Section 5.1, the elastic results may be given a linear elastic fracture mechanics interpretation. This approach requires, among other things, the extraction of the bending stress intensity data from the finite element results. Since displacement data are more accurate than stress data in finite element studies, the displacement results are compared with the Williams [19] solution in terms of the bending stress intensity factor. For convenience, data along the crack face are used. That is, using the expression from [19] for the transverse deflection w results in in-plane displacements $u = -z\frac{\partial w}{\partial x}$ and $v = -z\frac{\partial w}{\partial y}$ of the form

$$u = -\frac{3z}{2} b_1 r^{\frac{1}{2}}\left[\cos\theta\left(-\cos\frac{3\theta}{2}+\frac{3(1-\nu)}{7+\nu}\cos\frac{\theta}{2}\right) - \sin\theta\left(\sin\frac{3\theta}{2}-\frac{(1-\nu)}{7+\nu}\sin\frac{\theta}{2}\right]\right.$$

$$\left. - 2zb_2 r\left[\cos\theta\left(\cos 2\theta+\frac{1-\nu}{1+\nu}\right) + \sin\theta\sin 2\theta\right] - z\gamma r^{3/2} - \cdots\right.$$

(5-1)

$$v = -\frac{3}{2} zb_1 r^{\frac{1}{2}}\left\{\sin\theta\left[-\cos\frac{3\theta}{2}+\frac{3(1-\nu)}{7+\nu}\cos\frac{\theta}{2}\right] + \cos\theta\left[\sin\frac{3\theta}{2}-\frac{(1-\nu)}{(7+\nu)}\sin\frac{\theta}{2}\right]\right\}$$

$$- 2zrb_2\sin\theta\left[\cos 2\theta+\frac{1-\nu}{1+\nu}\right] - \cos\theta\sin 2\theta - z\alpha r^{3/2} - \cdots$$

FIGURE 5-10
STRESS VARIATION WITH ANGLE COMPARING THE NO CLOSURE SOLUTION WITH WILLIAMS [19] SOLUTION

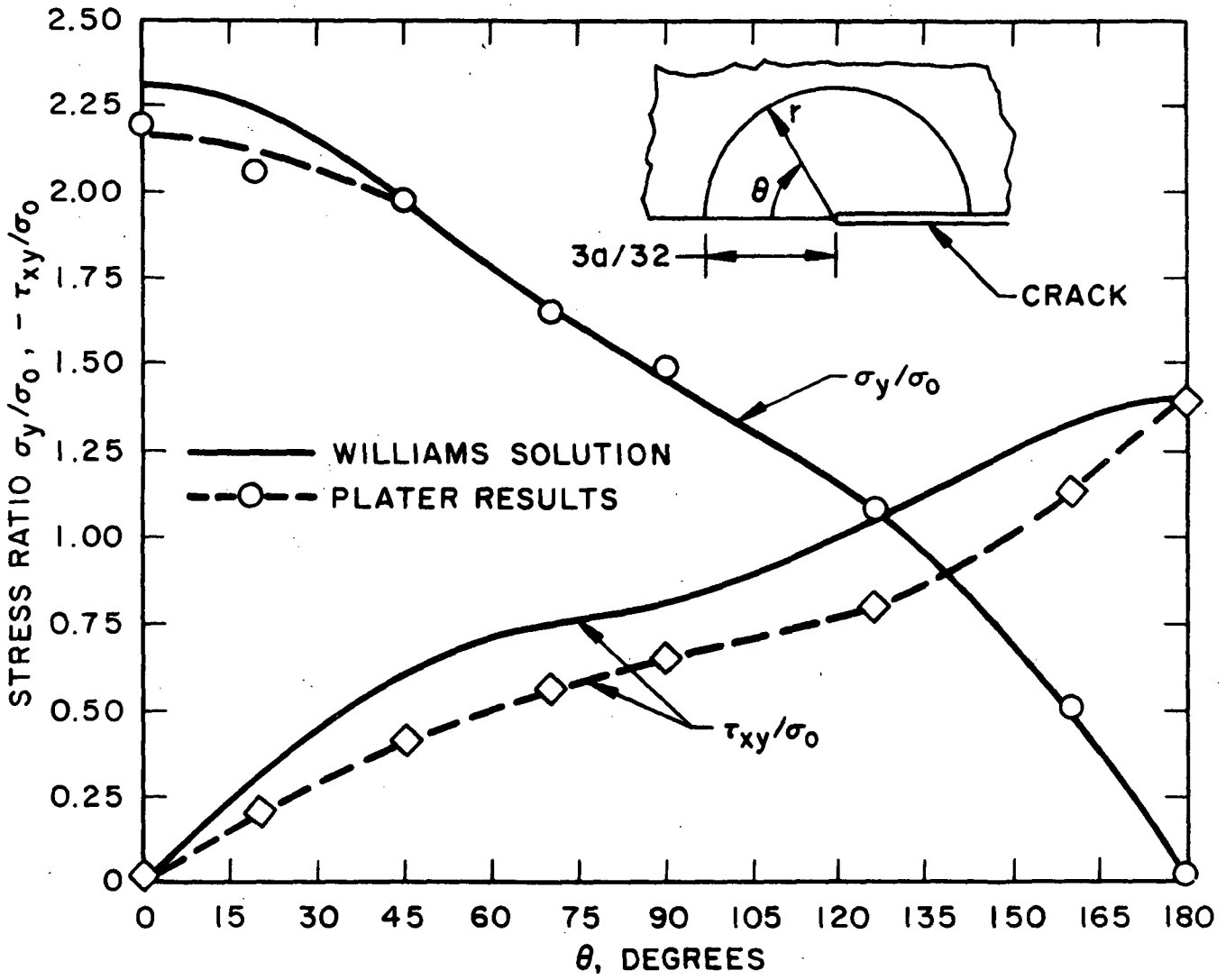

FIGURE 5-11
MOMENT VARIATION WITH ANGLE
FOR ELASTIC RESPONSE

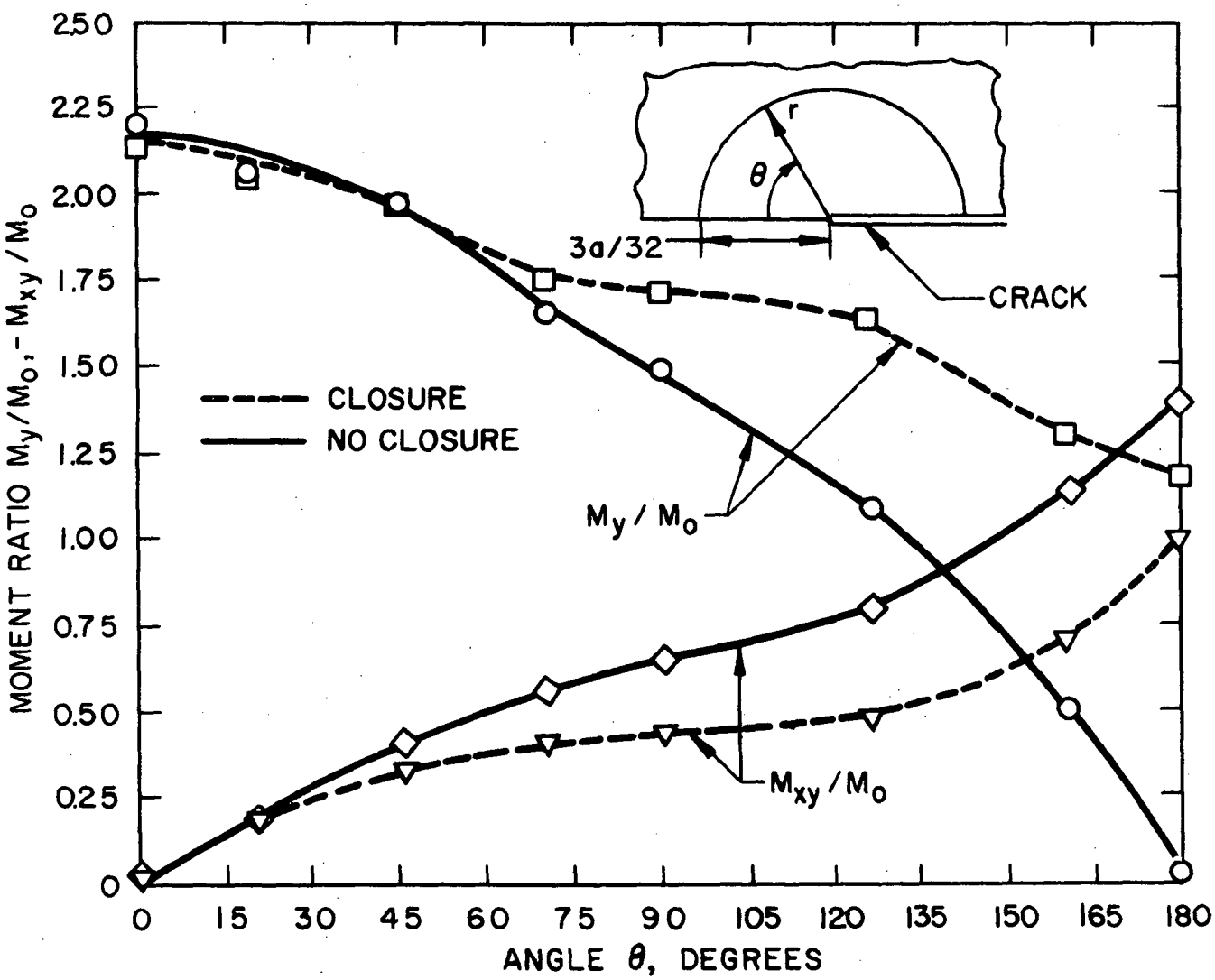

FIGURE 5-12
MOMENT DISTRIBUTION ALONG θ=90°

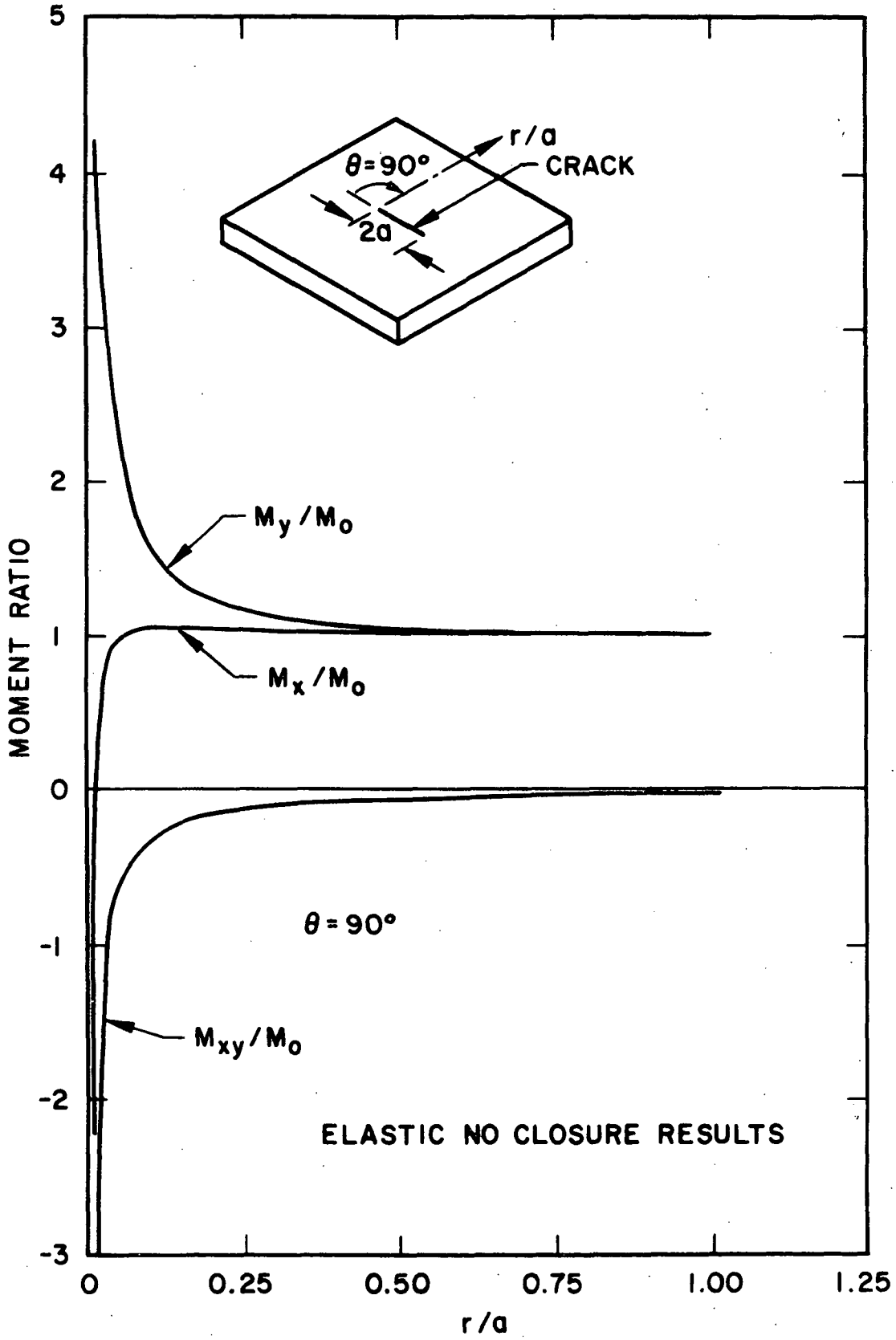

Along the crack face where $\theta = 180^{o}$, the expressions for u and v at $z = - h/2$ are

$$u = - \frac{2hb_2 r}{1+\nu} + \gamma r^{3/2}$$

$$v = + \frac{6hb_1 r^{1/2}}{7+\nu} + \alpha r^{3/2}$$

where b_2, γ, α are constants and

$$b_1 = \frac{2(7+\nu)(1+\nu)}{3(3+\nu)Eh\sqrt{2\pi}} K_B \qquad (5\text{-}2)$$

$$K_B = \frac{6M_o}{h^2} (\pi a)^{\frac{1}{2}}$$

Dividing both sides of Equations (5-2) by $\sqrt{r/a}$, it is possible to get the v displacement in the form

$$\frac{v}{\sqrt{r/a}} = \alpha(\frac{r}{a}) + \beta \qquad (5\text{-}3)$$

where

α is a constant coefficient for the higher order terms of the Williams solution, and

$$\beta = \frac{4(1+\nu)}{E(3+\nu)\sqrt{2\pi}} K_B$$

As in all finite element studies, the results near the crack tip are not as good as those away from the crack tip. However, by plotting $v/\sqrt{r/a}$ from the finite element results and extrapolating to the crack tip, values of α and β are obtained from which K_B is calculated. Figure (5-13a) shows results of this procedure for the no closure model with the value obtained from the extrapolation being 14% lower than $K_B = 6M_o/h^2(\pi a)^{\frac{1}{2}}$. This is indicative of the systemic error of the finite element model and is unimportant since a comparison between the closure/no closure model is of prime interest. Figure (5-13b) shows the closure results obtained through the same process. Figure (5-14) compares the results through the thickness for the closure/no closure problems. Note that K_B is zero at the compressive edge for the closure problem and at the mid-plane for the no closure problem. The value of K_B is also negative on the compressive edge in the no closure problem. This leads to ambiguity as to the physical interpretation if any, that can be applied to the bending stress intensity. The linearity is due to the Kirchhoff assumptions. The K_B is about 20% higher on the tension surface for the closure problem than for the no closure case. This is trend is fairly consistent with experimental observation in photoelastic materials [24]. Actually, from photoelastic studies, Smith and Smith [24] obtained 40% higher values of K_B but they could not entirely isolate the closure effects in their experiments because of a number of other events that operate simultaneously (e.g., three-dimensional effects such as crack extension and crack face warping.)

FIGURE 5-13

DETERMINATION OF ELASTIC BENDING STRESS INTENSITY FACTORS ON THE TENSION SURFACE

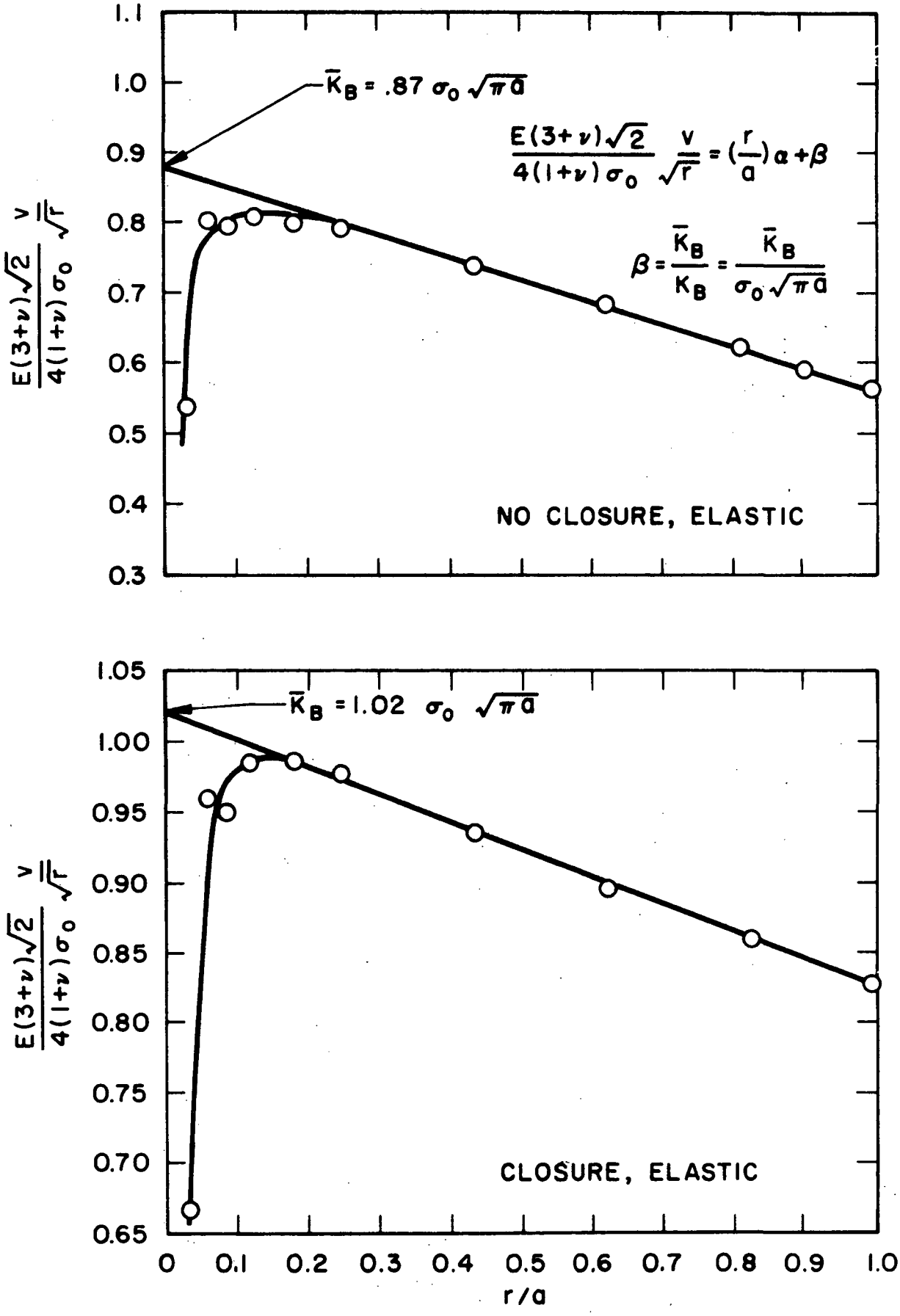

FIGURE 5-14
COMPARISON OF BENDING STRESS INTENSITY DATA

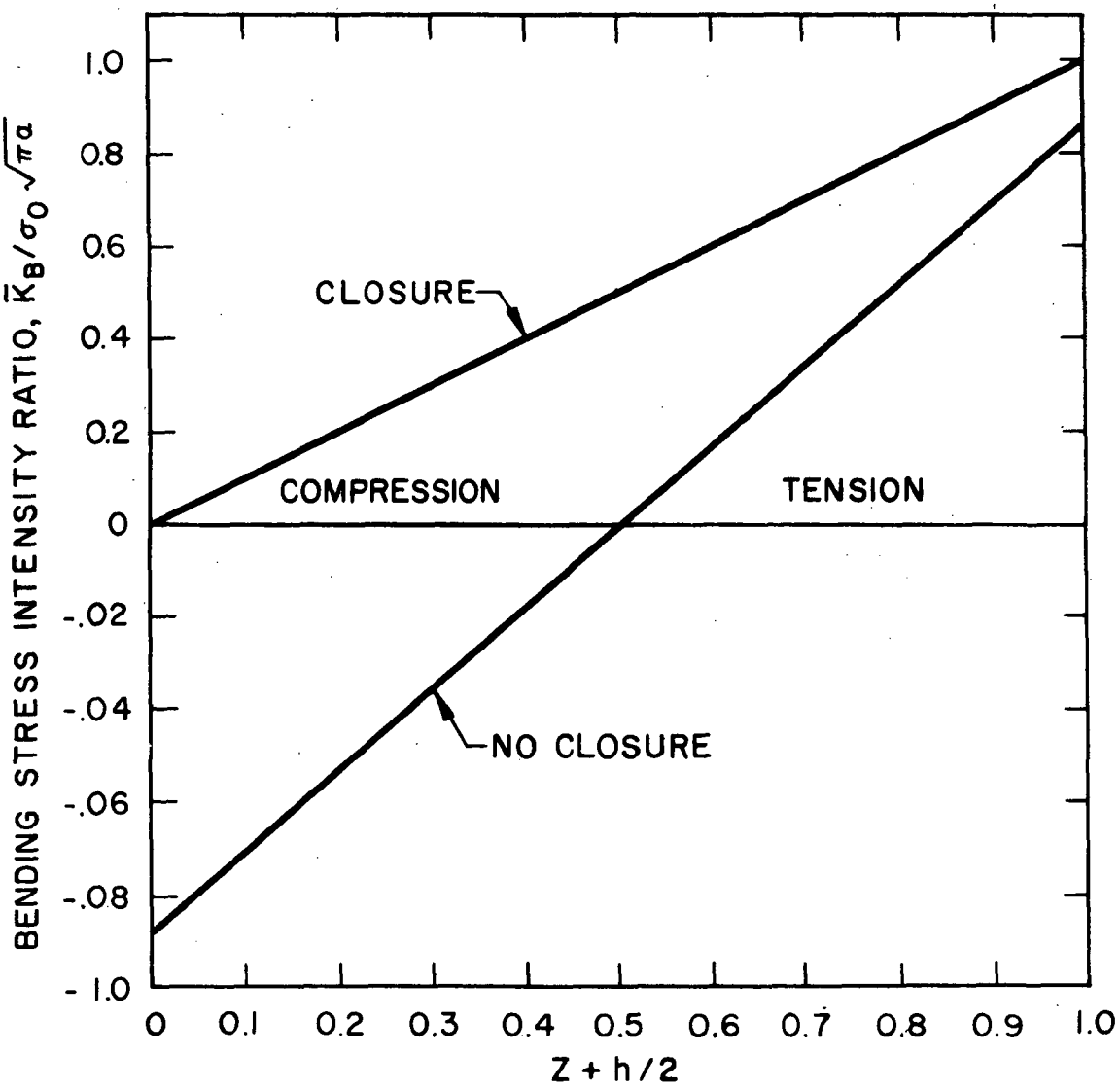

5.4 Neutral Surface Shifts

The strongest indicator of the crack closure phenomenon is the shift in the neutral surface. Actually, the definition of a neutral surface is arbitrary in the sense that either zero forces, strains, or displacements may be used to determine it. Only kinematic quantities will be used here; specifically either $\varepsilon_y = 0$ or $v = 0$ will define the neutral surfaces.

In his work on the combined bending/extension elastic problem, Wynn [5] applied an extensional load at the exterior plate boundaries in such a magnitude as to preclude contact of the crack face surfaces during bending. Under these circumstances, crack closure is obviously no problem. However, adjusting the superimposed extensional load in the exact amount to relieve the contact on the compressive surface does not correctly model the crack closure phenomenon. This process puts the plate in tension while the actual mechanics along the crack face applies a compressive loading along the line of contact. Also, these forces are variable along the crack face as the wedging actions of the crack closure changes. This difference in mechanism is indicated by the shift in neutral surface defined by $\varepsilon_y = 0$ shown in Figure (5-15). If an exterior tension had been applied, the neutral surface would shift toward the compressive side of the plate. However, the constraint against material overlap is guaranteed by contact of the compressive surface which adds a compressive force and a normal bending moment along the crack face. As shown in Figure (5-15), this results in a shift of neutral surface (as defined by $\varepsilon_y = 0$) toward the tension surface.

FIGURE 5-15
NEUTRAL SURFACE AS DEFINED BY
$\epsilon_y = 0$ FOR THE ELASTIC CLOSURE PROBLEM

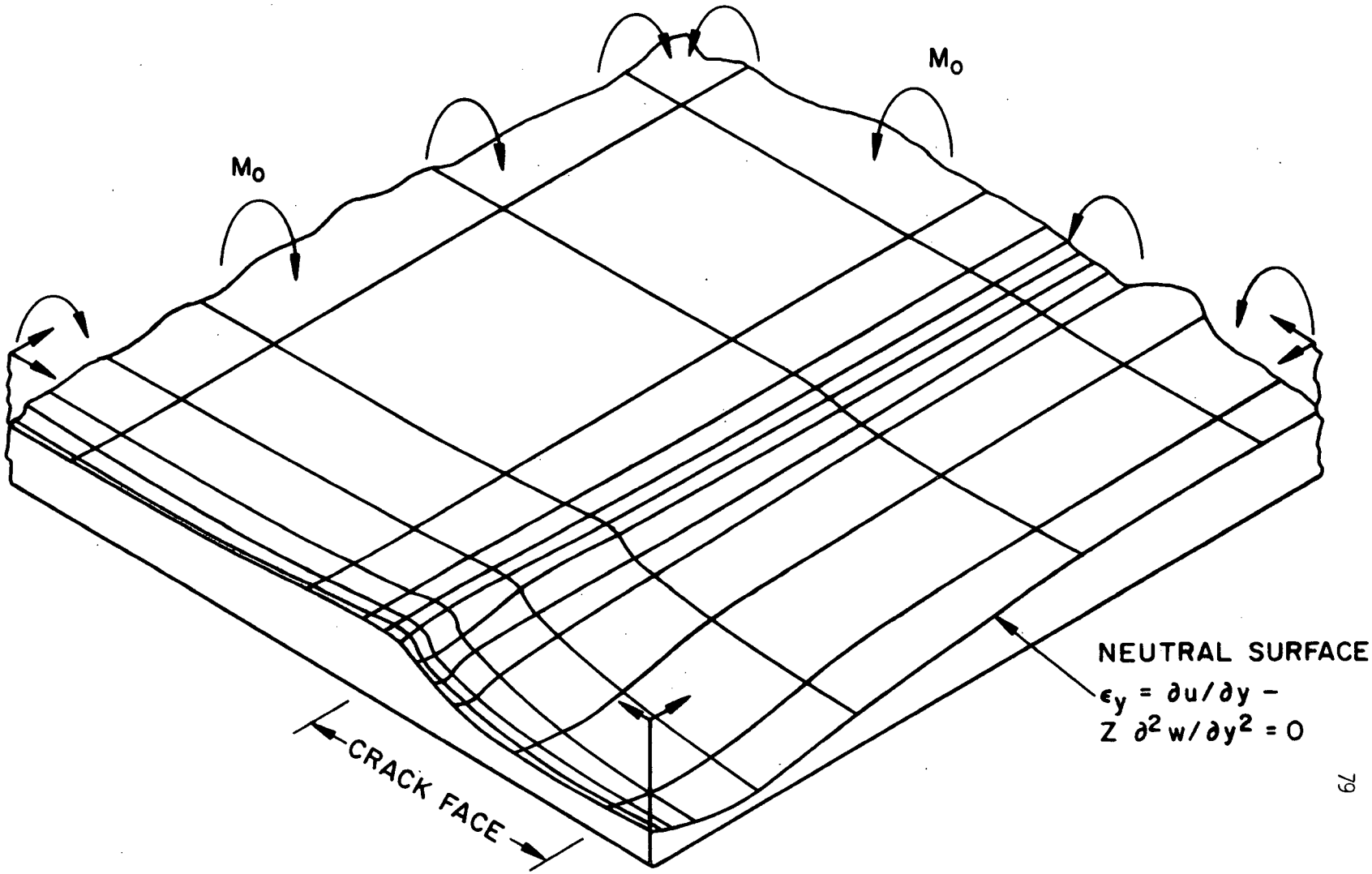

By defining the neutral surface as $\gamma = 0$, the shift is toward the compressive surface as shown in Figure (5-16). In fact, the neutral surface is identical to the compressive contact line at the crack face, and decays toward the mid-plane away from the crack face. The neutral surface is coincident with the mid-plane at a distance of three plate thicknesses from the crack face. The maximum shift is at the plate center and gradually becomes less pronounced as the crack tip is approached. Figure (5-16) shows the neutral surface shift at various stations of x.

5.5 Elasto-Plastic Results

The growth of plastic yield zones is the most dramatic feature of the elasto-plastic results. Yielding is defined at those points for which τ_{OCT} vs. γ_{OCT} is nonlinear. For the no closure problem, the yield zones are symmetric about the mid-plane as required by the Kirchhoff bending theory (see Figure (5-17)). Also a consequence of the Kirchhoff theory is the dominance of the singular shear stress term along the crack face approaching the crack tip. This dominates the plasticity behavior and forces the yield zones to generate along the crack face first and then to propogate into the material. Without the singular shear stress, it is presumed that the yield zone shape at any surface parallel to the mid-plane, would be similar to that found in extensional plane stress (see [6]).

Comparing the no closure results with the analyses of Brinson and Gonzalez [12] and Brinson, et al. [48], using the Dugdale model, indicates that the elastic core present in this analysis is a very important feature

FIGURE 5-16

NEUTRAL SURFACE SHIFT AS DEFINED BY v = 0

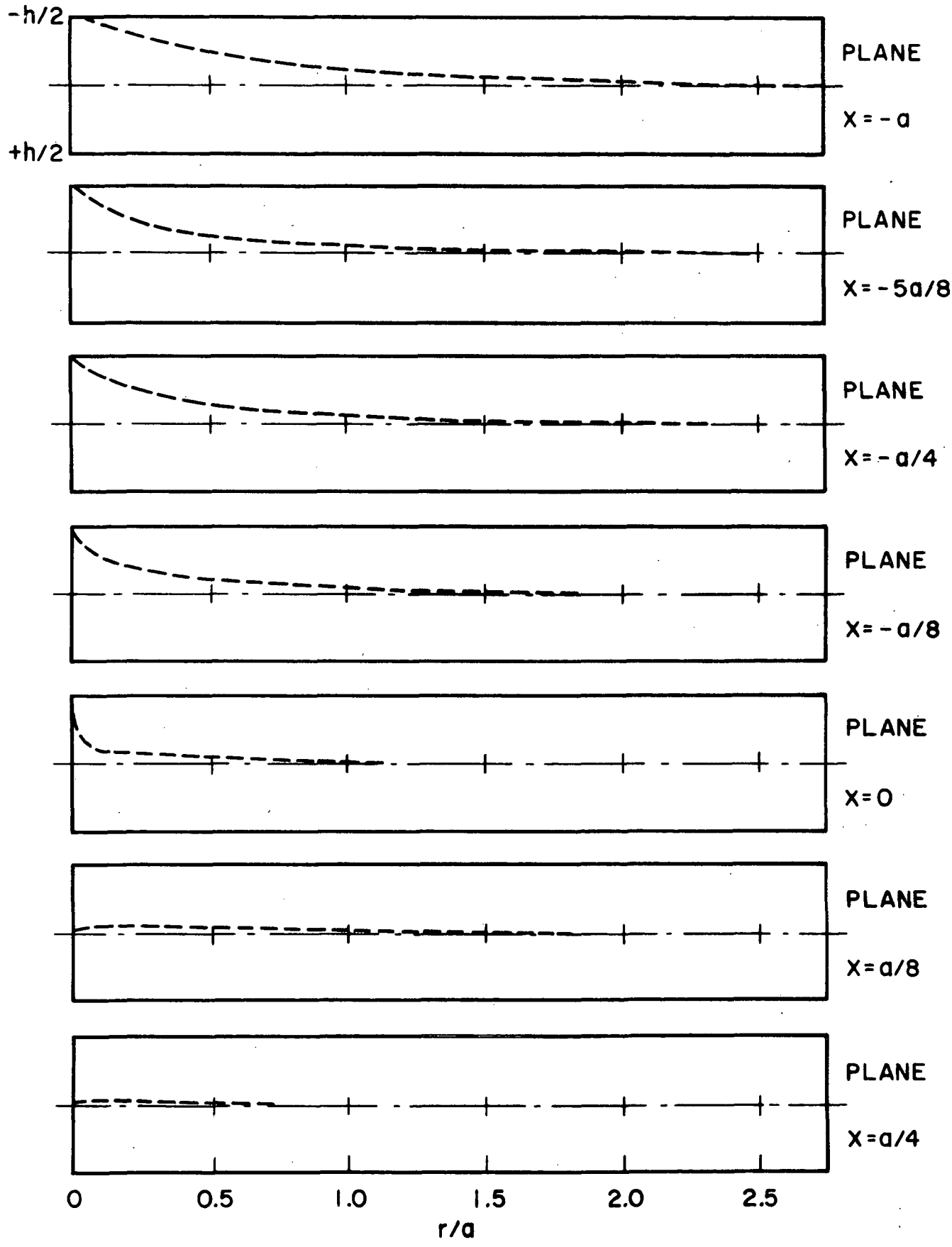

FIGURE 5-17
YIELD ZONES FOR THE NO CLOSURE PROBLEMS

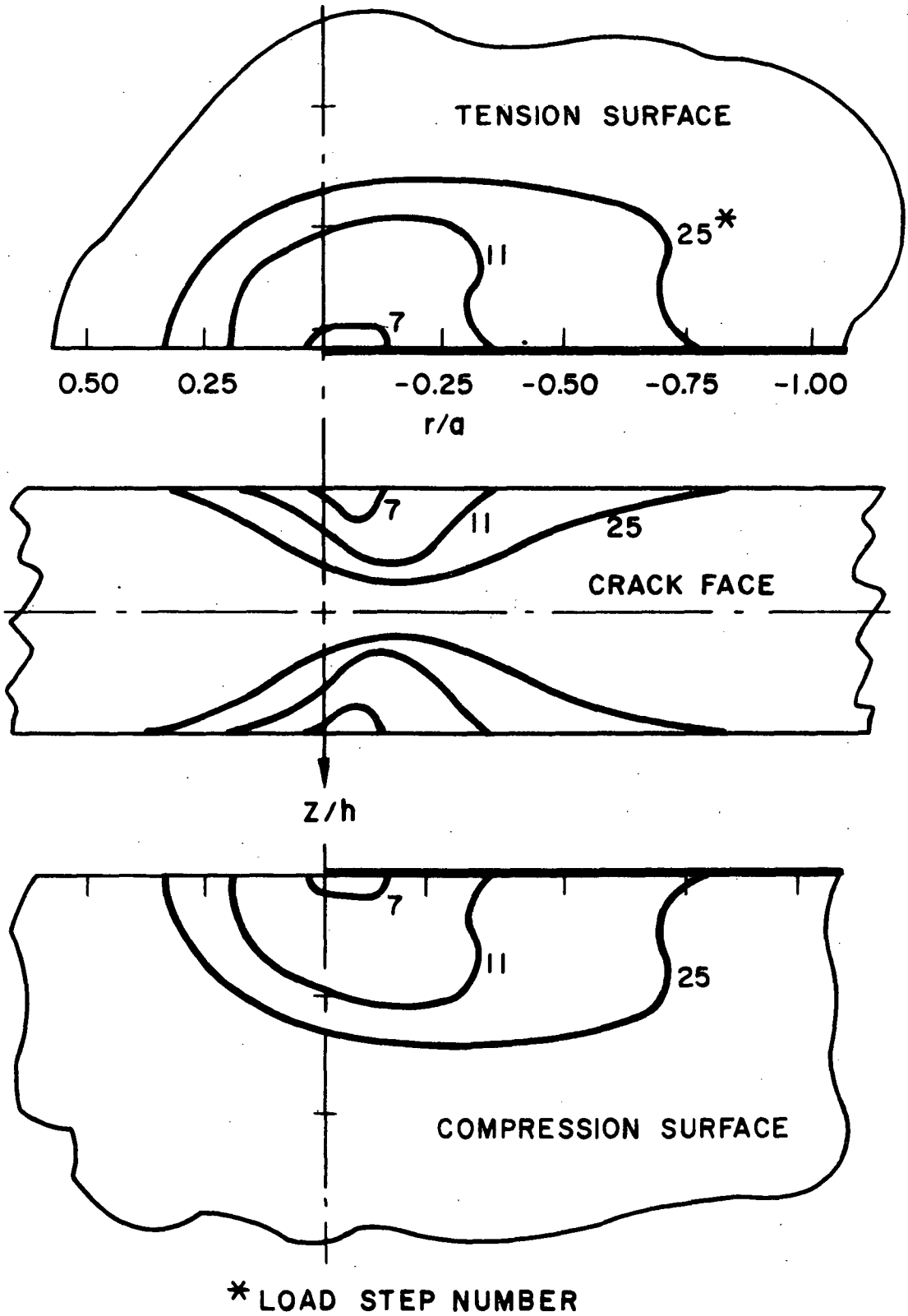

*LOAD STEP NUMBER

in the elasto-plastic bending of the plate. Being a rigid/perfectly plastic model, the Dugdale (or strip) model requires full penetration of the yield zones, i.e., no elastic core present at the crack tip. Figure (5-17b) shows that the yield zone shape through the thickness obtained from this analysis is not cusp shaped as in the strip model and that the plate has a definite elastic core.

The formation of yield zones is completely different in the case of the closure model. As shown in Figure (5-18), the yield zones form on the tension surface first and proceed through the thickness before yielding on the compressive edge. It is noted in Figure (5-18a) that the in-plane yield zone growth appears to be a combination of the plane stress extensional case and the bending case with no closure. The important feature, though, is that yielding progresses on the tension surface first prior to initial yield on the compressive contact surface. The yield zones tend to grow along the crack face for the closure problem due to the compressive stress field built up by the contact of the crack face and the shear stress due to Kirchhoff boundary conditions. Although the stresses are a bit higher in the closure case, the yield zones are smaller. This is due to the greater constraint of the crack surface in the closure case causing compressive fields along the crack face which inhibits yielding.

The through thickness stress distributions in Figure (5-19) show neutral axis shifts and nonlinear stress behavior as loading builds up. The crack closure results in shifting the neutral surface and in causing

FIGURE 5-18
YIELD ZONES FOR THE CLOSURE PROBLEM

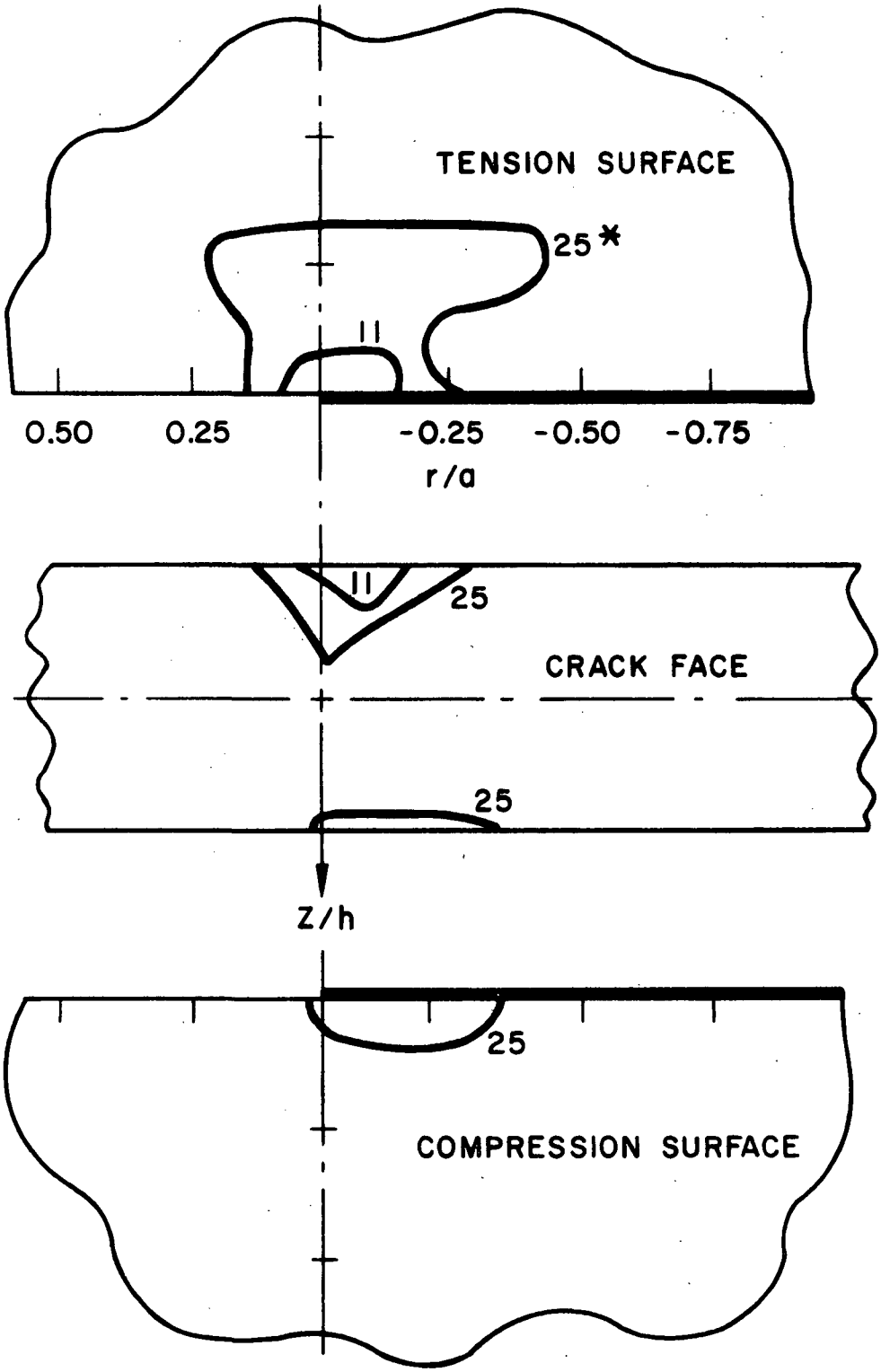

*LOAD STEP NUMBER

FIGURE 5-19
THROUGH THICKNESS STRESS DISTRIBUTIONS FOR THE ELASTO-PLASTIC PROBLEMS

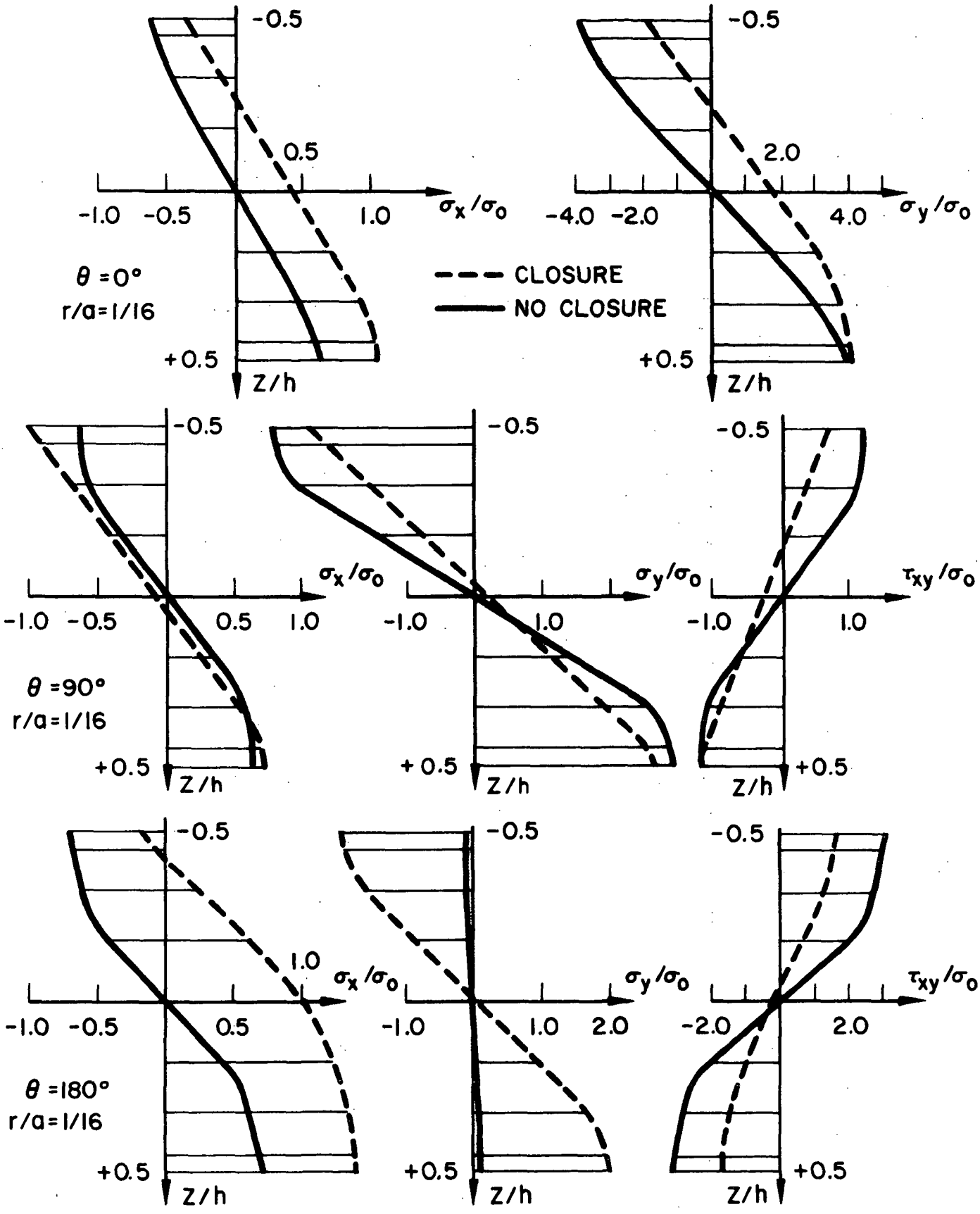

$M_{NO\ CLOSURE}$ = 793 IN.-LBS/IN. $M_{CLOSURE}$ = 703 IN.-LBS/IN.

initial yielding to occur on the tension surface. As yielding proceeds, the elastic core takes up more of the load until yielding is initiated on the compressive surface.

The moment redistribution as loading proceeds is indicated in Figure (5-20). By comparing the closure case with the no closure case, it is seen that for a given load, more redistribution takes place with the closure model. This is consistent with the fact that for a given applied moment, less material is yielded due to the constraint of the crack face for the closure model.

The neutral axis shift, as defined by the surface where $v = 0$, is not greatly affected by the yielding process. The neutral surface does shift back toward the mid-plane of the plate as the plasticity builds up, but this behavior is only local to the crack tip. It does appear though, if large scale yielding would take place, crack closure would have a lessening effect on the plate behavior.

A further indication of greater constraint of yielding in the crack closure case is the relatively less crack tip blunting in the closure case than in the no closure case. The relative crack openings are shown in Figure (5-21). The crack opening displacements are normalized to the crack opening displacement at the plate center. It can be inferred from the data that for a given load, less plastic straining occurs in the closure case than in the no closure case.

FIGURE 5-20
MOMENT REDISTRIBUTION FOR
THE ELASTO-PLASTIC PROBLEMS

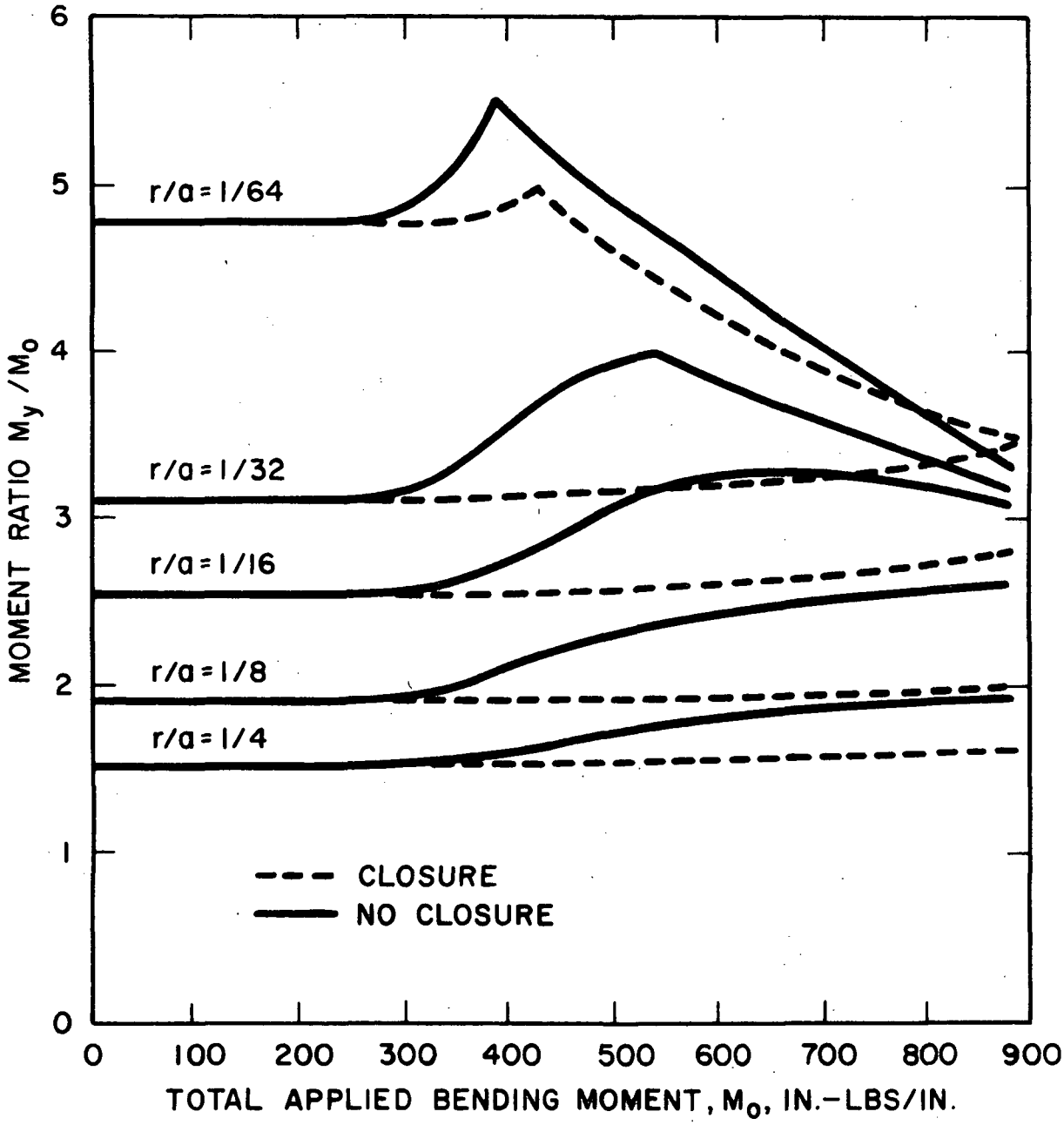

FIGURE 5-21
CRACK TIP BLUNTING DUE
TO ELASTO-PLASTIC FLOW

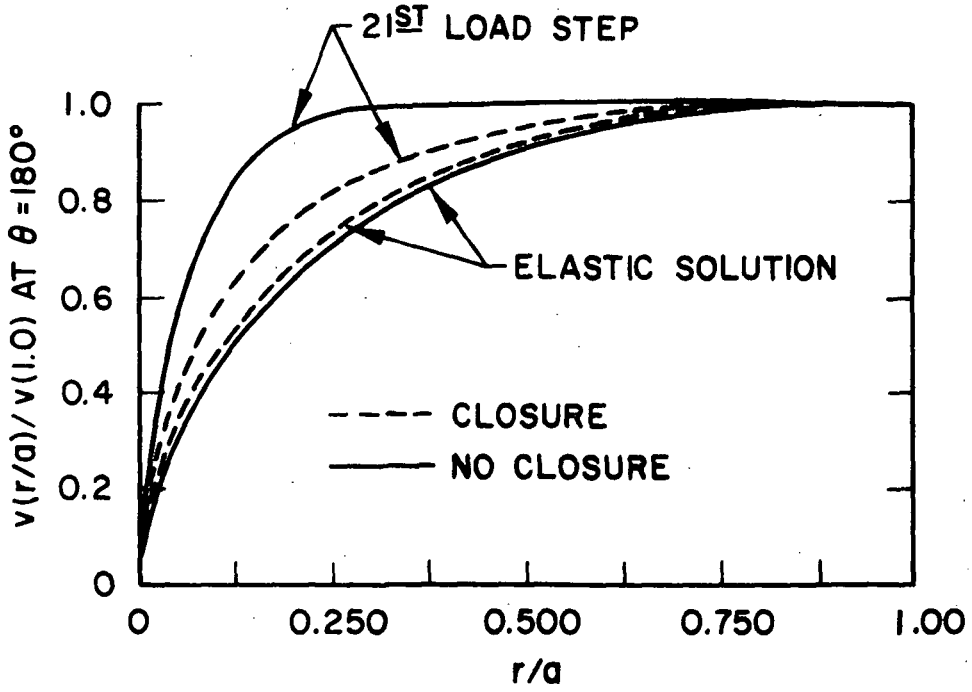

In Figures (5-22), contour plots of w, $\frac{\partial w}{\partial x}$, and $\frac{\partial w}{\partial y}$ are shown. Comparing these with the elastic results of Figures (5-2), (5-3), and (5-4) show that yielding has caused little change in behavior. This is due to the very local character of the crack tip yielding not affecting overall plate behavior.

FIGURE 5-22
CONTOUR PLOTS OF W, $\partial w/\partial x$ & $\partial w/\partial y$ AT THE MAXIMUM LOAD STEPS

NO CLOSURE

CLOSURE

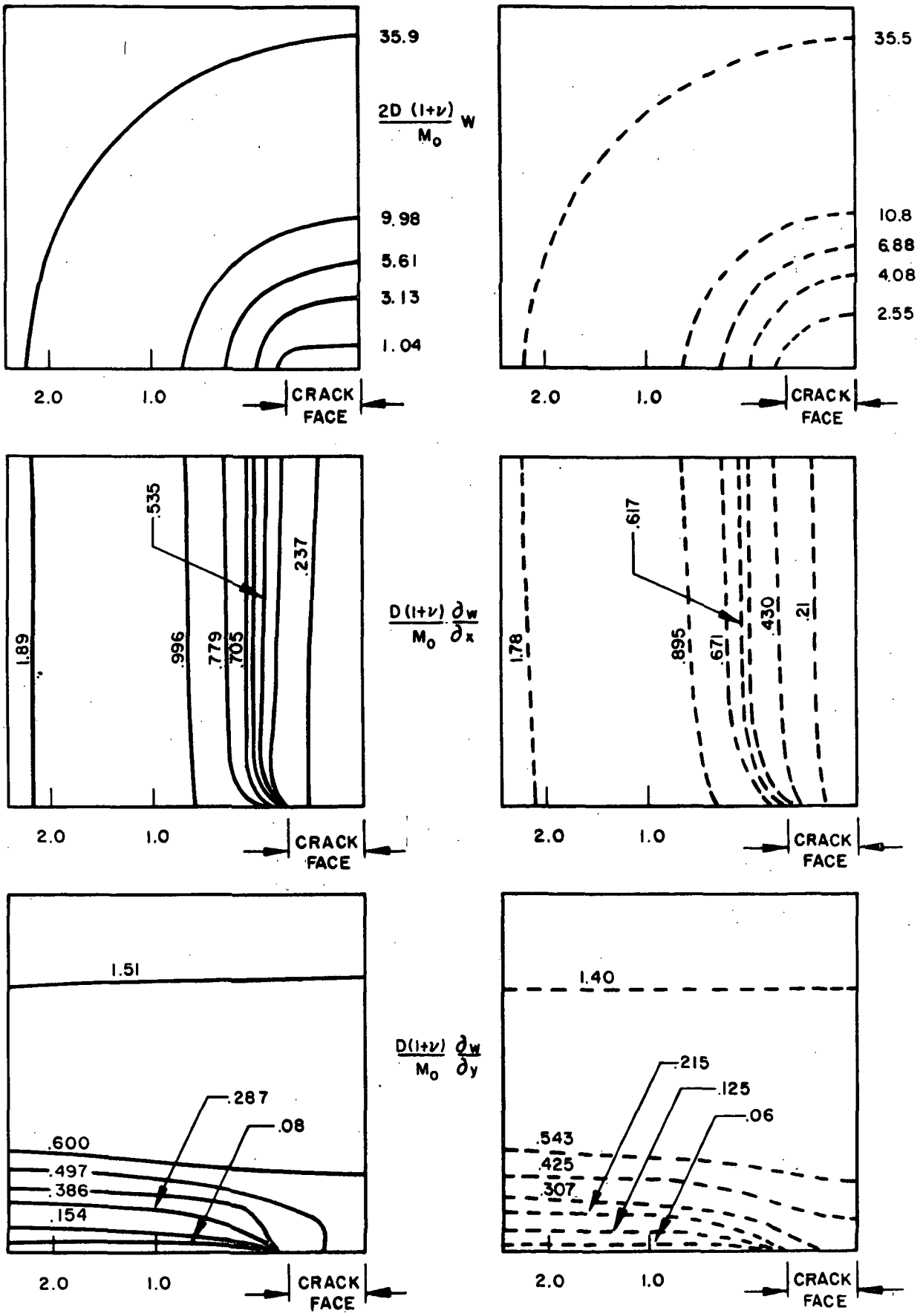

CHAPTER VI

FURTHER REMARKS

A numerical solution to the problem of a centrally cracked plate subject to a circular bending field has been obtained. The distinguishing features of the solutions are that they allow isolation of the effects of crack closure and elasto-plastic material behavior. The numerical capability used to generate the solutions incorporates classic Kirchhoff plate theory assumptions with elasto-plastic work hardening material behavior. The results indicate that crack closure and elasto-plasticity are important considerations in the mechanics of through cracked plates subject to bending.

6.1 Conclusions

Specific conclusions with regard to this work are as follows:

1. The effects of crack closure are significant in the mechanics of through crack bending and must be given consideration in the physical assessment of the problem.
2. Neglect of the crack closure phenomena results in non-conservative calculations for crack opening displacements and bending stress intensities based on linear elastic fracture mechanics concepts.
3. The most sensitive parameter to the crack closure phenomena is the transverse slope with respect to the direction normal to the crack face. ($\partial w/\partial y$)

4. Neutral axis shifts, based on displacement measurements, clearly monitor the crack closure phenomena. As plastic yielding builds up, neutral axis shifts become less pronounced.
5. Superimposing tension on exterior boundaries to preclude contact on the compressive surface due to bending does not model the crack closure phenomena in a physically realistic fashion.
6. The Dugdale or strip model as applied to plate bending does not adequately model the elasto-plastic problem as it does not include the elastic core consideration.
7. Plastic straining first occurs on the tensile surface of the plate and proceeds part-way through the thickness before yielding occurs on the compressive edge for the closure case.
8. Inclusion of crack closure in the analysis inhibits plastic straining when compared to analysis neglecting closure, at least for the circular bending problem.

6.2 Recommendations for Further Research

The principal difficulty encountered in this work was the free surface approximation required by Kirchhoff plate theory. Knowles and Wang [3] have shown that reformulation of the problem in terms of Reissner sixth order theory precludes this difficulty and results in solutions more compatible with the extensional case. Still, the crack closure phenomena has not been included and, based on these findings using Kirchhoff theory,

its significance needs to be evaluated using the higher order theory. A possible approach in this direction would be to employ Reissner plate theory in conjunction with the crack closure treatment used here.

The inclusion of the geometric non-linearities with the associated coupling of in-plane and bending behavior needs to be evaluated especially with reference to the combined extension/bending problem. Formulation of this type of complex problem can be made more tractable through numerical determination of stationary points of functionals as used in this work. The conjugate gradient method may be formulated to find stationary values of non-linear problems as in [30] and [33].

Short of solving the complete three dimensional contact problem, experimental investigations are required to verify the assumptions made here regarding crack closure and to further evaluate the three dimensional effects of the crack closure phenomena. Particular interest lies in the evaluation of crack face warping, generation of through thickness stress variations, plate thickness to crack length ratio effects, and the influence of plate exterior boundaries on the stress and strain field data.

Use of the solution capability to solve other bending problems of technical interest is also indicated. Elasto-plastic solutions to plates with patterned cutouts and under various boundary conditions are possible. Using the linear constraint equation concept, connection matrices between structures can be developed that model many different boundary flexibilities. This is a useful capability both in the practical engineering sense and as a research tool.

BIBLIOGRAPHY

1. Inglis, C. E., "Stresses in a Plate Due to the Presence of Cracks and Sharp Corners," Trans. Institute of Naval Architects, Vol. 60, (1913), pp. 219-230.

2. Williams, M. L., "Surface Stress Singularities Resulting from Various Boundary Conditions in Angular Corners of Plates Under Bending," Proceedings, First U. S. National Congress of Applied Mechanics, (June 1951), pp. 325-329.

3. Knowles, J. K. and N. K. Wang, "On the Bending of an Elastic Plate Containing a Crack, Journal of Mathematics and Physics, (1961), pp. 223-236.

4. Folias, E. S., "A Finite Line Crack in a Pressurized Spherical Shell," International Journal of Fracture Mechanics, Vol. 1, (March 1965), pp. 20-46.

5. Wynn, R. H., "Fracture of Centrally Cracked Plates Under Combined Bending and Extensional Loading," Ph.D. Thesis, Virginia Polytechnic Institute, Engineering Mechanics, (February 1969).

6. Swedlow, J. L., M. L. Williams, and W. H. Yang, "Elasto-Plastic Stresses and Strains in Cracked Plates," Proceedings of the First International Conference on Fracture, (1965), Vol. 1, pp. 259-282.

7. Miyamoto H., M. Shiratori, and T. Miyoshi, "Analysis of Stress and Strain Distribution at the Crack Tip by Finite Element Method," Recent Advances in Matrix Methods of Structural Analysis and Design, The University of Alabama Press, University of Alabama, (1971), pp. 317-341.

8. Lee, C. H. and S. Kobayashi, "Elasto-Plastic Analysis of Plane Strain and Axisymmetric Flat Punch Indentation by the Finite Element Method," International Journal of Mechanical Sciences, Vol. 12, (1970), pp. 349-370.

9. Hutchinson, J. W., "Singular Behavior at the End of a Tensile Crack in a Hardening Material," Journal of Mechanics Physics Solids, Vol. 16, (1968), pp. 13-31.

10. Rice, J. R. and G. R. Rosengren, "Plane Strain Deformation Near a Crack Tip in a Power Law Hardening Material," Journal of Mechanics Physics Solids, Vol. 16, (1968), pp. 1-12.

11. Hutchinson, J. W., "Plastic Stress and Strain Fields at a Crack Tip," Journal of Mechanics Physics Solids, Vol. 16, (1968), pp. 337-347.

12. Gonzalez, H. Jr., and H. F. Brinson, "The Bending Dugdale Model," Virginia Polytechnic Institute and State University Report VPI-E-70-14, (August 1970).

13. Smith, D. G. and C. W. Smith, "A Photoelastic Evaluation of the Influence of Closure and Other Effects Upon the Local Bending Stresses in Cracked Plates," International Journal of Fracture Mechanics, Vol. 6, No. 3, (September 1970), pp. 305-318.

14. Williams, M. L. and R. H. Owens, "Stress Singularities in Angular Corners of Plates having Linear Flexural Rigidities for Various Boundary Conditions," Proceedings, Second U. S. National Congress of Applied Mechanics, (June 1954), pp. 407-411.

15. Williams, M. L., "Stress Singularities Resulting from Various Boundary Conditions in Angular Corners of Plates in Extension," Journal of Applied Mechanics, (December 1952), pp. 526-528.

16. Williams, M. L., "On the Stress Distribution at the Base of a Stationary Crack," Journal of Applied Mechanics, Vol. 24, (March 1957), pp. 109-114.

17. Irwin, G. R., "Analysis of Stresses and Strains Near the End of a Crack Transversing a Plate," Journal of Applied Mechanics, Vol. 24, (1957), pp. 361-364.

18. Westergaard, H. M., "Bearing Pressures and Cracks," Trans. ASME, Vol. 61, (1939), pp. A49-A53.

19. Williams, M. L., "The Bending Stress Distribution at the Base of a Stationary Crack," Journal of Applied Mechanics, Vol. 28, (March 1961), pp. 78-82.

20. Sih, F., P. Paris, and F. Erdogan, "Crack Tip Stress Intensity Factors for Plane Extension and Plate Bending Problems," Journal of Applied Mechanics, (June 1962), pp. 306-312.

21. Muskhelishvili, N. I., Some Basic Problems of Mathematical Theory of Elasticity, English translation, P. Noordhoff and Co., (1953).

22. Hartranft, R. J. and G. C. Sih, "Effect of Plate Thickness on the Bending Stress Distribution Around Through Cracks," Journal of Mathematics and Physics, 47, 3 (1968), pp. 276-281.

23. Erdogan, F., O. Tuncel, and P. Paris, "An Experimental Investigation of the Crack Tip Stress Intensity Factors in Plates Under Cylindrical Bending," Trans. ASME, Journal of Basic Engineering, (1962), pp. 542-546.

24. Smith, D. G. and C. W. Smith, "Influence of Precatastrophic Extension and Other Effects on Local Stresses in Cracked Plates Under Bending Fields," VPI-E-70-19, (November 1970).

25. Rice, J. R., "A Path Independent Integral and the Approximate Analysis of Strain Concentration by Notches and Cracks," Journal of Applied Mechanics, Vol. 35, (1968), pp. 379-386.

26. Rice, J. R. and D. M. Tracey, "Computational Fracture Mechanics," presented at the International Symposium on Numerical and Computer Methods in Structural Mechanics, Sponsored by the Office of Naval Research and the University of Illinois at Urbana-Champaign, Urbana, Illinois, (September 8-10, 1971).

27. Swedlow, J. L., "Initial Comparisons between Experiment and Theory of the Strain Fields in a Cracked Copper Plate," International Journal of Fracture Mechanics, Vol. 5, (March 1969), pp. 25-31.

28. Levy, N., P. V. Marcal, W. J. Ostergren, and J. R. Rice, "Small Scale Yielding Near a Crack in Plane Strain: A Finite Element Analysis," International Journal of Fracture Mechanics, Vol. 7, (1971), pp. 143-156.

29. Swedlow, J. L., "Character of the Equations of Elasto-Plastic Flow in Three Independent Variables," Int. J. Non-Linear Mechanics, Vol. 3, pp. 325-336, (1968).

30. Bogner, F. K., R. L. Fox, and L. A. Schmit, "Finite Deflection Analysis Using Plate and Cylindrical Shell Discrete Elements," AIAA/ASME 8th Structures, Structural Dynamics and Materials Conference, AIAA, New York, (1967), pp. 197-211.

31. Tong, P. and T. H. H. Pian, "The Convergence of Finite Element Methods in Solving Linear Elastic Problems," International Journal of Solids and Structures 3, (1967), pp. 865-879.

32. Birkhoff, G., M. H. Schultz, and R. S. Varga, "Piecewise Hermite Interpolation in One and Two Variables with Application to Partial Differential Equation," Numerical Mathematik 14, (1968), pp. 232-256.

33. Fox, R. L. and E. L. Stanton, "Developments in Structural Analysis by Direct Energy Minimization," AIAA Journal 6, (June 1968), pp. 1036-1042.

34. Beckman, F. S., "The Solution of Linear Equations by the Conjugate Gradient Method," Mathematical Methods for Digital Computers, Ralston, A., and Wilf, H. S. (Eds.), Wiley, (1960), pp. 62-72.

35. Bogner, F. K., "Finite Deflection, Discrete Element Analysis of Shells," AFFDL-TR-67-185, Air Force Flight Dynamics Laboratory, Wright-Patterson Air Foce Base, Ohio (June 1968).

36. Shieh, W., "Analysis of Plate and Shell Structures by Triangular Finite Elements," Ph.D. Dissertation, Northwestern University (1968).

37. Stanton, E. L. and L. A. Schmit, "A Discrete Element Stress and Displacement Analysis of Elasto-Plastic Plates," AIAA Journal 8, 7, (July 1970), pp. 1245-1251.

38. Key, S. W., "A Convergence Investigation of the Direct Stiffness Method," Ph.D. Thesis, Dept. of Aeronautics and Astronautices, University of Washington, Seattle, Washington (1968).

39. Hildebrand, F. B., Introduction to Numerical Analysis, McGraw-Hill Book Co., New York (1956).

40. Gisvold, K. M. and J. Moe, "Buckling Analysis by Means of Non-Linear Programming," International Journal for Numerical Methods in Engineering 2, (1970), pp. 351-361.

41. Beveridge, G. S. G. and R. S. Schechter, Optimization Theory and Practice, McGraw-Hill Book Co., (1970).

42. Box, M. J., "A New Method of Constrained Optimization and Comparison with Other Methods," Computer Journal 8, (April 1965), pp. 42-52.

43. Timoshenko, S. P. and Woinowsky-Krieger, Theory of Plates and Shells, McGraw-Hill Book Co., New York, (1959).

44. Swedlow, J. L. and M. L. Williams, "A Review of Recent Investigations into Fracture at GALCIT," A.R.L. 64-175, (October 1964).

45. Callabresi, M. L., "Inelastic Stress Analysis of Solids," Ph.D. Thesis, University of Arizona, Civil Engineering, (1970).

46. Fried, I., "A Gradient Computational Procedure for the Solution of Large Problems Arising from the Finite Element Discretization Method," International Journal for Numerical Methods in Engineering, Vol. 2, (1970), pp. 477-494.

47. Jones, D. P., "A Discrete Element Analysis of Elasto-Plastic Beam and Plate Structures by Energy Minimization," Carnegie-Mellon University, Dept. of Mechanical Engineering, Report SM-61, (May 1971).

48. Brinson, H. F., J. H. Underwood, and A. R. Rosenfield, "Yield Zones in Polymeric and Metallic Plates Under Pure Bending Containing a Through Crack," Virginia Polytechnic Institute and State University, College of Engineering, VPI-E-72-7, (April 1972).

APPENDIX A

CONSTITUTIVE EQUATION FOR PLANE STRESS

For plane stress, the constitutive relation of Equation (3-9) is:

$$[E] = \frac{E}{(1-\nu^2)\Delta}\begin{bmatrix} 1+FS_y^2 + \frac{2F}{1+\nu}S_{xy}^2 & \nu-FS_xS_y + \frac{2\nu F}{1+\nu}S_{xy}^2 & -\frac{F}{1+\nu}(S_x+\nu S_y)S_{xy} \\ \nu-FS_yS_x+\frac{2\nu F}{1+\nu}S_{xy}^2 & 1+FS_x^2 + \frac{2F}{1+\nu}S_{xy}^2 & -\frac{F}{1+\nu}(\nu S_x+S_y)S_{xy} \\ -\frac{F}{1+\nu}(\nu S_y+S_x)S_{xy} & -\frac{F}{1+\nu}(S_y+\nu S_x)S_{xy} & \frac{1-\nu}{2}+\frac{F}{2(1+\nu)}[S_x^2+S_y^2+2\nu S_xS_y] \end{bmatrix}$$

where

$$\Delta = 1 + \frac{F}{1-\nu^2}(S_x + S_y)^2 + \frac{2F}{1+\nu}(S_{xy}^2 - S_xS_y)$$

$$S_x = 1/3(2\sigma_x - \sigma_y) \qquad S_y = 1/3(2\sigma_y - \sigma_x)$$

$$F = E/6\tau_o^2\mu_{eq} \qquad 2\mu_{eq} = d\tau_{eq}/d\tau_{eq}$$

For relations useful in Equation (3-8),

$$\phi = 2J_2/3, \quad \phi_{ij} = S_{ij}/3\phi, \quad (\tau_{eq} = \tau_o)$$

$$d\varepsilon_{eq}^{(p)} = 3d\varepsilon_{ij}^{(p)}\, d\varepsilon_{ij}^{(p)}$$

APPENDIX B

BICUBIC HERMITE INTERPOLATION FORMULAS

Displacement rate vector $\{\dot{u}\}$ and bicubic Hermite interpolation formulas used in Section IV.

$$\{\dot{u}\} = \begin{Bmatrix} \dot{u}_{11} \\ \dot{u}_{x11} \\ \dot{u}_{y11} \\ \dot{u}_{xy11} \\ \dot{u}_{12} \\ \dot{u}_{x12} \\ \dot{u}_{y12} \\ \dot{u}_{xy12} \\ \dot{u}_{21} \\ \dot{u}_{x21} \\ \dot{u}_{y21} \\ \dot{u}_{xy21} \\ \dot{u}_{22} \\ \dot{u}_{x22} \\ \dot{u}_{y22} \\ \dot{u}_{xy22} \end{Bmatrix} \qquad \{P(x,y)\} = \begin{Bmatrix} H_{01}(x) \cdot H_{01}(y) \\ H_{11}(x) \cdot H_{01}(y) \\ H_{01}(x) \cdot H_{11}(y) \\ H_{11}(x) \cdot H_{11}(y) \\ H_{01}(x) \cdot H_{02}(y) \\ H_{11}(x) \cdot H_{02}(y) \\ H_{01}(x) \cdot H_{12}(y) \\ H_{11}(x) \cdot H_{12}(y) \\ H_{02}(x) \cdot H_{01}(y) \\ H_{12}(x) \cdot H_{01}(y) \\ H_{02}(x) \cdot H_{11}(y) \\ H_{12}(x) \cdot H_{11}(y) \\ H_{02}(x) \cdot H_{02}(y) \\ H_{12}(x) \cdot H_{02}(y) \\ H_{02}(x) \cdot H_{12}(y) \\ H_{12}(x) \cdot H_{12}(y) \end{Bmatrix}$$

$$\dot{u}_{xij} = \left.\frac{\partial \dot{u}}{\partial x}\right|_{\text{at corner } i,j}; \qquad H_{ij} = \text{Hermite Interpolation Formula}$$

Displacement rates $\{\dot{v}\}$ and $\{\dot{w}\}$ are similar to $\{\dot{u}\}$.

APPENDIX C

ON THE DERIVATION OF FIELD EQUATIONS CHARACTERIZING THE ELASTO-PLASTIC BEHAVIOR OF VARIOUS SITUATIONS

Using Theorem I developed in Chapter III, it is possible to derive field equations of elasto-plastic flow for various physical situations. Using the strain-rate, displacement-rate relation

$$\dot{\varepsilon}_{ij} = \tfrac{1}{2}(\dot{u}_{i,j} + \dot{u}_{j,i}) \tag{c-1}$$

Equation (3-18), which is the condition for equilibrium, can be written as

$$\int_V E_{ijk\ell}\dot{u}_{i,j}\delta\dot{u}_{k,\ell}dV - \int_{S_\sigma} \overset{\nu}{\dot{T}}_k\delta\dot{u}_k dS = 0 \tag{c-2}$$

Integrating Equation (c-2) by parts produces surface and volume integrals plus constants of integration. Using the fundamental lemma of calculus of variations, this procedure will lead to field equations and complete boundary conditions.

In the following sections, theories for plane stress/strain, St. Venant torsion, simple beam theory, and plate bending theory are presented to show both the adequacy of Equation (c-2) and to provide a convenient reference for the various elasto-plastic field theories.

C-1 Plane Stress/Strain

Referring to Figure C-1, the usual plane stress assumptions are

$$\dot{\sigma}_{xz} = \dot{\sigma}_{yz} = \dot{\sigma}_{zz} = 0 \tag{c-3}$$

The constitutive equations are of the form

$$\begin{Bmatrix} \dot{\sigma}_x \\ \dot{\sigma}_y \\ \dot{\tau}_{xy} \end{Bmatrix} = [E] \begin{Bmatrix} \dot{\varepsilon}_x \\ \dot{\varepsilon}_y \\ \dot{\gamma}_{xy} \end{Bmatrix} \tag{c-4}$$

where [E] is given in detail for plane stress and plane strain in Appendix A. The volume integral can then be written per unit thickness as

$$\begin{aligned} \int_V E_{ijk\ell} \dot{u}_{i,j} \delta \dot{u}_{k,\ell} dV = \int_0^{x_o} \int_0^{y_o} \{ & [E_{11}\dot{u}_x + E_{12}\dot{v}_y + E_{13}(\dot{u}_y + \dot{v}_x)]\delta\dot{u}_x \\ & + [E_{13}\dot{u}_x + E_{22}\dot{v}_y + E_{23}(\dot{u}_y + \dot{v}_x)]\delta v_y \\ & + [E_{13}\dot{u}_x + E_{23}\dot{v}_y + E_{33}(\dot{u}_y + v_x)]\delta(\dot{u}_y + \dot{v}_x)\} dxdy \end{aligned} \tag{c-5}$$

The surface integral is

$$\int_{S_\nabla} \dot{T}_i \delta \dot{u}_i dS = -\int_0^{y_o} \dot{N}_x \delta\dot{u} dy - \int_0^{y_o} \dot{N}_{xy} \delta\dot{v} dy - \int_0^{x_o} \dot{N}_{yx} \delta\dot{u} dx - \int_0^{x_o} \dot{N}_y \delta\dot{v} dx \tag{c-6}$$

FIGURE C-1
PLANE STRESS GEOMETRY FOR THE STRETCHING THEORY

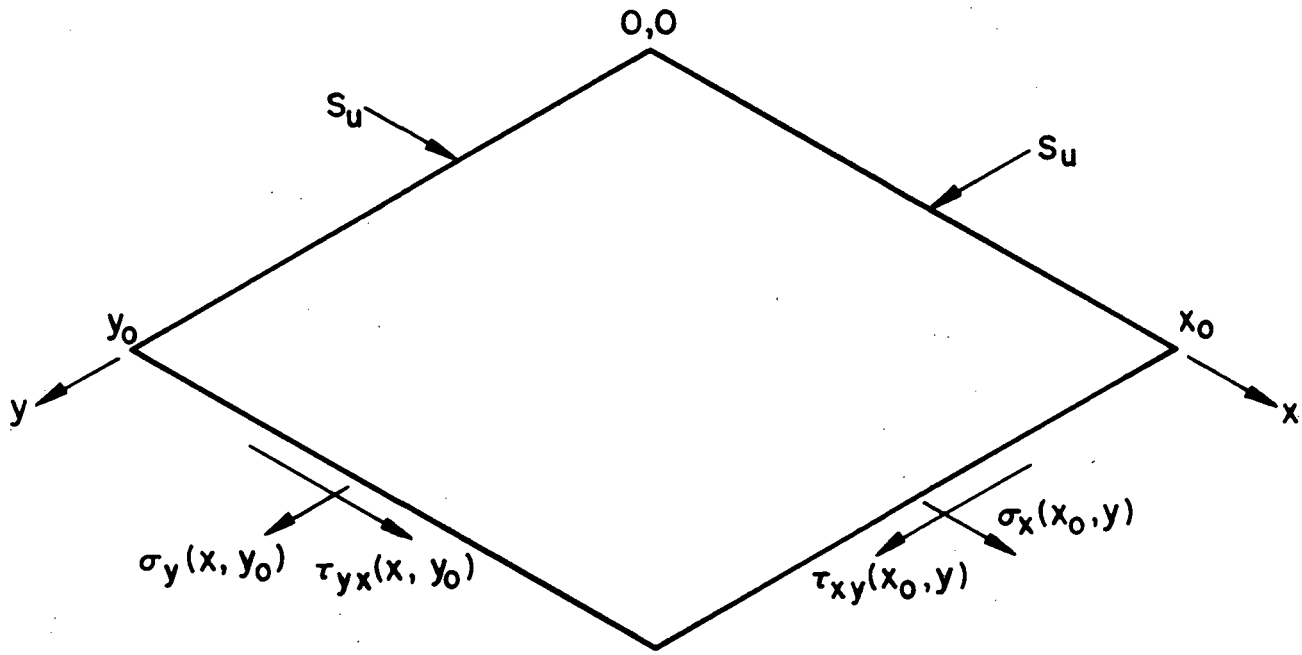

SURFACE TRACTIONS:

$$N_x = \int_0^{y_o} \sigma_x(x_o, y)\, dy$$

$$N_y = \int_0^{x_o} \sigma_y(x, y_o)\, dx$$

$$N_{xy} = \int_0^{y_o} \tau_{xy}(x_o, y)\, dy$$

Integrating by parts and applying the fundamental lemma of variational calculus results in the field equations

$$E_{11}\dot{u}_{xx} + 2E_{13}\dot{u}_{xy} + (E_{33} + E_{12})\dot{v}_{xy} + E_{13}\dot{v}_{xx} + E_{23}\dot{v}_{yy}$$

$$+ (E_{11,x} + E_{13,y})\dot{u}_x + (E_{12,x} + E_{23,y})\dot{v}_y$$

$$+ (E_{13,x} + E_{33,y})(\dot{u}_y + \dot{v}_x) = 0 \qquad (c\text{-}7)^*$$

and

$$E_{22}\dot{v}_{yy} + 2E_{23}\dot{v}_{xy} + E_{33}\dot{v}_{xx} + E_{23}\dot{u}_{yy} + (E_{33} + E_{12})\dot{u}_{xy} + E_{13}\dot{u}_{xx}$$

$$+ (E_{22,y} + E_{23,x})\dot{v}_y + (E_{12,y} + E_{13,x})\dot{u}_x$$

$$+ (E_{33,x} + E_{23,y})(\dot{v}_x + \dot{u}_y) = 0 \qquad (c\text{-}8)^*$$

with the complete boundary conditions at $y = y_o$ or $y = 0$

$$\begin{cases} E_{13}\dot{u}_x + E_{23}\dot{v}_y + E_{33}(\dot{u}_y + \dot{v}_x) - \dfrac{\dot{N}_{yx}}{2Z_o} = 0 & \text{or } \dot{u} \text{ Specified} \\ E_{12}\dot{u}_x + E_{22}\dot{v}_y + E_{23}(\dot{u}_y + \dot{v}_x) - \dfrac{\dot{N}_y}{2Z_o} = 0 & \text{or } \dot{v} \text{ Specified} \end{cases} \qquad (c\text{-}9)$$

---

* See J. L. Swedlow, "Character of the Equations of Elasto-Plastic Flow in Three Independent Variables," Int. J. Non-Linear Mechanics, Vol. 3, pp. 325-336, 1968, for verification of these equations.

at $x = x_o$ or $x = 0$

$$\begin{cases} E_{11}\dot{u}_x + E_{12}\dot{v}_y + E_{13}(\dot{u}_y + \dot{v}_x) - \dfrac{N_x}{2Z_o} = 0 \quad \text{or } \dot{u} \quad \text{Specified} \\ E_{13}\dot{u}_x + E_{23}\dot{v}_y + E_{33}(\dot{u}_y + \dot{v}_x) - \dfrac{N_{xy}}{2Z_o} = 0 \quad \text{or } \dot{v} \quad \text{Specified} \end{cases} \tag{c-10}$$

C-2 St. Venant Torsion

The usual St. Venant torsion assumptions using the notation of Figure C-2 are

$$\dot{\sigma}_x = \dot{\sigma}_y = \dot{\sigma}_z = \dot{\tau}_{xy} = 0 \tag{c-11}$$

and kinematically

$$\dot{u} = -\theta(t)yx \qquad \dot{v} = \theta(t)xz \qquad \dot{w} = \dot{w}(x,y,t) \tag{c-12}$$

The constitutive relation is

$$\begin{Bmatrix} \dot{\varepsilon}_{xz} \\ \dot{\varepsilon}_{yz} \end{Bmatrix} = \frac{1}{\mu} \begin{bmatrix} 1 + \dfrac{\beta^2 \tau_{xz}^2}{J_2} & \dfrac{\beta^2 \tau_{yz}\tau_{xz}}{J_2} \\ \dfrac{\beta^2 \tau_{yz}\tau_{xz}}{J_2} & 1 + \dfrac{\beta^2 \tau_{yz}^2}{J_2} \end{bmatrix} \begin{Bmatrix} \dot{\tau}_{xz} \\ \dot{\tau}_{yz} \end{Bmatrix} \tag{c-13}$$

FIGURE C-2
GEOMETRY FOR ST. VENANT TORSION THEORY

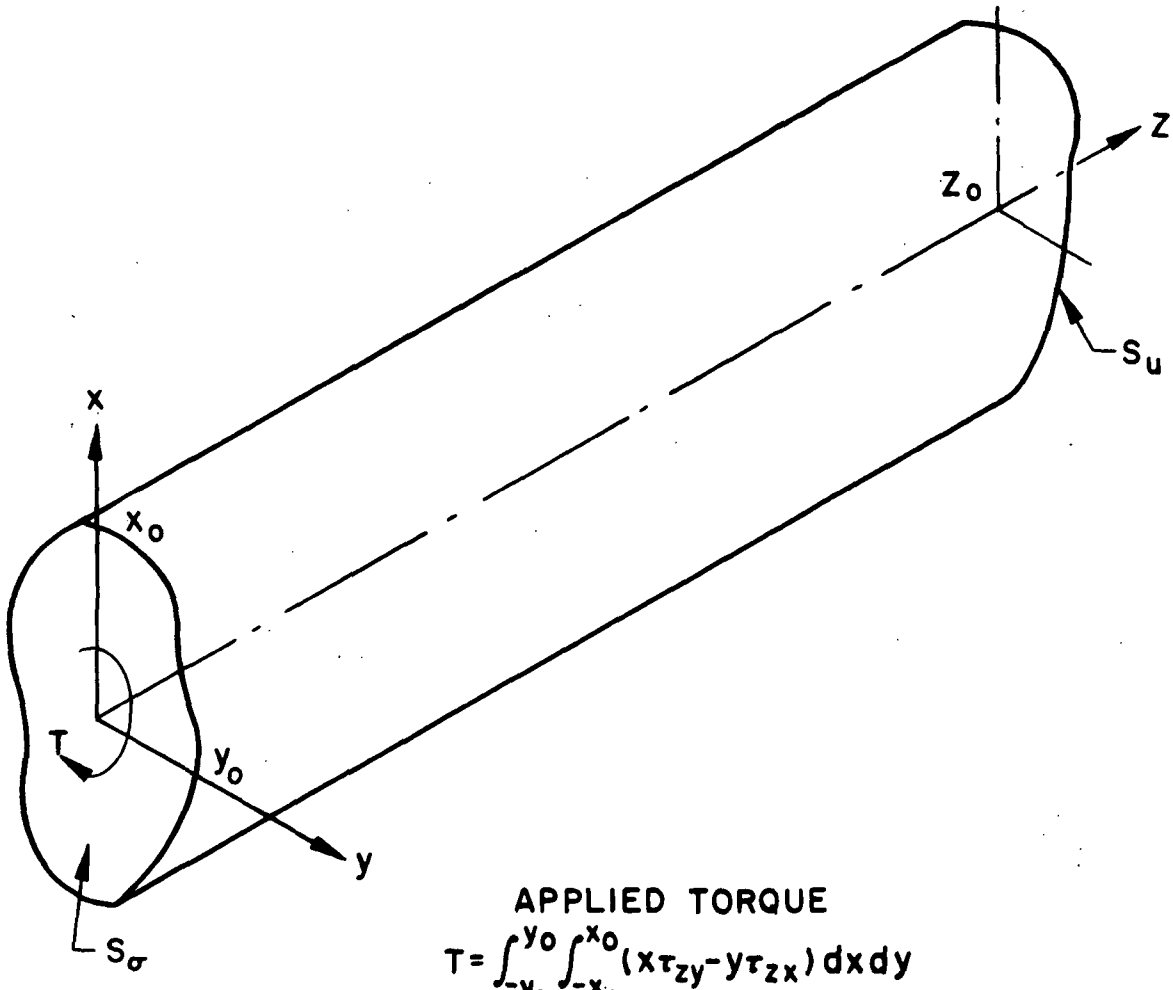

APPLIED TORQUE

$$T = \int_{-y_o}^{y_o} \int_{-x_o}^{x_o} (x\tau_{zy} - y\tau_{zx})\, dx\, dy$$

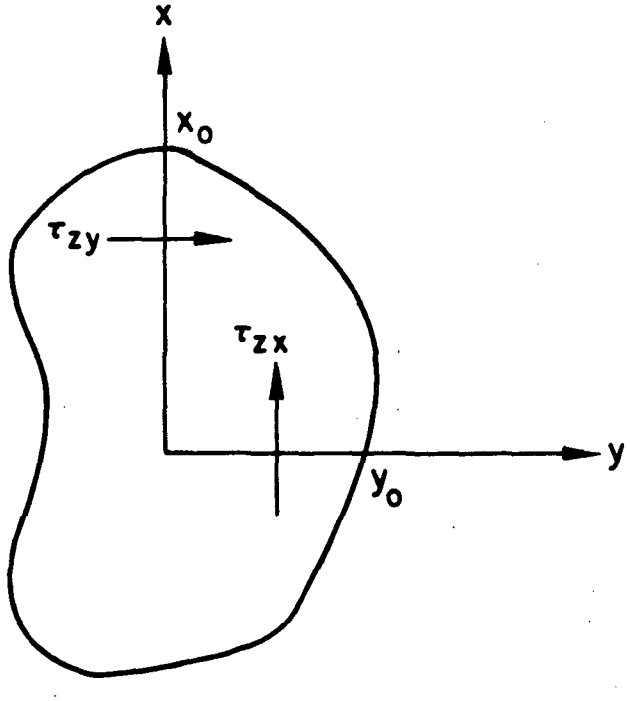

This can be inverted to be in the form

$$\{\dot{\tau}\} = [E]\{\dot{\varepsilon}\} \tag{c-14}$$

The strain-rate, displacement-rate equations are

$$\dot{\varepsilon}_{xz} = [\dot{w}_x + \dot{u}_z] \quad \dot{\varepsilon}_{yz} = [\dot{v}_z + \dot{w}_y] \tag{c-15}$$

Equation (c-2) can now be written as

$$\int_V [E] \begin{Bmatrix} \dot{w}_x + \dot{u}_z \\ \dot{v}_z + \dot{w}_y \end{Bmatrix} \delta \begin{Bmatrix} \dot{w}_x + \dot{u}_z \\ \dot{v}_z + \dot{w}_y \end{Bmatrix} dV - \int_{S_\sigma} \overset{\nu}{\dot{T}}_i \delta \dot{u}_i dS = 0 \tag{c-16}$$

with the surface term being

$$\int_{S_\sigma} \overset{\nu}{\dot{T}}_i \delta \dot{u}_i dS = \int_{-x_o}^{x_o} \int_{-y_o}^{y_o} (\tau_{zx}\dot{v} + \tau_{zy}\dot{u}) \Big|_{z=z_o} dxdy \tag{c-17}$$

Integrating Equation (c-16) and (c-17) by parts and applying the fundamental lemma results in the following theory for St. Venant torsion of an elasto-plastic rod;

Differential equation

$$E_{11}\dot{w}_{xx} + 2E_{12}\dot{w}_{xy} + E_{22}\dot{w}_{yy} + \alpha_1\dot{w}_x + \alpha_2\dot{w}_y = -\alpha_1\dot{u}_z - \alpha_2\dot{v}_z$$

where

$$\alpha_1 = E_{11,x} + E_{12,y}$$

$$\alpha_2 = E_{22,y} + E_{12,x} \qquad \text{(c-18)}$$

subject to the boundary conditions at $z = z_o$

$$\begin{cases} E_{11}\dot{w}_x + E_{11}\dot{u}_z + E_{12}(\dot{w}_y + \dot{v}_z) - \tau_{xz} = 0 \quad \text{or} \quad \dot{u} \quad \text{Specified} \\ \text{and} \\ E_{12}(\dot{w}_x + \dot{u}_z) + E_{22}[\dot{v}_z + \dot{w}_y] - \tau_{yz} = 0 \quad \text{or} \quad \dot{v} \quad \text{Specified} \end{cases} \qquad \text{(c-19)}^*$$

$$\begin{cases} E_{11}(\dot{w}_x + \dot{u}_z) + E_{12}(\dot{w}_y + \dot{v}_z) = 0 \quad @\ x = x_o \text{ or } \dot{w} \quad \text{Specified} \\ \\ E_{12}(\dot{w}_x + \dot{u}_z) + E_{22}(\dot{w}_y + \dot{v}_z) = 0 \quad @\ y = y_o \text{ or } \dot{w} \quad \text{Specified} \end{cases} \qquad \text{(c-20)}^*$$

where

$$\dot{v}_z = \theta(t)x \quad \text{and} \quad \dot{u}_z = -\theta(t)y$$

τ_{xz}, τ_{yz} are specified on the boundary such that the applied torque at the $z = z_o$ end would be

$$T = \int_{-y_o}^{y_o} \int_{-x_o}^{x_o} (x\tau_{yz} - y\tau_{xz})dxdy \qquad \text{(c-21)}$$

---

* See J. L. Swedlow, "Character of the Equations of Elasto-Plastic Flow in Three Independent Variables," Int. J. Non-Linear Mechanics, Vol. 3, pp. 325-336, 1968, for verification of these equations.

C-3 Simple Beam Theory

The usual assumptions accompanying simple beam theory consistent with the notation of Figure C-3 are:

1. Planes remain plane; i.e., the total strain distribution through thickness of the beam is linear.
2. Effects of z-direction are neglected.
3. Transverse deflection is a function of x only.

From assumption 1, the strain, displacement-rate equation can be written as

$$\dot{\varepsilon}_x = \dot{u}^S_x - y\dot{v}_{xx}, \qquad \dot{\varepsilon}_y = \dot{\varepsilon}_z = \dot{\gamma}_{xy} = \dot{\gamma}_{xz} = \dot{\gamma}_{yz} = 0 \qquad \text{(c-22)}$$

where $\dot{u}^S$ implies the extensional displacement associated with the mid-plane of the beam.

The constitutive relation of the plane stress problem reduces to

$$\dot{\sigma}_x = E_{11}\dot{\varepsilon}_x$$

The volume integral of Equation

$$\int_V E_{ijk\ell}\dot{u}_{i,j}\delta\dot{u}_{k,\ell}dV = \int_{-z_o}^{z_o}\int_{-y_o}^{y_o}\int_o^{\ell}\{E_{11}\dot{u}^S_x\delta\dot{u}^S_x - E_{11}y[\dot{u}^S_x\delta\dot{v}_{xx} + \dot{v}_{xx}\delta\dot{u}^S_x] + E_{11}y^2\dot{v}_{xx}\delta\dot{v}_{xx}\}dxdydz \qquad \text{(c-23)}$$

FIGURE C-3
GEOMETRY AND LOADING FOR BEAM THEORY

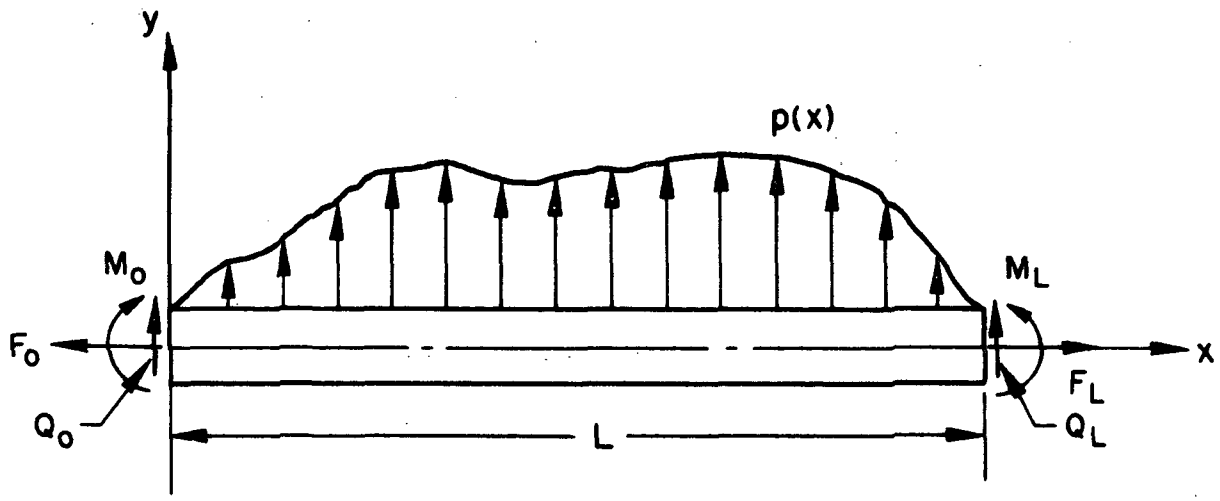

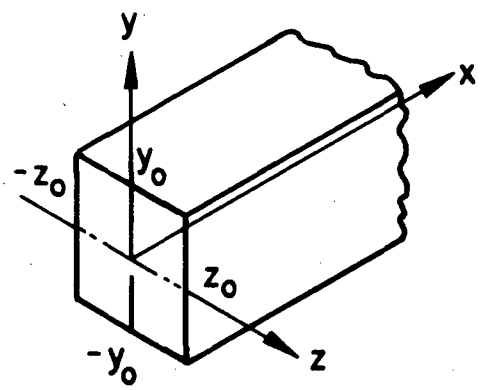

$$F = \int_{-y_o}^{y_o} \sigma_x \, dy$$

$$M = \int_{-y_o}^{y_o} \sigma_x \, y \, dy$$

$$Q = \int_{-y_o}^{y_o} \tau_{xy} \, dy$$

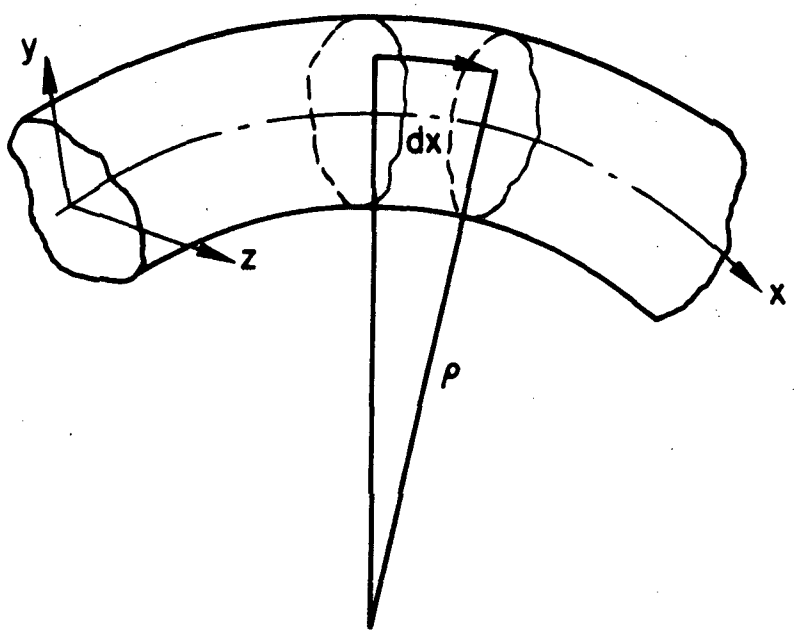

Defining

$$C_1 = 2t\int_{-y_o}^{y_o} E_{11}dy \quad C_2 = 2t\int_{-y_o}^{y_o} E_{11}ydy \quad C_3 = 2t\int_{-y_o}^{y_o} E_{11}y^2dy$$

then Equation (c-23) becomes

$$\int_V E_{ijk\ell}\dot{u}_{i,j}\delta\dot{u}_{k,\ell}dV = \int_o^L [C_1\dot{u}_x^S\delta\dot{u}_x^S - C_2(\dot{u}_x^S\delta\dot{v}_{xx} + \dot{v}_{xx}\delta\dot{u}_{xx}^S) + C_3\dot{v}_{xx}\delta\dot{v}_{xx}]dx \qquad (c\text{-}24)$$

Note that for elasticity, $E_{11} = E/1-\nu^2$ a constant. Hence, $C_1 = 4Ety_o/1-\nu^2$, $C_2 = 0$, and $C_3 = EI/(1-\nu^2)$. Since $C_2 = 0$, the bending and stretching modes decouple in the elastic case. However, the coupling between in-plane and transverse displacements is present in elasto-plastic beam theory.

The surface integral is written as

$$\int_{S_\sigma} \dot{T}\delta u_i dS = \int_o^L p\delta\dot{v}dx - M_o\delta\dot{v}_x\Big|_o + M_L\delta\dot{v}_x\Big|_L + Q_o\delta\dot{v}\Big|_o - Q_L\delta\dot{v}\Big|_L + F_L\delta\dot{u}\Big|_L - F_o\delta\dot{u}\Big|_o \qquad (c\text{-}25)$$

Integrating Equations (c-24) and (c-25) by parts twice and applying the fundamental lemma, the resulting differential equations theory for elasto-plastic beams is

$$\begin{cases} (C_2\dot{u}_x^S)_{xx} - (C_3\dot{v}_{xx})_{xx} = -p \\ (C_1\dot{u}_x^S)_x - (C_2\dot{v}_{xx})_x = 0 \end{cases} \qquad \text{(c-26)}$$

subject to the boundary conditions at x = L

$$\begin{cases} C_1\dot{u}_x^S - C_2\dot{v}_{xx} - F_L = 0 & \text{or} \quad \dot{u}^S \quad \text{Specified} \\ (C_2\dot{u}_x^S)_x - (C_3\dot{v}_{xx})_x + Q_L = 0 & \text{or} \quad \dot{v} \quad \text{Specified} \\ -(C_2\dot{u}_x^S) + C_3\dot{v}_{xx} - M_L = 0 & \text{or} \quad \dot{v}_x \quad \text{Specified} \end{cases} \qquad \text{(c-27)}$$

at x = 0

$$\begin{cases} -C_1\dot{u}_x^S + C_2\dot{v}_{xx} + F_o = 0 & \text{or} \quad \dot{u}^S \quad \text{Specified} \\ -(C_2\dot{u}_x^S)_x + (C_3\dot{v}_{xx})_x - Q_o = 0 & \text{or} \quad \dot{v} \quad \text{Speicified} \\ C_2\dot{u}_x^S - C_3\dot{v}_{xx} + M_o = 0 & \text{or} \quad \dot{v}_x \quad \text{Specified} \end{cases} \qquad \text{(c-28)}$$

For elastic problems as noted, $C_2 = 0$ and the above equations reduce to uncoupled elastic simple beam and uniaxial tension problem.

C-4 Plate Bending Theory

Elasto-plastic plate bending theory may be derived by making kinematic assumptions similar to Kirchhoff bending theory. These assumptions include:

1. Deflections are small compared to the thickness of the plate and the slope is small compared to one.
2. State of plane stress exists in the plane of the plate, i.e., $\dot{\sigma}_z = \dot{\tau}_{xz} = \dot{\tau}_{yz} = 0$.
3. Total strain distribution is linear through the plate thickness.

For elasto-plastic plate theory, it is necessary to include the in-plane or membrane behavior as they do not decouple from the bending behavior as in elasticity. The plate and coordinate system are shown in Figure C-4.

The strain displacement relations are

$$\begin{aligned} \dot{\varepsilon}_x &= \dot{u}_x - Z\dot{w}_{xx} \\ \dot{\varepsilon}_y &= \dot{v}_y - Z\dot{w}_{yy} \\ \dot{\gamma}_{xy} &= \dot{u}_y + \dot{v}_x - 2Z\dot{w}_{xy} \end{aligned} \qquad \text{(c-29)}$$

and the constitutive law is identical to the plane stress case given in Equation (c-4).

FIGURE C-4
GEOMETRY AND LOADING FOR BENDING-STRETCHING THEORY

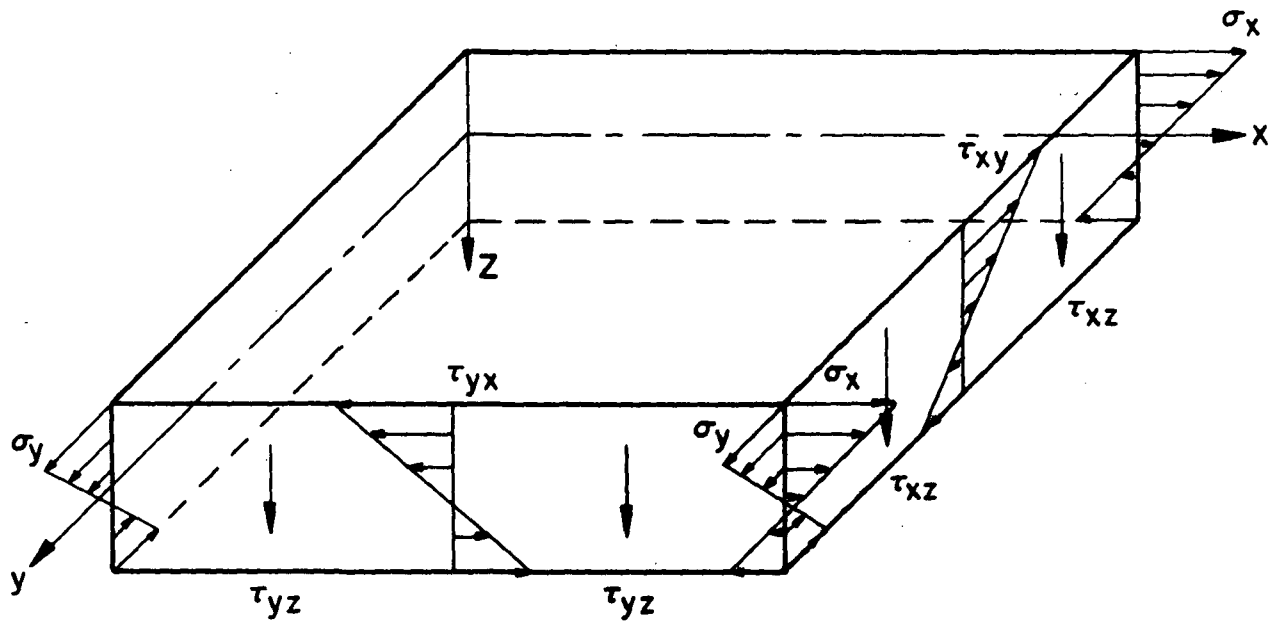

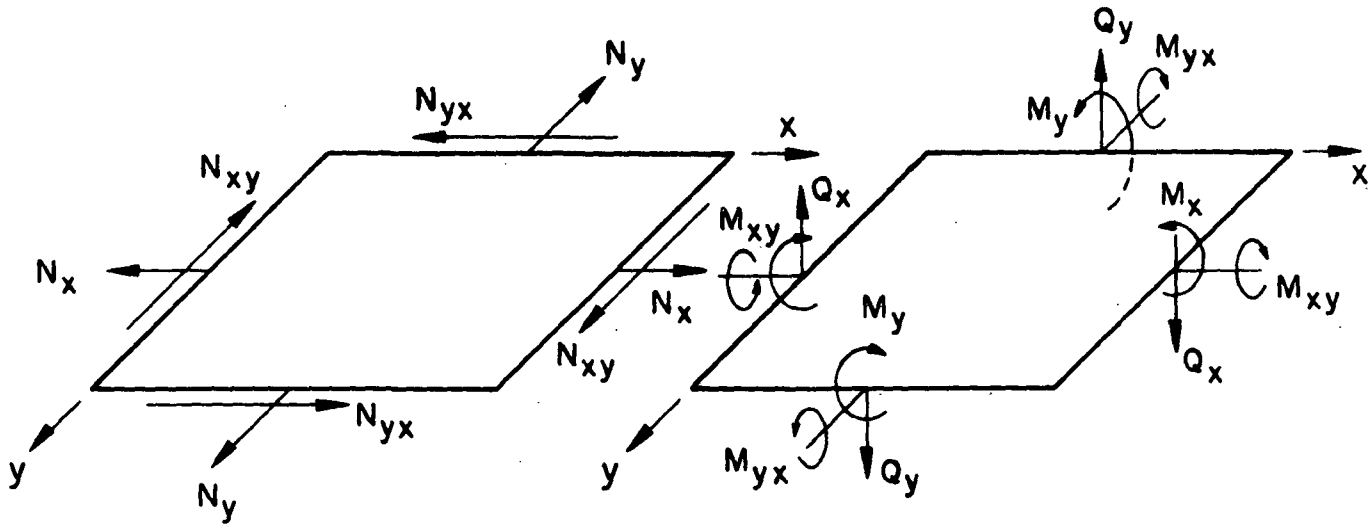

MEMBRANE (AVERAGE) LOADS

BENDING (LINEAR) LOADS

Using Equations (c-29) and (c-4), the volume integral of Equation (c-2) can be written as

$$\tfrac{1}{2}\int_V E_{ijk\ell}\dot{u}_{i,j}\,\dot{u}_{k,\ell}\,dV = \int_V \tfrac{1}{2}\{E_{11}[\dot{u}_x - Z\dot{w}_{xx}]^2 + 2E_{12}[\dot{u}_x - Z\dot{w}_{xx}][\dot{v}_y - Z\dot{w}_{yy}]$$

$$+ E_{22}[\dot{v}_y - Z\dot{w}_{yy}]^2 + 2E_{13}[\dot{u}_x - Z\dot{w}_{xx}][\dot{u}_y + \dot{v}_x - 2Z\dot{w}_{xy}]$$

$$+ 2E_{23}[\dot{v}_y - Z\dot{w}_{yy}][\dot{u}_y + \dot{v}_x - 2Z\dot{w}_{xy}]^2 + E_{33}[\dot{u}_y + \dot{v}_x - 2Z\dot{w}_{xy}]^2\}dV \qquad \text{(c-30)}$$

Since E_{ij} is the only quantity that is a function of z, the integration can be reduced by defining

$$\bar{E}_{ij} = \int_{-z_o}^{z_o} E_{ij}dZ \qquad C_{ij} = \int_{-z_o}^{z_o} ZE_{ij}dZ \qquad D_{ij} = \int_{-z_o}^{z_o} Z^2E_{ij}dZ \qquad \text{(c-31)}$$

With $\bar{E}_{ij}$, C_{ij}, and D_{ij} introduced into Equation (c-30) and expanding terms, the volume integral may be written as

$$\int_V E_{ijk\ell}\dot{u}_{i,j}\delta\dot{u}_{k,\ell}\,dV = \int_0^{y_o}\int_0^{x_o} \{[\bar{E}_{11}\dot{u}_x + \bar{E}_{12}\dot{v}_y + \bar{E}_{13}(\dot{u}_y + \dot{v}_x)]\delta\dot{u}_x$$

$$+ [\bar{E}_{13}\dot{u}_x + \bar{E}_{22}\dot{v}_y + \bar{E}_{23}(\dot{u}_y + \dot{v}_x)]\delta\dot{v}_y + [\bar{E}_{13}\dot{u}_x + \bar{E}_{23}\dot{v}_y + \bar{E}_{33}(\dot{u}_y + \dot{v}_x)]\delta(\dot{u}_y + \dot{v}_x)$$

$$- [C_{11}\dot{w}_{xx} + C_{12}\dot{w}_{yy} + 2C_{13}\dot{w}_{xy}]\delta\dot{u}_x - [C_{12}\dot{w}_{xx} + C_{22}\dot{w}_{yy} + 2C_{23}\dot{w}_{xy}]\delta\dot{v}_y$$

$$- [C_{13}\dot{w}_{xx} + C_{23}\dot{w}_{yy} + 2C_{33}\dot{w}_{xy}]\delta(\dot{u}_y + \dot{v}_x) - [C_{11}\dot{u}_x + C_{12}\dot{v}_y + C_{13}(\dot{u}_y + \dot{v}_x)]\delta\dot{w}_{xx}$$

(This equation is continued on the next page.)

$$- [C_{12}\dot{u}_x + C_{22}\dot{v}_y + C_{23}(\dot{u}_y + \dot{v}_x)]\delta\dot{w}_{yy} - 2[C_{13}\dot{u}_x + C_{23}\dot{v}_y + C_{33}(\dot{u}_y + \dot{v}_x)]\delta\dot{w}_{xy}$$

$$+ [D_{11}\dot{w}_{xx} + D_{12}\dot{w}_{yy} + 4D_{13}\dot{w}_{xy}]\delta\dot{w}_{xx} + [D_{12}\dot{w}_{xx} + D_{22}\dot{w}_{yy} + 4D_{23}\dot{w}_{xy}]\delta\dot{w}_{yy}$$

$$+ 4[D_{13}\dot{w}_{xx} + D_{23}\dot{w}_{yy} + D_{33}\dot{w}_{xy}]\delta\dot{w}_{xy}\}dxdy \qquad \text{(c-32)}$$

The surface integral of Equation (c-2) is

$$\int_{S_\sigma} \dot{\nu}\dot{T}_i\delta\dot{u}_i dS = + \int_0^{y_o} [N_x\delta\dot{u} + N_{xy}\delta\dot{v} + M_x\delta\dot{w}_x + M_{xy}\delta\dot{w}_y - Q_x\delta\dot{w}]dy$$

$$+ \int_0^{x_o} [N_y\delta\dot{v} + N_{xy}\delta\dot{u} + M_y\delta\dot{w}_y + M_{yx}\delta\dot{w}_x - Q_y\delta\dot{w}]dx$$

$$+ \int_0^{x_o}\int_0^{y_o} p\delta w dxdy \qquad \text{(c-33)}$$

where

$$\begin{Bmatrix} N_x \\ N_y \\ N_{xy} \end{Bmatrix} = \int_{-z_o}^{z_o} \begin{Bmatrix} \sigma_x \\ \sigma_y \\ \tau_{xy} \end{Bmatrix} dz, \quad \begin{Bmatrix} M_x \\ M_y \\ M_{xy} \end{Bmatrix} = \int_{-z_o}^{z_o} Z \begin{Bmatrix} \sigma_x \\ \sigma_y \\ \tau_{xy} \end{Bmatrix} dz, \quad \begin{Bmatrix} Q_x \\ Q_y \end{Bmatrix} = \int_{-z_o}^{z_o} \begin{Bmatrix} \tau_{xz} \\ \tau_{yz} \end{Bmatrix} dz \qquad \text{(c-34)}$$

Integrating by parts and applying the fundamental lemma of variational calculus results in the field equations which couple the in-

plane and transverse displacements through the C_{ij}'s. These equations are:

$$D_{11}\dot{w}_{xxxx} + 2[D_{12} + 2D_{33}]\dot{w}_{xxyy} + D_{22}\dot{w}_{yyyy} + 8[D_{23}\dot{w}_{xyyy} + D_{13}\dot{w}_{xxxy}]$$
$$+ [D_{11,xx} + D_{12,yy} + 4D_{13,xy}]\dot{w}_{xx} + [D_{12,xx} + D_{22,yy} + 4D_{23,xy}]\dot{w}_{yy}$$
$$+ 4[D_{13,xx} + D_{23,yy} + D_{33,xy}]\dot{w}_{xy} - C_{11}\dot{u}_{xxx} - 3C_{13}\dot{u}_{xxy}$$
$$- [C_{12} + 2C_{33}][\dot{u}_{xyy} + \dot{v}_{yxx}] - C_{23}\dot{u}_{yyy} - C_{13}\dot{v}_{xxx} \qquad \text{(c-35)}$$
$$- 3C_{23}\dot{v}_{xyy} - C_{22}\dot{v}_{yyy} - [C_{11,xx} + C_{12,yy} + 2C_{13,xy}]\dot{u}_x$$
$$- [C_{12,xx} + C_{22,yy} + C_{23,xy}]\dot{v}_y - [C_{13,xx} + C_{23,yy} + 2C_{33,xy}][\dot{u}_y + \dot{v}_x] = p$$

$$\bar{E}_{11}\dot{u}_{xx} + 2\bar{E}_{13}\dot{u}_{xy} + \bar{E}_{33}\dot{u}_{yy} + (\bar{E}_{33} + \bar{E}_{12})\dot{v}_{xy} + \bar{E}_{13}\dot{v}_{xx} + \bar{E}_{23}\dot{v}_{yy}$$
$$+ [\bar{E}_{11,x} + \bar{E}_{13,y}]\dot{u}_x + [\bar{E}_{12,x} + \bar{E}_{23,y}]\dot{v}_y + [\bar{E}_{13,x} + \bar{E}_{33,y}](\dot{u}_y + \dot{v}_x)$$
$$- C_{11}\dot{w}_{xxx} - 3C_{13}\dot{w}_{xxy} - (C_{12} + 2C_{33})\dot{w}_{xyy} - C_{23}\dot{w}_{yyy} \qquad \text{(c-36)}$$
$$- [C_{11,x} + C_{13,y}]\dot{w}_{xx} - 2[C_{13,x} + C_{33,y}]\dot{w}_{xy} - [C_{12,x} + C_{23,y}]\dot{w}_{yy} = 0$$

$$\bar{E}_{22}\dot{v}_{yy} + 2\bar{E}_{23}\dot{v}_{xy} + \bar{E}_{33}\dot{v}_{xx} + \bar{E}_{23}\dot{u}_{yy} + [\bar{E}_{33} + \bar{E}_{12}]\dot{u}_{xy} + E_{13}\dot{u}_{xx}$$

$$+ [\bar{E}_{22,y} + \bar{E}_{23,x}]\dot{v}_y + [\bar{E}_{12,y} + \bar{E}_{13,x}]\dot{u}_x + [\bar{E}_{33,x} + \bar{E}_{23,y}][\dot{v}_x + \dot{u}_y]$$

$$- C_{13}\dot{w}_{xxx} - (C_{12} + 2C_{33})\dot{w}_{xxy} - 3C_{23}\dot{w}_{xyy} + C_{22}\dot{w}_{yyy}$$

$$- [C_{12,y} + C_{13,x}]\dot{w}_{xx} - 2[C_{23,y} + C_{33,x}]\dot{w}_{xy}$$

$$- [C_{22,y} + C_{23,x}]w_{yy} = 0 \qquad \text{(c-37)}$$

The complete boundary conditions are:

At the corner point $x = x_o$ and $y = y_o$

$$M_{xy} + M_{yx} + 4[D_{13}\dot{w}_{xx} + D_{23}\dot{w}_{yy} + D_{33}\dot{w}_{xy}] - 2[C_{13}\dot{u}_x + C_{23}\dot{v}_y + C_{33}(\dot{u}_y + \dot{v}_x)] = 0$$

$$\text{or} \quad \dot{w} \quad \text{Specified} \qquad \text{(c-38)}$$

Along the line $x = x_o$ for all y, there are four conditions as follows:

$$\bar{E}_{11}\dot{u}_x + \bar{E}_{12}\dot{v}_y + \bar{E}_{13}(\dot{u}_y + \dot{v}_x) - C_{11}\dot{w}_{xx} - C_{12}\dot{w}_{yy} - 2C_{13}\dot{w}_{xy} - \frac{N_x}{2Z_o} = 0$$

$$\text{or} \quad \dot{u} \quad \text{Specified} \qquad \text{(c-39)}$$

$$\bar{E}_{13}\dot{u}_x + \bar{E}_{23}\dot{v}_y + \bar{E}_{33}(\dot{u}_y + \dot{v}_x) - C_{13}\dot{w}_{xx} - C_{23}\dot{w}_{yy} - 2C_{33}\dot{w}_{xy} - \frac{N_{xy}}{2Z_o} = 0$$

or $\dot{v}$ Specified (c-40)

$$-\frac{\partial M_{xy}}{\partial y} - [(D_{11}\dot{w}_{xx})_x + (D_{12}\dot{w}_{yy})_x + 4(D_{13}\dot{w}_{xx})_y + 4(D_{13}\dot{w}_{xy})_x$$

$$+ 4(D_{23}\dot{w}_{yy})_y + 4(D_{33}\dot{w}_{xy})_y] + Q_x + [(C_{11}\dot{u}_x)_x + (C_{12}\dot{v}_y)_x$$

$$+ (C_{13}\dot{u}_y)_x + (C_{13}\dot{v}_x)_x + 2(C_{13}\dot{u}_x)_y + 2(C_{23}\dot{v}_y)_y + 2(C_{33}\dot{u}_y)_y$$

$$+ 2(C_{33}\dot{v}_x)_y] = 0 \qquad \text{or } \dot{w} \text{ Specified} \qquad \text{(c-41)}$$

$$D_{11}\dot{w}_{xx} + D_{12}\dot{w}_{yy} + 4D_{13}\dot{w}_{xy} - [C_{11}\dot{u}_x + C_{12}\dot{v}_y + C_{13}(\dot{u}_y + \dot{v}_x)] = M_x$$

or $\dot{w}_x$ Specified (c-42)

Along the line $y = y_o$ for all x,

$$\bar{E}_{13}\dot{u}_x + \bar{E}_{23}\dot{v}_y + \bar{E}_{33}(\dot{u}_y + \dot{v}_x) - [C_{13}\dot{w}_{xx} + C_{23}\dot{w}_{yy} + 2C_{33}\dot{w}_{xy}] - \frac{N_{yx}}{2Z_o} = 0$$

or $\dot{u}$ Specified (c-43)

$$\bar{E}_{12}\dot{u}_x + \bar{E}_{22}\dot{v}_y + \bar{E}_{23}(\dot{u}_y + \dot{v}_x) - [C_{12}\dot{w}_{xx} + C_{22}\dot{w}_{yy} + 2C_{23}\dot{w}_{xy}] - \frac{N_y}{2Z_o} = 0$$

or $\dot{v}$ Specified (c-44)

C-20

$$-\frac{\partial M_{yx}}{\partial x} - [4(D_{13}\dot{w}_{xx})_x + 4(D_{23}\dot{w}_{yy})_x + 4(D_{33}\dot{w}_{xy})_y + (D_{12}\dot{w}_{xx})_y + (D_{22}\dot{w}_{yy})_y + 4(D_{23}\dot{w}_{xy})_y] + [(C_{12}\dot{u}_x)_y + (C_{22}\dot{v}_y)_y + (C_{23}\dot{u}_y)_y + (C_{23}\dot{v}_x)_y + 2(C_{13}\dot{u}_x)_x + 2(C_{23}\dot{v}_y)_x + 2[C_{33}(\dot{u}_y + \dot{v}_x)]_x + Q_y = 0$$

or $\dot{w}$ Specified

(c-45)

$$D_{12}\dot{w}_{xx} + D_{22}\dot{w}_{yy} + 4D_{23}\dot{w}_{xy} - [C_{12}\dot{u}_x + C_{22}\dot{v}_y + C_{23}(\dot{u}_y + \dot{v}_x)] = M_y$$

or $\dot{w}_y$ Specified

(c-46)

APPENDIX D

BOUNDARY CONDITIONS AT CORNER POINTS IN KIRCHHOFF PLATE THEORY

As noted in Equation (c-38), there are reactive forces present at corner points in fourth order plate theory. In this appendix, the boundary conditions at points where boundaries are discontinuous are derived via the variational principal stated in Equation (c-2). The plate under examination (Figure D-1) has no applied in-plane loadings and is assumed to be elastic.

The volume integral of Equation (c-32) is reduced to include only the transverse deflection noting that for elastic behavior, $C_{ij} = 0$. However, the surface integral, $\int_{S_\sigma} \overset{\nu}{T}_i u_i dS$, which includes the bending moments M_n and M_{nt}, and the transverse shear force Q_n along with the transverse pressure p, becomes

$$\int_{S_\sigma} \overset{\nu}{T}_i u_i dS = - \int_o^s \left[M_n \frac{\partial w}{\partial n} + M_{nt} \frac{\partial w}{\partial t} - Q_n w \right] dS \qquad (d\text{-}1)$$

By setting the first variation of the volume plus surface integrals to zero, the boundary conditions for the case where surface tractions are applied over the surface $S\sigma_1$ and $S\sigma_2$ in Figure D-1 can be found. At the intersection of $S\sigma_1$ and $S\sigma_2$, either the transverse deflection w is zero, or

$$\frac{D(1-\nu)}{2} [(w_{xx} - w_{yy})(\sin 2\alpha_1 - \sin 2\alpha_2) - 2w_{xy}(\cos 2\alpha_1 - \cos 2\alpha_2)] - M_{nt}\Big|_{\text{on } S_1} + M_{nt}\Big|_{\text{on } S_2} = 0 \qquad (d\text{-}2)$$

FIGURE D-1
PLATE GEOMETRY FOR CORNER EXAMINATION

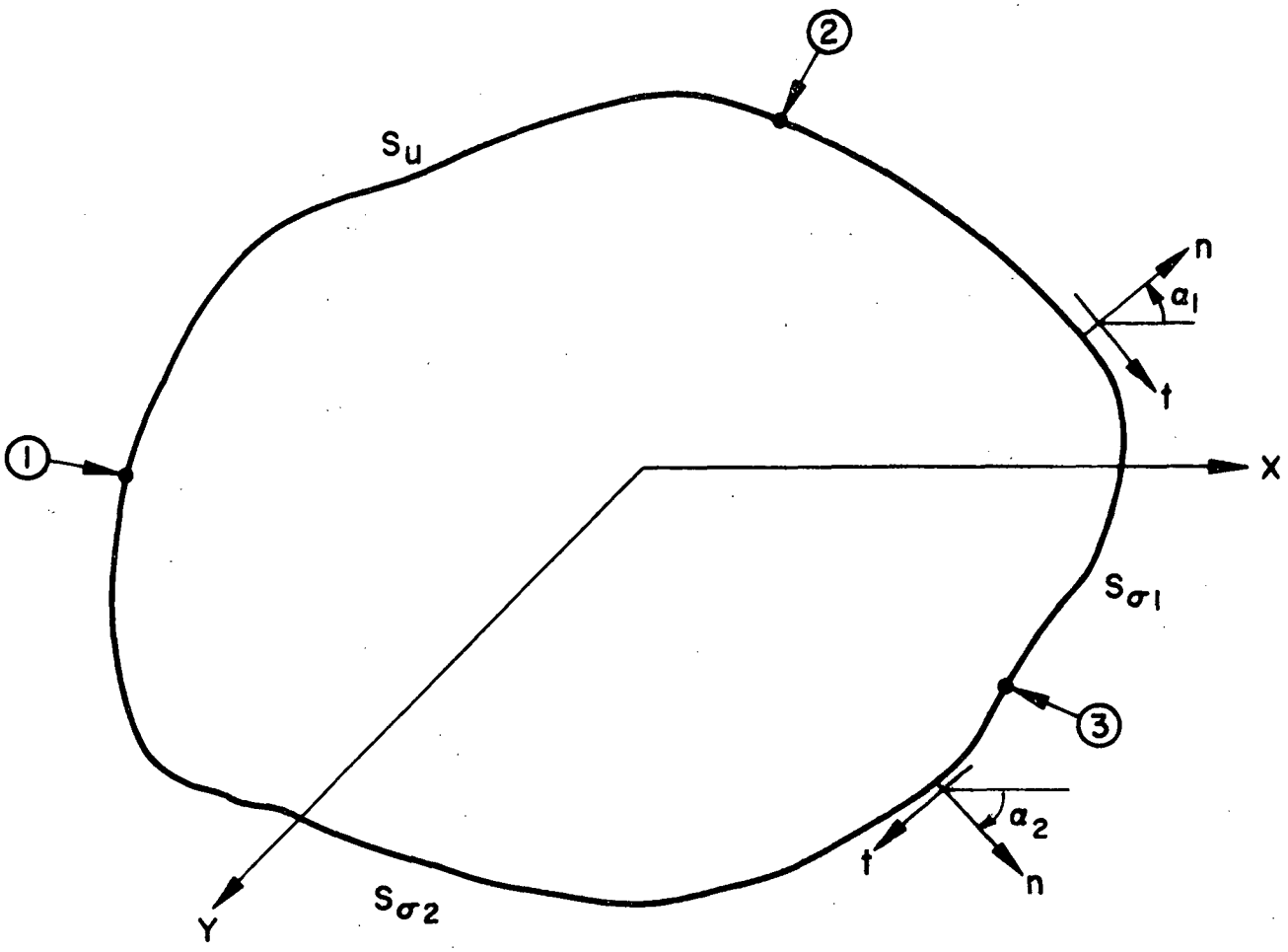

NOTES :

1. APPLIED TRACTIONS ON $S_{\sigma 1}$ & $S_{\sigma 2}$
2. APPLIED DISPLACEMENTS ON S_u
3. n & t REFER TO NORMAL AND TANGENTIAL DIRECTIONS AT A POINT
4. X & Y ARE CARTESIAN COORDINATES

The various corner configurations of Figure D-2 are examined in light of Equation c-47 and are listed in Table D-1. It is noted that the reactive conditions at the intersection vary from zero for a smooth intersection to a maximum for the exterior corner, back to zero for the crack tip, and to a minimum for the interior corner.

FIGURE D-2
CORNER CONFIGURATIONS

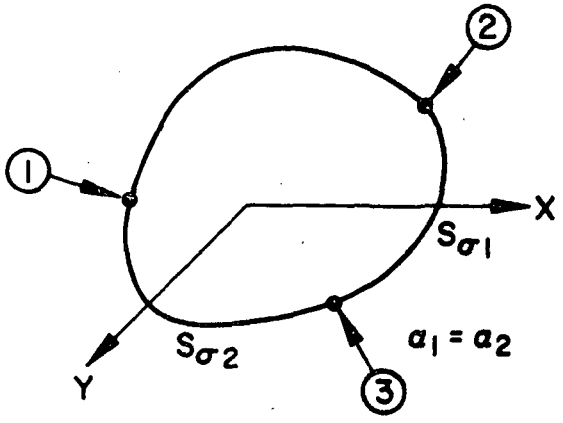

a. SMOOTH INTERSECTION

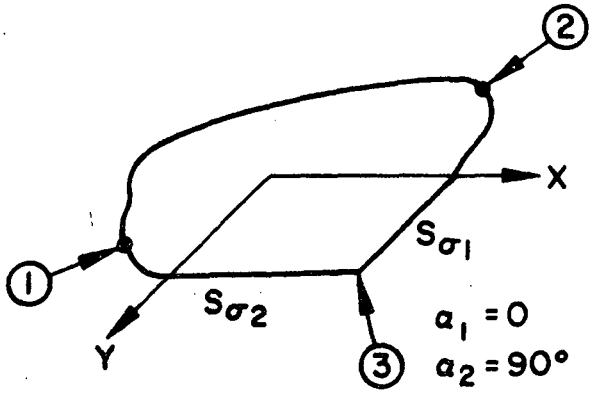

b. EXTERIOR CORNER

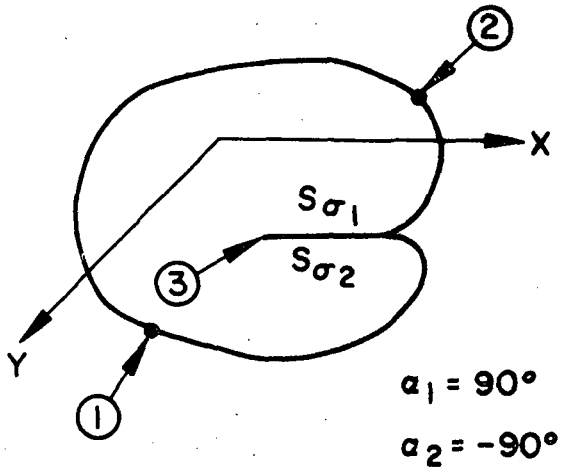

c. CRACK TIP

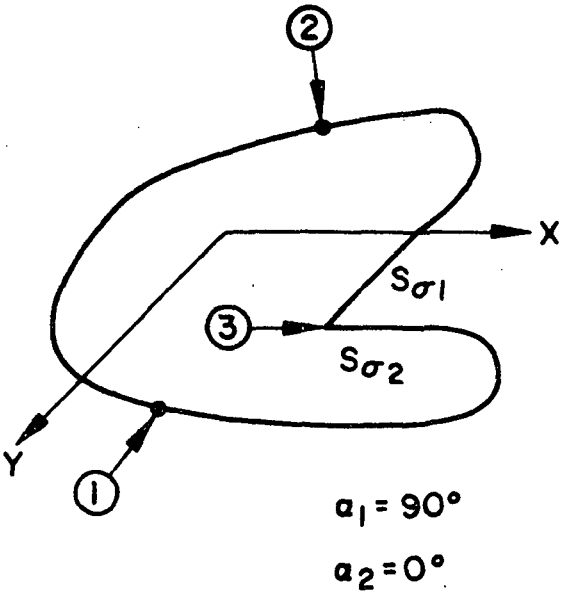

d. INTERIOR CORNER

TABLE D-1

Corner Reactions in Elastic Plate Bending Theory

FIGURE	α_1	α_2	M_{nt} on $S\sigma_1$	M_{nt} on $S\sigma_2$	CORNER REACTION EQUATION (d-2)
Smooth Intersection Figure A-6.a D-2	α	α	M_{nt}	M_{nt}	0
Exterior Corner Figure A-6.b D-2	0	90^o	M_{xy}	M_{yx}	$M_{yx} - M_{xy} = -2D(1-\nu)w_{xy}$
Crack Tip Figure A-6.c D-2	90^o	-90^o	M_{yx}	M_{yx}	0
Interior Corner Figure A-6.d D-2	90^o	0^o	M_{yx}	M_{xy}	$M_{xy} - M_{yx} = -2D(1-\nu)w_{xy}$

1. Report No.	2. Government Accession No.	3. Recipient's Catalog No.
4. Title and Subtitle ELASTO-PLASTIC BENDING OF CRACKED PLATES, INCLUDING THE EFFECTS OF CRACK CLOSURE		5. Report Date October 1972 6. Performing Organization Code
7. Author(s) David Paul Jones		8. Performing Organization Report No. SM-83A 10. Work Unit No.
9. Performing Organization Name and Address Carnegie-Mellon University Pittsburgh, Pennsylvania 15213		11. Contract or Grant No. NGL 39-002-023 13. Type of Report and Period Covered
12. Sponsoring Agency Name and Address Contractor Report		14. Sponsoring Agency Code

15. Supplementary Notes

16. Abstract

A capability for solving elasto-plastic plate bending problems is developed using assumptions consistent with Kirchhoff plate theory. Both bending and extensional modes of deformation are admitted with the two modes becoming coupled as yielding proceeds. The material work-hardens and, consistent with the fundamental theory of elasto-plasticity, loading is incremental and local unloading is permitted to occur. Equilibrium solutions are obtained numerically by determination of the stationary point of a functional which is analogous to the potential strain energy. The stationary value of the functional for each load increment is efficiently obtained through use of the conjugate gradient method (CGM) at modest computer storage requirements. The CGM was modified to take advantage of initial search direction vectors to provide possible reductions in computing time from one load increment to the next.

This technique is applied to the problem of a large centrally through cracked plate subject to remote circular bending. Comparison is drawn between two cases of the bending problem. The first neglects the possibility of crack face interference with bending, and the second includes a kinematic prohibition against the crack face from passing through the symmetry plane. Results are reported which isolate the effects of elasto-plastic flow and crack closure.

17. Key Words (Suggested by Author(s))	18. Distribution Statement
Cracked plates Plate bending Elasto-plastic bending	UNCLASSIFIED

19. Security Classif. (of this report)	20. Security Classif. (of this page)	21. No. of Pages	22. Price*
UNCLASSIFIED	UNCLASSIFIED		